ABSTRACT

Title of Document: DETECTION OF RAIN-ON-SNOW EVENTS AND ITS IMPACT ON PASSIVE MICROWAVE-BASED SNOW WATER EQUIVALENT RETRIEVAL

Elizabeth Meghan Ryan, Master of Science, 2018

Directed By: Assistant Professor, Barton A. Forman
Department of Civil and Environmental Engineering

Rain-on-snow (ROS) events can impact snow stratigraphy via generation of wet snow and ice crust(s) within the snowpack. Considering the assumptions of most passive microwave-based snow water equivalent (SWE) retrievals, which include a dry and homogenous snowpack, ROS events could significantly impact SWE retrieval accuracy. This study explored the feasibility of various approaches to detect ROS events using multiple data types (i.e., satellite observations, model output, and in-situ measurements). Agreement in ROS events detected varied among the different data types. Only ~10% of suspected ROS events were flagged using the satellite-based algorithm. Alternatively, ~50% of suspected ROS events were flagged using the model-based algorithm, whereas ~40% of suspected ROS events were flagged using the in-situ measurements-based algorithm. Findings were unable to speak to the impact of ROS events on SWE retrieval accuracy due to the lack of in-situ SWE measurements; however, a slight pattern in local fluctuations was observed.

DETECTION OF RAIN-ON-SNOW EVENTS AND ITS IMPACT ON PASSIVE MICROWAVE-BASED SNOW WATER EQUIVALENT RETRIEVAL

By

Elizabeth Meghan Ryan

Thesis submitted to the Faculty of the Graduate School of the
University of Maryland, College Park, in partial fulfillment
of the requirements for the degree of
Master of Science
2018

Advisory Committee:
Assistant Professor Barton A. Forman, Chair
Professor Richard H. McCuen
Associate Professor Kaye L. Brubaker

© Copyright by
Elizabeth Meghan Ryan
2018

ACKNOWLEDGEMENTS

Firstly, I would like to give a special thank you to my advisor, Dr. Barton Forman, for his constant support and optimism. I am very thankful for all the opportunities he has given me. He has such a contagious enthusiasm, both inside and outside the classroom, for the field, and I greatly appreciate his consistent willingness to meet with me whenever I requested. Today I am a smarter, more inquisitive, stronger communicator, and critical thinker because of him.

I want to thank my other advisor and supervisor, Dr. Ludovic Brucker, for all of his time and feedback throughout these last three years, in addition to setting up some partial financial support from the Universities Space Research Association (USRA). Dr. Brucker is an exceptional example of a scientist that I aspire to become and has made a considerable impact on my development as a graduate student and scientist/engineer within the field of remote sensing. I very much enjoyed my time working at National Aeronautics and Space Administration (NASA) Goddard with him, and interacting with other Goddard employees, contractors and summer interns.

An enormous thank you to Dr. Kaye Brubaker and Dr. Richard McCuen for their challenging classes, countless office hours, constructive criticism and kind words. Not only have I gained a tremendous amount of knowledge about modeling, fluid dynamics, storm water management and statistics, but also the fundamental tools that I need to make a difference as an engineer and a newfound inspiration for the field. There have been numerous highs and lows along my journey as a graduate student in the Civil and Environmental Engineering graduate program and I am extremely thankful for my entire committees' patience and mentorship.

Thank you, Dr. Galloway, for your patience and wisdom. Working with you has entirely changed my perspective on water resources management, research processes and mastering the art of balancing all life's stressors. There aren't many professors left like you.

I would also like to recognize Dr. Forman's research team, especially Yuan Xue, Lu Liu, Jing Wang and Jawairia Ahmad. Each and every one of you provided me tremendous support and feedback, and it was an honor working beside you guys. I know you all will go on to do great things!

My deepest gratitude to my biggest mentors, my parents, who inspire me every day. I am forever in debt to the emotional and financial support you have provided and can only hope to be half the parents you are to me. Thank you to my boyfriend of four plus years, Timothy Saad, for always standing by my side and pushing me to my fullest potential in every aspect of my life. I would not even be in graduate school, if it weren't for you. Thank you for celebrating all my triumphs and loving me even more through all my failures. You are my rock, I love you.

Thank you to my other cheerleaders and supporters, including Dr. Bruce James, Dr. Wendy Whittemore, Antti Koskelo, Rachael Taylorson, Michele Holzhauser, Lauren and Jacob Ryan, Arjun Durr, Louis Coplan and Matthew Alexander.

Lastly, thank you to the University of Maryland, College Park for facilitating my academic career and being my home since January 2010, Go Terps!

Table of Contents

List of Tables

List of Figures

List of Notation and Abbreviations

AMSR-E	Advanced Microwave Scanning Radiometer - Earth Observing System
CATCHMENT	NASA Catchment land surface model
D_S	Depth of Snow
EASE-Grid 2.0	Equal-Area Scalable Earth -2 Grid
fd	Forest density
ff	Forest fraction
FU	BIM ROS detection algorithm Refreeze flag
GHz	Gigahertz
GR	Gradient ratio
$GR_p^{v1,v2}$	Gradient ratio of frequencies (v1 and v2) at polarization (p)
H	Horizontal polarization
K	Kelvin
L	Length dimension
p	Polarization of a given wavelength
GSOD	Global Summary of the Day
LL	BIM ROS detection algorithm Liquid layer Flag
LLs	BIM ROS detection algorithm Liquid layer Spectral Flag
LLt	BIM ROS detection algorithm Liquid layer Temporal Flag
m	Meters
M	Mass dimension
MERRA-2	Modern Era Retrospective-analysis for Research and Applications-2
NASA	National Aeronautics and Space Administration
NOAA	National Atmospheric and Oceanic Administration
NSIDC	National Snow and Ice Data Center
PFU	BIM ROS detection algorithm Post-refreeze Flag
PR^v	Polarization ratio at frequency (v)
ROS	Rain-on-snow
SLC	Snow liquid water content
SWE	Snow water equivalent
Tb	Brightness temperature
Tb_{vp}	Brightness temperature at frequency (v) [GHz] and polarization (p)
V	Vertical polarization
ρ_S	Density of Snow
ρ_W	Density of Water

Chapter 1: Introduction and Literature Review

1.1 Introduction

Over the past decade, Anchorage, Alaska, has had nearly all of its weather-related school closures as a result of winter rain. A November 2010 storm, nicknamed the "Icepocalypse", developed an ice layer so thick that it remained on several streets for the entire winter season. Icy conditions have become the menace of local transportation departments; enough to have caused Alaska to become the first state to use an ice-grinding device on its roadways (Rosen, 2014). The scope of these winter rainstorms does not stop at endangering transportation infrastructure: an October rainstorm witnessed in 2003 is strongly considered to be the root cause of death for over 20,000 musk oxen in Banks Island, Canada (Grenfell, et al., 2008). The resultant ice crust, formed from the rain event, was too thick for the herbivorous animals to burrow through and access its only food source. Local hunters found emaciated carcasses and even observed oxen, desperate for food, wandering onto pack ice and drifting out to sea (Grenfell, et al., 2008). Ecologists have uncovered numerous other ecologic impacts of these storms from a decline in peregrine falcon populations due to increased exposure of chicks to hypothermia to long-term withering of yellow cedar due to freezing roots with little insulating snow layer, degraded by rain (Rosen, 2014).

There is also solid evidence to suggest that high latitude snowpacks that experienced rain event(s) have altered microwave emissions, relative to an unaffected snowpack. These passive microwave emissions are observed using remote sensing instruments, such as radiometers on-board satellite platforms, and heavily used in retrieval-based estimations that rely on many assumptions, some of which include a dry, homogenous snowpack. Winter season rain events

resulting in wet snow conditions and ice crusts can violate these basic assumptions and may produce less accurate estimations. Accuracy of snowpack features estimated using satellite observations is crucial for the understanding of water and energy systems, water resource management, climate prediction and models. Thus, further exploration of such phenomenon and its potential impacts is crucial and was the primary motivation for the study.

Although the current knowledge on the impact of these rainstorms is growing, there is still much unknown about the duration, frequency, and intensity of these storms, in addition to their widespread impacts. The thesis further investigates the phenomenon by examining methods to determine the temporal and global polar distribution of these events using the three pillars of scientific estimation (i.e., in-situ measurements, model estimations, and remote sensing observations) and the impact of winter rain events on microwave-based retrieval snowpack characterization.

1.2 Rain-on-Snow (ROS) Events

High latitude rain-on-snow (ROS) events, described simply as liquid precipitation falling onto a snowpack, can lead to the formation of ice crusts on or within the snowpack such as those created in Figure 1.1. Winter season liquid precipitation can occur when air temperatures are close to or exceed freezing in either the atmosphere in which the raindrop formed or passing through as it falls. Liquid precipitation percolating within or accumulating on top of the snowpack may then freeze into an ice crust as the air temperature returns to sub-freezing ranges. Over time an ice layer can go through freeze-thaw cycles that cause it to evolve and harden into a stronger/ thicker ice crust. ROS events vary greatly in duration, intensity and frequency, and consequently the ice crusts formed by them.

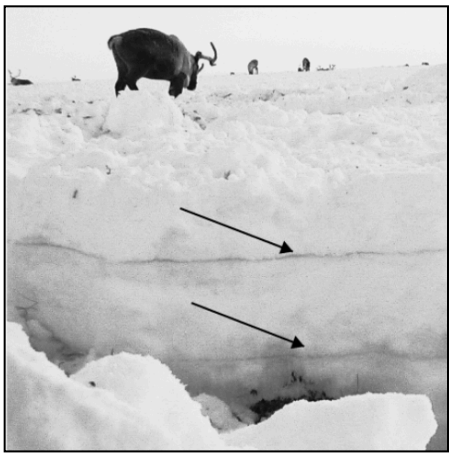

Figure 1.1. Ice crusts formed from an ROS event in November 2006 on the southern Yamal Peninsula, Russia (Detection of snow surface thawing and refreezing in the eurasian arctic with quikscat: implications for reindeer herding, 2010).

Multiple peer-reviewed papers have discussed observations of ROS events and theorized a steady increase of said events, as winters will continue to warmer in the higher latitudes (Winter Rain on Snow and its Association with Air Temperature in Norther Eurasia, 2008; Grenfell, et al., 2008; Ecological Implications of Changes in the Arctic Cryosphere, 2011; Callaghan, et al., 2010; Liston, et al., 2011; Passive-Microwave-Based Detection of Rain-on-Snow Events over sub-Arctic Regions, 2014; Bjerke, et al., 2011). However, ROS events are exceptionally undocumented, largely as a result of sparse observational weather networks, where a small localized ROS event covering a distance on the order of a few hundred square kilometers can be completely concealed but is still large enough to cause impact local ungulates and microwave observations (Jentsch, et al., 2007). There continues to be difficulty in both finding the location of where the event occurs and the form of precipitation falling during the event, as the current technology at the sites cannot determine the phase of precipitation falling into instrument. Almost all of our knowledge on ROS events is based on anecdotal evidence (Grenfell, et al., 2008), which is surprising considering the potential impact these events have on the surface energy balance and hydrologic cycles as well as the terrestrial and ecological

systems. Dr. Putkonen from the University of North Dakota describes the study of ROS events as "one of those fairly rare occasions where there is a very interesting scientific problem to understand natural properties that we know very little about, but [which] have very high societal value" (Stemp-Morlock, 2008).

It is theorized that the high latitudes will warm at a faster rate than the rest of the globe and that ROS events may become more common in regions where it has not occurred previously (Winter Rain on Snow and its Association with Air Temperature in Norther Eurasia, 2008) (Liston, et al., 2011). The northern hemisphere's higher latitudes are a "particularly sensitive component of the Earth's climate system" (Observational evidence of recent change in the northern high-latitude environment, 2000). The International Panel on Climate Change speculates an increase in high-latitude liquid precipitation as the Arctic warms. John Walsh, chief scientist at University of Alaska Fairbank's International Arctic Research Center, theorizes that high latitude winters will continue to be warmer and as ice coverage declines and more regions experience more open water, more heat will be absorbed and ultimately returned back into the atmosphere, in addition to moisture and that effectively will cause heavy downpours in late-fall and early winters (Rosen, 2014). One study concluded that it was the increases in air temperatures during the winter season that caused an increase in rainfall days as more moisture was retained by the atmosphere, causing an increase in ROS events over the northern part of European Russia (Winter Rain on Snow and its Association with Air Temperature in Norther Eurasia, 2008). A persistent jet stream pattern was theorized as the reason for an unusually warm Alaskan 2013-2014 winter, which may have been caused by exceptionally warm ocean temperatures in the south of Alaska (Galloway, et al., 2014).

1.3 ROS Ecological Impacts

Large changes to snowpack composition, specifically the development of an ice crust(s), has been documented to result in the demise of native ungulate herds like caribou, reindeer and musk oxen. An ice crust can reduce foraging capabilities to such a degree that starvation occurs and the animals perish and has a resonating impact on the local communities in the region.

Ice crusts created by an ROS event have the potential to significantly impact local wildlife and consequently the indigenous communities reliant on them. Indigenous herbivorous species rely on the lichen and vegetation lying underneath the snowpack and use their hooves to dig through the snow to reach their food source. Over the last two decades several hunters and indigenous communities in remote polar regions have witnessed ROS events that have led to massive die offs of local herds in the region. For example, one historical ROS event in Banks Island, Canada is believed to have caused the death of an estimated 20,000 musk oxen in October of 2003 (Grenfell, et al., 2008). A decade later, in November 2013, on the southern Yamal Peninsula of Russia, local herders observed a region where approximately 61,000 reindeer perished believed as a result of another large ROS event, marked as the largest regional die off or reindeer ever to be documented (Guarino, 2016). The Yamal peninsula also had a recorded ROS event in November of 2006 where local herders estimated a loss amounted to about 25% of their animals or 20,000 reindeer, where an ice barrier in reindeer pastures was observed by researchers (Detection of snow surface thawing and refreezing in the eurasian arctic with quikscat: implications for reindeer herding, 2010). ROS events and short periods of warm weather during the winter season have many local hunters/herders concerned about the future of their livelihoods and conservation of the ungulate species and taiga ecosystem. Therefore, further investigation into where, when and how frequent these ROS events are occurring might help mitigate the

future impacts these phenomena could have on indigenous wildlife and the communities that rely on them.

"December 2014 brought Norway its biggest December rainfall totals since 1975 and forced some hibernating bears out of their wet dens in Finland." (Rosen, 2014) "Bruce C. Forbes, an expert on permafrost ecology at the University of Lapland in Finland recommends mobile slaughterhouses could be deployed so that reindeer can be slaughtered humanely and herders could receive compensation (Guarino, 2016).

Figure 1.2. Ungulates (Reindeer, Caribou and Musk oxen) impacted by ROS events.

1.4 ROS Impact on Snowpack Estimation

There is concern for not only the tundra and taiga wildlife, but also the influence ROS events have on snowpack estimation based on satellite observations.

1.4.1 Importance of Snowpack Estimation

Snowpack estimation is important for a variety of water resource management applications, including climate prediction and modeling. There are various features of a snowpack that can be measured and/or estimated, including snowpack density, snow depth, and snow water equivalent (SWE). SWE is an estimate of the equivalent of liquid water present within a snowpack. Such estimates are valuable for a variety of purposes ranging from spring

snowmelt projections to energy balance equations for climate models. SWE can be described as a numerical length value assigned to quantify the amount water held within a snowpack and can be expressed as:

$$SWE = D_s * \frac{Density\ of\ Snow(\rho_S)}{Density\ of\ Water\ (\rho_W)} = [L] * \frac{[ML^{-3}]}{[ML^{-3}]} = [L] \quad (1\text{-}1)$$

where SWE is the snow water equivalent [m]; D_s is the snow depth [m]; ρ_S is the snow density [$kg\ m^{-3}$]; ρ_W is the water density [$kg\ m^{-3}$]; L is the length dimension; and M is the mass dimension. A more densely compacted snowpack will contain more water than a lightly compacted snowpack of the same snow depth, thus highlighting the need to use SWE to help accurately characterize a given snowpack.

1.4.1.1 Methods of Snowpack Characterization

There are three main approaches to characterizing snowpack features: (1) remote sensing observations, (2) model estimation, and (3) in-situ measurements.

1.4.1.1.1 *Snowpack Characterization using In-situ Measurements*

In-situ measurements yield estimates of snowpack features closest to the truth because they are the most direct. Measurements conducted by amateurs to highly trained professionals can be compared against the other two approaches (i.e., model estimates and remote sensing observations) for calibration and/or validation. Ground stations often measure snow depth, air temperature, and precipitation at frequent time intervals and field campaigns can measure specific features at a site. Some shortcomings with ground-based stations include limited spatial distribution, especially in polar regions. Ground stations that break down often go months before being fixed due to their remoteness. Also, the technology for these stations is dated, and many are not able to discern the phase of precipitation or provide a fraction of the phases falling, which

is important for ROS event detections where even though the air temperature recorded may be below freezing, liquid precipitation still occurs (Stemp-Morlock, 2008). However, some newer models are now able to determine about 36 different classifications of rain/snow combinations (reference).

High latitude ground stations largely consist of the use of tipping bucket rain gauges to measure precipitation and some use heated buckets to prevent freezing water from plugging the opening of the funnel (Grenfell, et al., 2008). World Meteorological Organization (WMO) developed synoptic weather types that are regularly logged and can help discern the kind of precipitation, however these codes do not shed much light on the fraction of solid to liquid precipitation or the snowpack state (Grenfell, et al., 2008).

1.4.1.1.2 *Snowpack Characterization using Model Estimates*

The British statistician, George E. P. Box, once said, "All models are wrong, but some are useful". Model estimations can provide high temporal and spatial resolution, however the amount of uncertainty can be high, depending on the accuracy of the forcings (a.k.a., boundary conditions) used, discretization of simulation time, applicability to the region studied, and underlying assumptions. There are numerous models and algorithms created and used to estimate snowpack features. Forcings can come from other models, in-situ measurements or passive or active remote sensing observations.

1.4.1.1.3 *Snowpack Characterization using Remote Sensing Observations*

Remote sensing technology allows scientists to study physical features without ever coming into direct contact with them. Remote sensing technology ranges from the camera on a mobile phone to an instrument as complex as a sensor onboard a satellite. Remote sensing

technology takes advantage of the electromagnetic spectrum by either passively or actively observing particular wavelengths emitted, reflected or absorbed from the feature of interest. Various natural phenomena can interact with different electromagnetic wavelengths in such a manner that they can be studied.

For example, by measuring the difference in near-infrared (NIR) light and red visible light over a given region, one can quantify the about of vegetation, known as the Normalized Difference Vegetation Index or NDVI. Such a phenomenon can be used as an indicator of drought, where healthy vegetation will reflect more NIR and green visible relative to other wavelengths.

Remote Sensing instruments, such as satellites, are useful because they can cover large regions, especially high latitude remote areas, at regular intervals. However, there is a tradeoff between temporal and spatial resolution. Spatial resolution is increased often at the cost of decreased temporal resolution. Polar regions generally have increased, temporal and spatial resolution, as polar orbiting satellites pass over regions several times during a day with complete spatial coverage. Geostationary satellites can be used to increase the temporal resolution of a given area closer to the equator, however their spatial distribution is limited to that particular region.

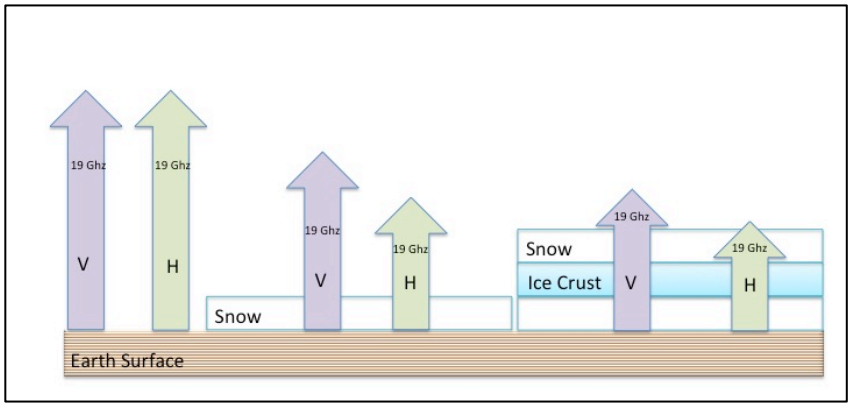

Figure 1.3. Diagram of the attenuation of a snowpack and ice crust to Earth's microwave emission.

In the context of snow characterization using remote sensing technology, the Earth naturally emits electromagnetic microwave radiation of which a satellite sensor can observe. The perceived radiance that reaches the sensor is known as a brightness temperature (Tb). A snowpack on the Earth's surface can absorb or attenuate the Earth's microwave emission and scientists can take advantage of the phenomenon to develop methods for estimating various snowpack features like snow depth and SWE. A snowpack's bulk emissivity primarily depends on various snow properties including liquid water content, grain size, surface roughness, a presence of dielectrocally distinct surface or internal water or ice layers, snow density, and the snow's physical temperature (Grenfell, et al., 2008) (Passive-Microwave-Based Detection of Rain-on-Snow Events over sub-Arctic Regions, 2014). However the emisivity can also be determined on a second order by factors such as soil mosiutre, atmosphere, lake fraction, and vegetation volume (Passive-Microwave-Based Detection of Rain-on-Snow Events over sub-Arctic Regions, 2014).

On board the Aqua satellite is a sensor that observes microwave brightness temperatures (6.9 GHz, 10.7 GHz, 18.7 GHz, 23.8 GHz, 36.5 GHz and 89.0 GHz), referred to as the Advance Microwave Scanning Radiometer-Earth Observing System (AMSR-E). The AMSR-E sensor has a total of twelve channels, including both the horizontal and vertical polarizations of all six different microwave frequencies. It is a conically-scanning radiometer collecting observations with an incidence angle of 54.8 degrees and a spatial resolution that ranges from 5.4 km at the 89 GHz channel to 56 km at the 6.9 GHz channel. The incidence angle is very close to the Brewster angle for the snow/air interface which is important so that V-pol is less attenuated than H-pol as snowpack's vertical density changes with snow layering.

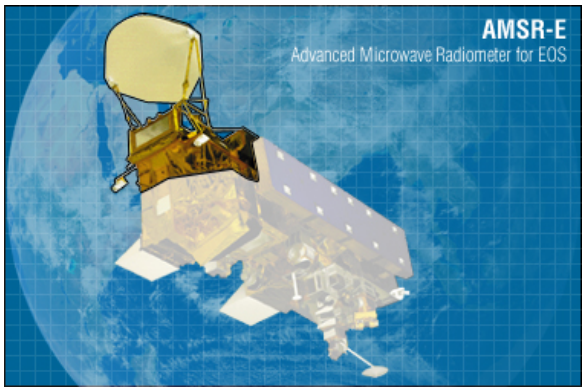

Figure 1.4. AMSR-E Sensor Onboard Aqua Satellite. Source http://aqua.nasa.gov.

SWE is estimated by first computing snow depth (D_S) using observed Tb from AMSR-E (Kelly, 2009) as:

$$D_S = ff\left[p1 * \frac{Tb_{18V} - Tb_{36V}}{1 - fd * 0.6}\right] + \cdots$$
$$\ldots (1 - ff)[p1 * (Tb_{10V} - Tb_{36V})] + [p2 * (Tb_{10V} - Tb_{18V})] \quad (1\text{-}2)$$

where D_S is snow depth [cm]; ff is the forest fraction [0 to 1]; fd is the forest density [g cm^{-3}]; Tb_{vp} is brightness temperature at (v) frequency and (p) polarization; and p1 and p2 are defined as:

$$p1 = \frac{1}{\log(Tb_{36V} - Tb_{36H})} \quad (1\text{-}4)$$

$$p2 = \frac{1}{\log(Tb_{18V} - Tb_{18H})} \quad (1\text{-}5)$$

where Tb_{vp} is brightness temperature at (v) frequency and (p) polarization. SWE is then further calculated as:

$$SWE_{AMSR-E} = D_S * \rho_S * 10.0 \quad (1\text{-}6)$$

where SWE_{AMSR-E} is the snow water equivalent [mm]; D_s is snow depth [cm]; ρ_S is snow density [g cm^{-3}]; and 10.0 is the conversion factor [mm] from cm to mm. Snow density is a static mask that doesn't change over the winter season, an average in-situ density was calculated and mapped for each of the six seasonal Sturm snow classes (A Seasonal Snow Cover Classification System for Local to Global Applications, 1995; Tedesco, 2012).

Snow depth can be estimated using brightness temperatures collected at three different frequencies - 10 GHz, 18 GHz, and 36 GHz - and their polarizations. Since only regions north of the 60^{th} parallel are studied, forest fraction is minimal, thereby enabling the SWE_{AMSR-E} equation to be simplified even further. Clouds can interfere with some of the microwave emssion observed as they themselves emit radition at the 89 GHz frequency.

1.4.2 ROS Impact on Snowpack Characterization

1.4.2.1 ROS Impact on Snowpack Composition

ROS event(s) have the potential to impact a snowpack in various ways depending on the duration, intensity, and the frequency in which the events occur in an affected region. Initially, when temperatures begin to approach freezing or warmer, even before precipitation occurs, there can be melting within the snowpack. With the addition of liquid precipitation as rain, the melting processes can be further accelerated. However, depending on the current composition of the snowpack, melted snowpack and/or percolating liquid precipitation could accumulate above an impermeable layer in the snowpack, and thus no water is leaving the system. Once precipitation ceases, if warm temperatures still persist, melting may continue to occur.

Once air temperatures drop back to subfreezing temperatures, liquid layer(s) in the snowpack will become an ice layer. The type of ice layer created is dependent on the rate of

temperature drop and current snowpack conditions. Over time the ice crust will evolve after multiple freeze-thaw cycles and can become highly compacted.

1.4.2.2 Potential ROS Impact on Retrieval-based Snowpack Characterization

In general, smaller wavelengths (i.e., higher frequencies) experience preferential scattering within the snowpack. Therefore, the longer wavelengths contain information relevant to deeper snow. ROS events may result in a wet snowpack and, when subfreezing temperatures return, the formation of one or more ice layers. A wet snowpack increases the microwave emission of the snowpack due to the increase in dielectric constant. Alternatively, ice crusts generally attenuate (scatter) microwave emission within the snowpack. Equation 1-2 accounts for a change in the difference of vertically and horizontally polarized light for 18 GHz, such a difference would increase if an ice crust was present, perhaps leading to a decrease in the $SWE_{AMSR\text{-}E}$ estimate. Increased emission of wet snow could result in very little change in the $SWE_{AMSR\text{-}E}$ estimate, if the radiance measured at all frequencies is increased.

In addition, liquid water on the surface of snow grains (or more simply wet snow) increases microwave absorption and reduces the microwave emission depth (penetration depth), thereby complicating SWE retrieval algorithms. Wet snow's thermal conductivity is very high and allows significant heat exchange between the soil below and the atmosphere above. Over time heat exchange can cause snow metamorphism that increases snowpack density and grain size and eventually into a hard, dense ice layer (Colbeck, 1982).

The presence of ice crusts within or on a snowpack can alter the ratio of polarized light attenuated in the snowpack. Quantifying the change in polarized light attenuated by the snowpack offers the potential to detect changes to the snowpack caused by an ROS event (Brucker, Ivanoff, & Maynard, 2014; Dolant, et al.; Langlois, et al., 2017). Due to the large

complexity of satellite-based snowpack estimation algorithms, many assumptions must be used, including the presence of a dry, homogenous snowpack without the existence of ice layer(s). Therefore, the presence of an ROS event phenomenon could lead to significant error in satellite-based SWE estimates.

1.5 Study Goal and Objectives

The goal of the study is to discern a linkage between local AMSR-E SWE (i.e. SWE_{AMSR-E}) fluctuations and ROS events to determine if ROS events should be flagged (i.e. may require additional modification) in passive microwave-based SWE retrievals at locations where a potential error may occur. The research goal comprised of two main objectives:

(A) Explore methods to detect ROS events in high latitude environments by:

1. Analyzing ROS events detected through the use of only satellite observations.
2. Detecting ROS events using estimates only from a land surface model output and atmospheric re-analysis tool.
3. Detecting ROS events using only ground station measurements.
4. Detecting ROS events using a combination of satellite observations, model estimates, and ground station measurements.

(B) Investigate if/how ROS events impact SWE_{AMSR-E} by:

1. Calculating the daily change in SWE_{AMSR-E} estimated before, the day of, and days following each ROS event (detected or documented).
2. Comparing each ROS event's daily SWE_{AMSR-E} changes to investigate if any patterns in local fluctuations occur.

3. Grouping ROS events by duration, antecedent snow depth, timing in winter season and region to determine if particular factors influence fluctuations in estimated SWE_{AMSR-E} during an ROS event.

Chapter 2: Methods and Data Sources

2.1 Introduction

The goal of the study was to determine if SWE_{AMSR-E} accuracy is negatively impacted by ROS events. Due to the lack of known ROS events, the study first explored some methods of detecting ROS events, known as Objective A. Objective B was to use the ROS events detected in Objective A to investigate SWE_{AMSR-E} accuracy. Chapter 2 discusses the methods of both objectives, A and B, in depth.

2.2 Methods of ROS Detection

Due to the remoteness of high latitude regions, there are only a handful of ROS events that have been documented, and even fewer that have been recorded by the sparsely-located, outdated, and inconsistent weather stations in these regions. As a result, only three well-known historical ROS events (see Figure 2.1) were used; Banks Island, Canada from 9 September - 3 October 2003; southern Yamal Peninsula, Russia from 5-7 November 2006; and Daring Lake, Northwest Territories, Canada on 8 April 2007. In order to further explore how ROS events impact SWE_{AMSR-E} (see Research Objective B outlined above), analysis of other ROS events beyond the three that have been documented, requires the exploration of new methods of ROS detection using existing data.

Each method of ROS detection employed a few simple conditional statements using one more data types: (1) satellite observations, (2) model estimates and (3) ground-based station measurements. The first three methods used only one dataset type, whereas the fourth method consisted of an amalgam of the previous three. Any ROS events that are detected using more than one of the first three methods is classified as an ROS event in Method 4. The fourth method

allows the incorporation of one or more dataset types, which is advantageous in mitigating the shortcomings of each type and helps to further narrow the number of ROS events detected to those that most likely occurred.

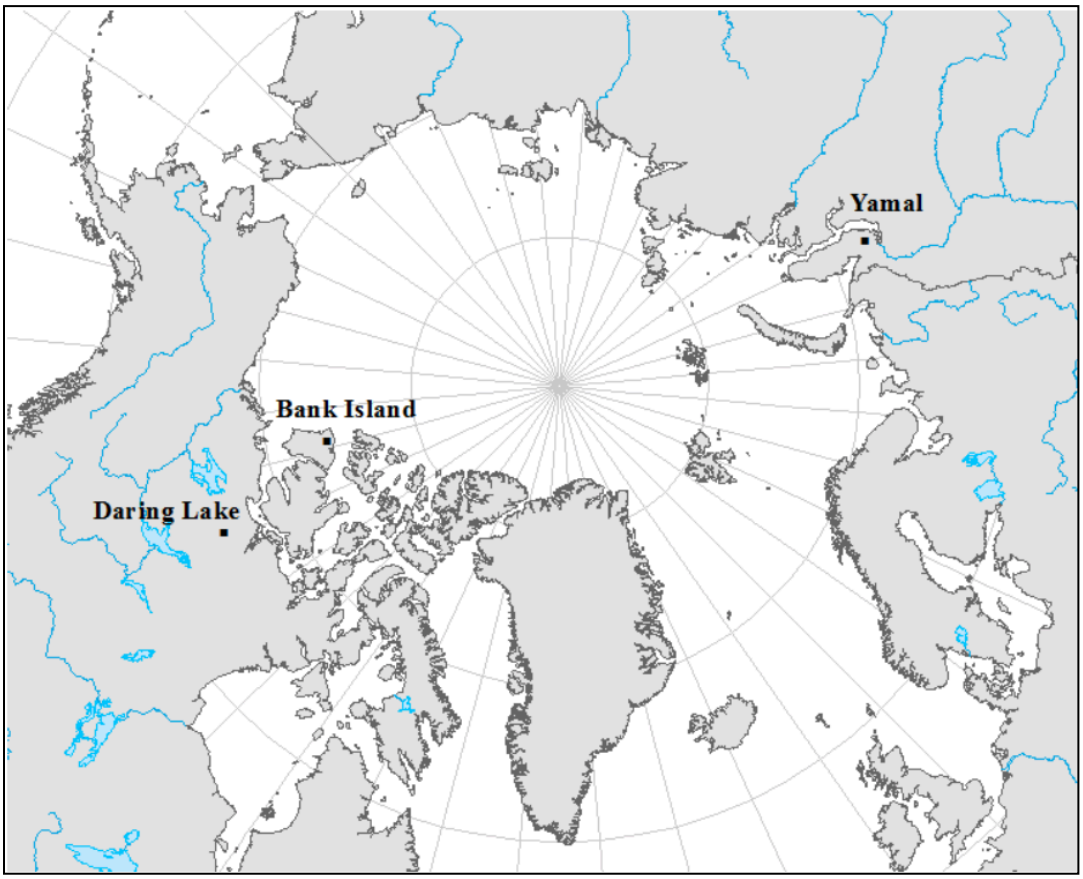

Figure 2.1. Location of the three documented ROS Events used: Banks Island, Canada; southern Yamal Peninsula, Russia; and Daring Lake, Northwest Territories, Canada (Passive-Microwave-Based Detection of Rain-on-Snow Events over sub-Arctic Regions, 2014).

Considering the primary focus was to investigate ROS event impact on Advanced Microwave Scanning Radiometer - Earth Observing System (AMSR-E) based snow water equivalent estimates (SWE_{AMSR-E}), the time period of investigation for Methods 1 - 4 encompassed the entire available record of the AMSR-E dataset from 19 June 2002 to 27 September 2011. Of that nine-year time period, only the winter seasons (i.e., months from

October-April) when snow cover was most likely were explored. Areas of interest were limited to polar regions north of the 60th parallel, in order to minimize the influence of vegetation, which tends to cause additional error in retrieval-based SWE estimates. Any detection over water, sea ice, or the Greenland ice sheet was removed with the use of the National Snow and Ice Data Center (NSIDC) land-sea-ice mask product. All detection methods assumed a homogenous distribution of snow depth, air temperature and precipitation across an entire 25 km x 25 km Equal Area Scalable Earth Grid-2 (EASE-Grid 2.0) cell provided by NSIDC (Brodzik, et al., 2011) (Brodzik, et al., 2014; Brodzik, et al., 2012).

2.2.1 Method 1: ROS Detection using Satellite Observations

Method 1 involved ROS detection though the sole use of passive microwave observations collected by AMSR-E, using an existing algorithm called the BIM ROS detection algorithm (Passive-Microwave-Based Detection of Rain-on-Snow Events over sub-Arctic Regions, 2014), herein referred to as Method 1. The radiance of each passive microwave frequency is measured by the AMSR-E sensor and referred to as its brightness temperature (Tb). Method 1 uses daily averaged Tb values obtained from NSIDC's AMSR-E/Aqua Daily L3 12.5 km Brightness Temperature, Sea Ice Concentration, and Snow Depth Polar Grids dataset (Cavalieri, et al., 2014). Four different microwave frequencies -18.7, 23.8, 36.5, and 89 GHz - were used in the algorithm. The horizontal and vertical polarization at each frequency was utilized, in addition to its polarization ratio. Polarization ratios (PR) quantify the difference in horizontally (H) and vertically (V) polarized light at a particular microwave frequency (ν) and are computed as:

$$\mathrm{PR}^{\nu} = \frac{\mathrm{Tb}_{\mathrm{V}}^{\nu} - \mathrm{Tb}_{\mathrm{H}}^{\nu}}{\mathrm{Tb}_{\mathrm{V}}^{\nu} + \mathrm{Tb}_{\mathrm{H}}^{\nu}} \qquad (2\text{-}1)$$

where PR^{v} is the polarization ratio [-] at frequency (v) [GHz]; and $\mathrm{Tb}_{\mathrm{p}}^{v}$ is the brightness temperature [K] at frequency (v) [GHz] and polarization (p) [-]; H is horizontally polarized light [-]; V is vertically polarized light [-]. Gradient ratios among the four different microwave frequencies were also used in Method 1. Gradient ratios (GR) quantify the difference between two different microwave frequencies (v_1 and v_2) of a specific polarization (p) and are computed as:

$$\mathrm{GR}_{\mathrm{p}}^{\mathrm{v1,v2}} = \frac{\mathrm{Tb}_{p}^{\mathrm{v1}} - \mathrm{Tb}_{\mathrm{p}}^{\mathrm{v2}}}{\mathrm{Tb}_{\mathrm{p}}^{\mathrm{v1}} + \mathrm{Tb}_{\mathrm{p}}^{\mathrm{v2}}} \tag{2-2}$$

where $\mathrm{GR}_{\mathrm{p}}^{\mathrm{v1,v2}}$ is the gradient ratio [-] for frequencies ($v1$ and $v2$) at polarization (p); and $\mathrm{Tb}_{\mathrm{p}}^{\mathrm{v}}$ is the brightness temperature [K] for frequency ($v1$ or $v2$) at polarization (p).

Both polarization and gradient ratios can provide insight into a snowpack's characteristics and their evolution. These ratios can be affected by fluctuations in a snowpack's vertical density profile or snow grain size. For example, an ice layer can increase a Tb's PR[19], the 19 GHz horizontally polarized light can be significantly attenuated by the ice layer, while the vertically polarized light remains relatively unchanged. (Passive-Microwave-Based Detection of Rain-on-Snow Events over sub-Arctic Regions, 2014), such phenomena can then be used to detect ice layers. $\mathrm{GR}_{\mathrm{V}}^{37,19}$ often increases in the presence of wet snow, which could be indicative of an ROS event. The same GR can then decrease after an ROS event, as a result of wet snow metamorphism increasing snowpack grain size and consequently the amount of scattering (Colbeck, 1982).

Method 1 aims to detect ROS events based on meeting certain thresholds for specific Tbs on the day preceding and day of a suspected ROS event. The algorithm consists of five types of ROS detection (i.e., flags). Flags 1-3 are indicative of a liquid layer (LL) on or within the

snowpack labeled as LLt, LLs, and LL, respectively. Flag 4 labeled ROS refreeze (FU) is indicative of an ice layer on or within the snowpack and can only occur if Flag 3 was raised the previous day. Flag 5 or post ROS refreeze (PFU) detects a metamorphosed ice layer in the snowpack and must proceed a Flag 4 from the previous day.

For the purposes of the study, an ROS event was considered detected for any region containing Flag 3 in the BIM ROS detection algorithm, indicating a liquid layer was detected in the snowpack. A liquid layer (LL or Flag 3) is not detected unless both LLt and LLs, Flags 1 and 2 respectively, are raised for that grid cell. Flag 1 or LLt is raised if changes in polarization and gradient ratios exceed specific thresholds over a 5-day moving window. Flag 2 or LLs is a spectral classification where the region's polarization and gradient ratios must meet a specified range for the flag to be raised. It is important to note here that a liquid layer could be detected during a surface melt event and not necessarily an ROS event because the spectral signatures can be similar between the two. Also, it is presumed that Method 1 would work better in cloud free conditions since 89 GHz is used in the detection. Clouds can magnify the radiation observed at the such wavelength, potentially leading to an inaccurate characterization of the snowpack.

Flags 4 and 5 play an important role in the algorithm by subsequently estimating if an ice crust exists and further evolved, respectively. Detection using Flags 1, 2, 4, or 5 were not used, mainly for simplicity. Method 1 results were regrided from the 12.5 km polar stereographic grid to a 25 km global EASE-Grid 2.0 (Brodzik, et al., 2014; Brodzik, et al., 2012). If one or more 12.5 km pixels detected an ROS event within a given 25 km EASE-Grid 2.0 pixel, the entire 25 km pixel was labeled as detecting an ROS event.

2.2.2 Method 2: ROS Detection using Model Estimates

Method 2 involved the use of forcing and output data from the NASA Catchment land surface model (here in referred to as CATCHMENT) (A catchment-based approach to modeling land surface processes in a general circulation model 1. Model Structure, 2000). CATCHMENT serves as the land surface component of the NASA Global Modeling and Assimilation Office Land Data Assimilation System (GMAO-LDAS). GMAO-LDAS is composed of various land-surface models that are uncoupled to the atmosphere and used to support water resource applications, research in weather prediction, water and energy cycles, and an approach to analyzing satellite and ground-based observations. The model divides a snowpack into three separate layers and estimates various states at each layer (e.g., snow density and snow temperature). The only model state used for Method 2 ROS detection was the current and previous day snow depths. CATCHMENT generates an hourly snow depth estimate that was aggregated up to a daily average.

CATCHMENT is forced by meteorological fields derived from NASA's Modern-Era Retrospective Analysis for Research and Applications-Version 2 (MERRA-2) product (Gelaro, et al., 2017) (Reichle, et al., 2017) (Development of the GEOS-5 atmospheric general circulation model: evolution from MERRA to MERRA2, 2015). MERRA-2 is a reanalysis product that aims to represent various physical processes and simulate a climate system on a global scale (Gelaro, et al., 2017). Output is produced at 1-hour intervals with a ½ degrees latitude (about 55.5 km) x 2/3 degrees longitude x 72 vertical level model configuration extending through the stratosphere (MERRA: NASA's Modern-Era Retrospective Analysis for Research and Applications, 2011). As opposed to MERRA-1, MERRA-2 incorporates advancements in meteorological assimilation by assimilating modern hyperspectral radiance microwave observations along with radio

occultation datasets. The reanalysis product also integrates post-2005 NASA ozone and space-based aerosol observations and includes advances in both the Global Earth Observing System (GEOS)-5 model and the Gridpoint Statistical Interpolation (GSI) assimilation system (Gelaro, et al., 2017).

Method 2 ROS detection uses MERRA-2 hourly air temperature and NOAA Climate Prediction Center Unified Gauge-Based Analysis of Global Daily Precipitation (CPCU)-corrected precipitation estimates as the meteorological boundary conditions to CATCHMENT. Temperature and precipitation values are aggregated up to a daily average in the CATCHMENT and used as forcings to derive a snow depth. MERRA-2 output is also regrided within the CATCHMENT to the EASE-Grid 2.0.

Numerous versions of Method 2 were generated where each version sets specific threshold values that must be met and/or exceeded for four different state variables; 1) current day daily-averaged snow depth, 2) previous day daily-averaged snow depth, 3) current day daily-averaged air temperature, and 4) current day daily-averaged precipitation. If all four thresholds were met and/or exceeded, the grid cell was considered to have had an ROS event. Note that two-thirds of the thresholds are derived from MERRA-2 forcings. Precipitation amount is indicated, and the form of precipitation is inferred from the air temperature estimates. CATCHMENT daily aggregated values are from 00:00-23:59 local time.

Thresholds were adjusted for each version of Method 2 based on the total number and spatial distribution of ROS events detected. Some versions included thresholds based on recorded observations, ground station measurements, and model estimates of regions where the three known ROS events occurred. CATCHMENT output used for ROS detection in Method 2 was already on the global EASE-Grid 2.0 grid cell.

2.2.3 Method 3: ROS Detection using In-situ Measurements

Method 3 uses ground station measurements from National Oceanic and Atmospheric Administration (NOAA)'s Global Summary of the Day (GSOD) dataset to detect ROS events. Data were obtained from https://data.noaa.gov/dataset/global-surface-summary-of-the-day-gsod. The data is derived from The Integrated Surface Hourly (ISH) dataset. During some periods, data may be unavailable due to data restrictions, communication problems, or equipment issues. See Chapter 1 for a more in-depth discussion of the obstacles that current polar-region ground stations experience. A minimum of four observations taken daily from the station is required for data to be reported. Deviations from the initially recorded value can also occur due rounding errors when the data are converted to constant units (e.g., 8.9 instead of 9). Mean values are based on hours of operation for the station and daily extremes and totals for precipitation and snow depth are reported only if station is reporting data succinctly to provide a valid value. Variables used in ROS detection were either a daily averaged mean air temperature or a maximum hourly temperature of the day in addition to a daily-averaged snow depth and daily-averaged precipitation. Precipitation type is not specified in the GSOD Network. Instead it is inferred from the recorded air temperatures; hence, precipitation at sub-freezing temperatures was considered to be snow. Conditional statements were created similar to Method 2 where a certain threshold had to be met or exceeded, and thresholds varied depending upon the particular version.

Figure 2.2 shows the global distribution of the NOAA GSOD network. Note the lack of coverage in high latitude polar regions. GSOD stations were regrided onto the global EASE-Grid 2.0 Grid using the Euclidean distance equation, used in Method 1 and described above (see Equation 6). Each station was assigned to the EASE-Grid 2.0 grid cell with the closest grid cell

center to the station's latitude and longitude coordinates. At times, more than one station was placed within the same grid cell. Only one ground station within the 25 km x 25 km grid cell needed to detect an ROS event in order for the whole grid cell to be labeled as an ROS event occurring. Therefore, it was assumed that entire grid cell experienced an ROS event, even though, in reality, the ROS event could have been localized to the region just where the ground station was located.

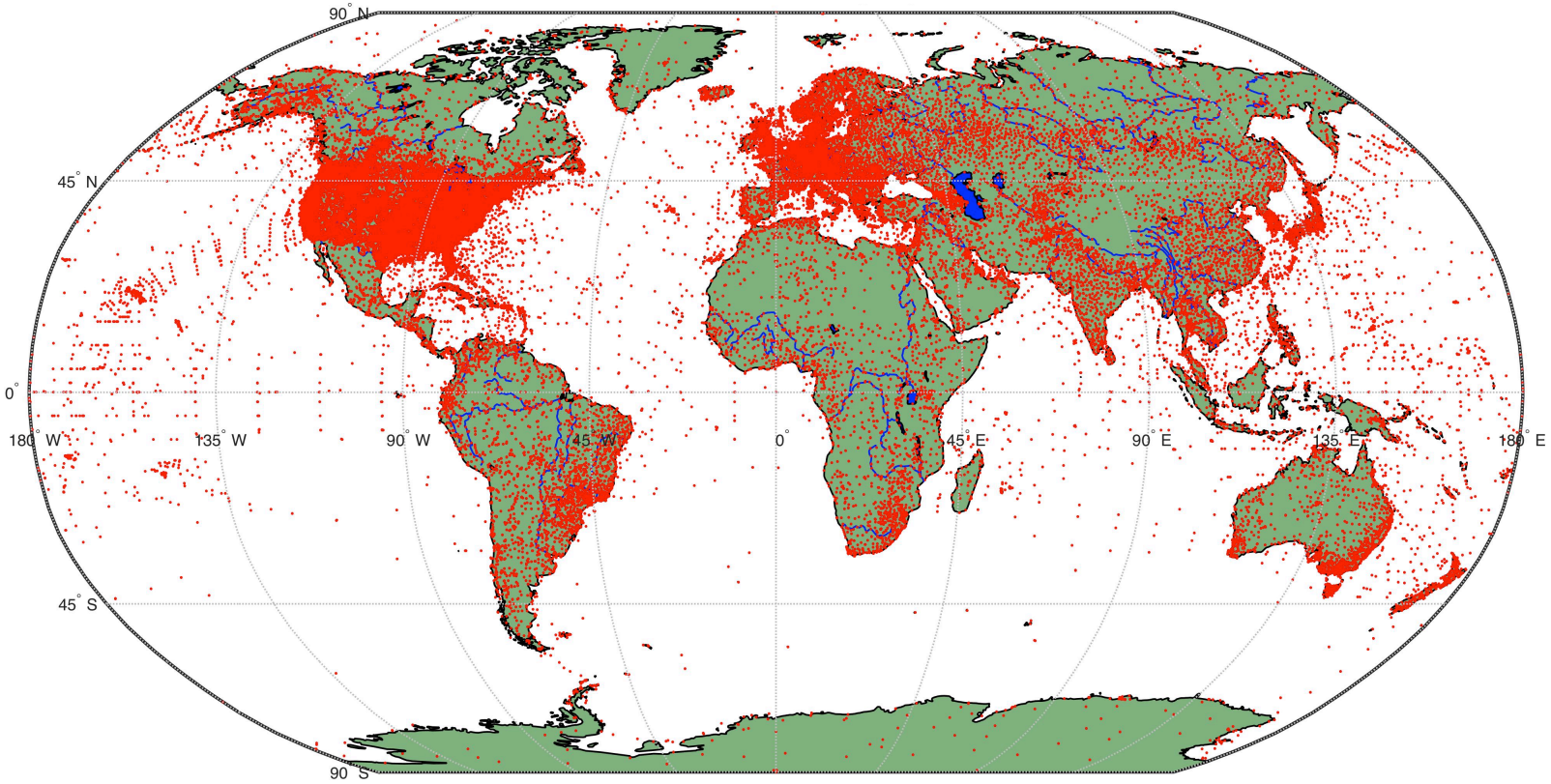

Figure 2.2. Global distribution of the National Oceanic and Atmospheric Administration Global Summary of the Day (GSOD) network. Note the lack of coverage in high-latitude regions

2.2.4 Method 4: ROS Detection using Multiple Data Types

The combined method (Method 4) involved using a version from each of the three previous methods (Methods 1-3) in order to generate a database of ROS events that were detected by two or more methods. The ROS events that were detected by multiple methods were then further studied in Objective B, which investigated the impact that ROS events have on $SWE_{AMSR\text{-}E}$. The approach in Method 4 was created to focus on the number of ROS events considered in Objective B. Table 2.1 summarizes the particular variables and datasets used for each of the four methods to detect ROS events.

Table 2.1. Summary of ROS Detection Methods

Method	Type	Variables	Dataset(s)
1	**Satellite Observations**	Brightness Temperatures: 18.7, 23.8, 36.5, and 89 GHz	NSIDC AMSR-E/Aqua Daily L3 12.5 km Tb, Sea Ice Concentration, and Snow Depth Polar Grids (Cavalieri, et al., 2014).
2	**Model Estimates**	Daily averaged MERRA-2 air temperature and precipitation CATCHMENT estimated daily-averaged snow depth	Catchment land surface model (CATCHMENT) using Modern-Era Retrospective Analysis for Research and Applications, Version 2 (MERRA-2) forcings (A catchment-based approach to modeling land surface processes in a general circulation model 1. Model Structure, 2000) (Reichle, et al., 2017) (Gelaro, et al., 2017) (Development of the GEOS-5 atmospheric general circulation model: evolution from MERRA to MERRA2, 2015)
3	**Ground Station Measurements**	Hourly maximum or mean air temperature Daily averaged precipitation and snow depth	NOAA's Global Surface Summary of the Day (GSOD) ground-based weather station network
4	**Combined**	Combination of the detected output of above Methods 1-3	-

2.3 Methods for Analyzing Impact of ROS Events on SWE_{AMSR-E}

The National Snow and Ice Center (NSIDC) AMSR-E/Aqua L3 Global SWE EASE- product (Kelly, 2009; Tedesco, et al., 2004) was used to observe the impact ROS events may have on SWE_{AMSR-E} estimation. First, a literature review of the three known ROS events was conducted, and any information about the event was summarized, including local observations of the event and any in-situ measurements. CATCHMENT estimates along with any available GSOD station data of snow depth, air temperature, and precipitation were examined for the

affected region. With consideration of all available information, an expected SWE time series was created and then compared to the $SWE_{AMSR\text{-}E}$ to investigate if $SWE_{AMSR\text{-}E}$ during a known ROS event roughly agreed with known information about the ROS event.

ROS events detected using Method 4 were regionally grouped if, for a given day, grid cells adjacent to one another detected ROS events. Eight possible adjacent grid cells, including the corner cells (see Figure 2.3), were available for a given detected grid cell. All detected grid cells that were adjacent to one another were domain averaged in order to calculate one given daily $SWE_{AMSR\text{-}E}$ estimate for that region. Once ROS events were grouped regionally, any ROS events detected in the same region for more than one consecutive day were eliminated. ROS events occurring over multiple days could not be used because daily changes in $SWE_{AMSR\text{-}E}$ were compared among ROS events.

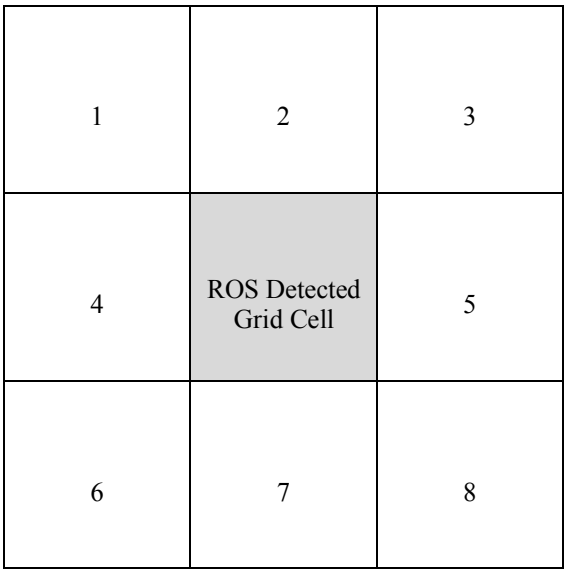

Figure 2.3. Diagram of surrounding adjacent cells to an ROS detected cell

For each of the ROS events (known or detected in Method 4) a time series of daily change in domain-averaged $SWE_{AMSR\text{-}E}$ before, during, and after an ROS event was calculated.

Each time series was then reviewed and compared to that of other ROS events to uncover any patterns in $SWE_{AMSR\text{-}E}$ estimate fluctuations over a suspected ROS event.

2.3.1 Methods for Factor Analysis: Impact of ROS Event Characteristics on SWE_{AMSR-E}

Further investigations were then conducted to determine if patterns in daily changes to SWE_{AMSR-E} depended on any of the four different factors (i-iv);

(i) The region where an ROS event occurred.

For regional factor analysis, six separate regions were delineated by the distribution of all the ROS events detected in Method 4.

(ii) The timing in winter season.

Factor analysis related to the timing in the winter season grouped ROS events into three winter periods: 1) Beginning: October-November, 2) Middle: December-February, and 3) End: March-April.

(iii) The duration of the ROS event.

Since all analyses conducted were only with ROS events occurring over one day, a factor analysis grouping of ROS events that occurred over multiple days was conducted to determine if snowpack's with longer duration ROS events (over one day) had similar daily SWE_{AMSR-E} fluctuations.

(iv) The amount of snow depth estimated around the time of the event.

With the snow depth factor analysis, for each ROS event detected using Method 4, a domain-averaged, CATCHMENT-based snow depth for the day preceding each ROS event was calculated and then all ROS events were separated into four different groups based on snow depth magnitude.

Analyses i-iv are referred to as the factor analysis and involved dividing the ROS events into different groups. For each of the four (i-iv) factor analyses previously described, daily

changes in SWE_{AMSR-E} estimates for each group were calculated to determine if any patterns emerged in a particular group. Patterns could suggest that time series should be separated according to a particular factor in order to further understand when SWE_{AMSR-E} might be most impacted by ROS events.

2.3.2 Methods for Quantifying ROS Impact on SWE_{AMSR-E}

Plotting daily time series of SWE_{AMSR-E} for each ROS event can provide a visual clue of if/how ROS events impact such retrieval. More specifically, the daily change in SWE_{AMSR-E} can help quantify the impact and provide a means for comparing among numerous ROS events. Additionally, the percentage of regionally averaged cells that had an increase, decrease, or no change in SWE_{AMSR-E} were calculated for the day preceding the ROS event, the day of the ROS event, and two days following the ROS event. These percentages (either positive, negative, or neutral) were compared between versions in Method 4 and the three known ROS events (see Figure 2.1) to ultimately ascertain the general patterns that occurred in local fluctuations in SWE_{AMSR-E}.

Chapter 3: ROS Detection Results

3.1 Introduction

According to the National Snow and Ice Data Center (NSIDC) land-sea-ice mask, mapped on the Equal-Area Scalable Earth (EASE)-2 Grid, approximately 49.6% of all grid cells north of the 60th parallel are characterized as water and approximately 5.8% as ice. Consequently, approximately 44.6% of all grid cells north of the 60th parallel were possible locations for ROS detection. As mentioned in Chapter 2, the Greenland ice sheet was masked from the study, with the exception of a few coastal areas. Chapter 3 describes and discusses the results generated from each ROS detection method.

3.2 Method 1: ROS Detection using Satellite Observations

Method 1 (see description above in Chapter 2), detected ROS events based entirely on satellite-derived passive microwave observations. Method 1 detected all three known ROS events, with a few slight exceptions. For the Daring Lake ROS event, and detected an ROS liquid layer developing (i.e., an ROS event) on 9 April 2007, which was the day after the ROS event actually occurred. Similarly, the detected southern Yamal Peninsula ROS event had the largest number of grid cells with detection on 8 November 2006, which was one day after the ROS event was known to end. These details do not necessary suggest inaccuracy of the Method 1, but rather could be a result of the timing in which the ROS event took place relative to the collection of AMSR-E observations used in Method 1. Although AMSR-E sensor passes over a given polar region about twice daily, the ROS event could have occurred after the second pass of

the day or had been relatively small up to that point, and therefore, was not observed (and thus detected) until the next day.

After the Method 1 output was regrided onto the EASE-Grid 2.0, approximately 77.3% of all land-based (excluding ice sheets and glaciers) grid cells could be used for detection using the algorithm. The gray areas (excluding the Greenland ice sheet) in Figure 3.8 show the remaining 22.7% of grid cells that were unable to detect an ROS event with the regridding technique used. The issue is exclusively a result of the regridding technique used where algorithm values were regrided from a polar grid to a global grid. In the future, a similar analysis could be conducted using a polar grid (rather than a global grid) in order to minimize the data gaps but was not done in order to maintain a tractable project scope.

Figure 3.1 shows the regional distribution of all ROS events detected using Method 1over the nine-year period. A majority of the detection occurred in Iceland, Quebec, Newfoundland and Labrador regions of Canada, as well as along the northwestern coast of Russia. Approximately 37.5% of all land (excluding ice sheets and glaciers) classified grid cells detected ROS events above the 60^{th} parallel.

The total number of grid cells detecting an ROS event was calculated for each day of the winter season over the entire nine-year period and plotted in Figure 3.2. The gray bars indicate that there was no algorithm output for two winter seasons: 2004-2005 and 2008-2009. The 2006-2007 winter season contained the highest daily value of 290 grid cells detecting ROS events on a single day. Method 1 suggests an ROS event if the BIM ROS detection algorithm detects a liquid layer within the snowpack based on changes in specific microwave frequencies. Therefore, a detected ROS event could be a melting event rather than a precipitation-related event. Such a false positive could be one reason for the relatively large number of detected ROS events.

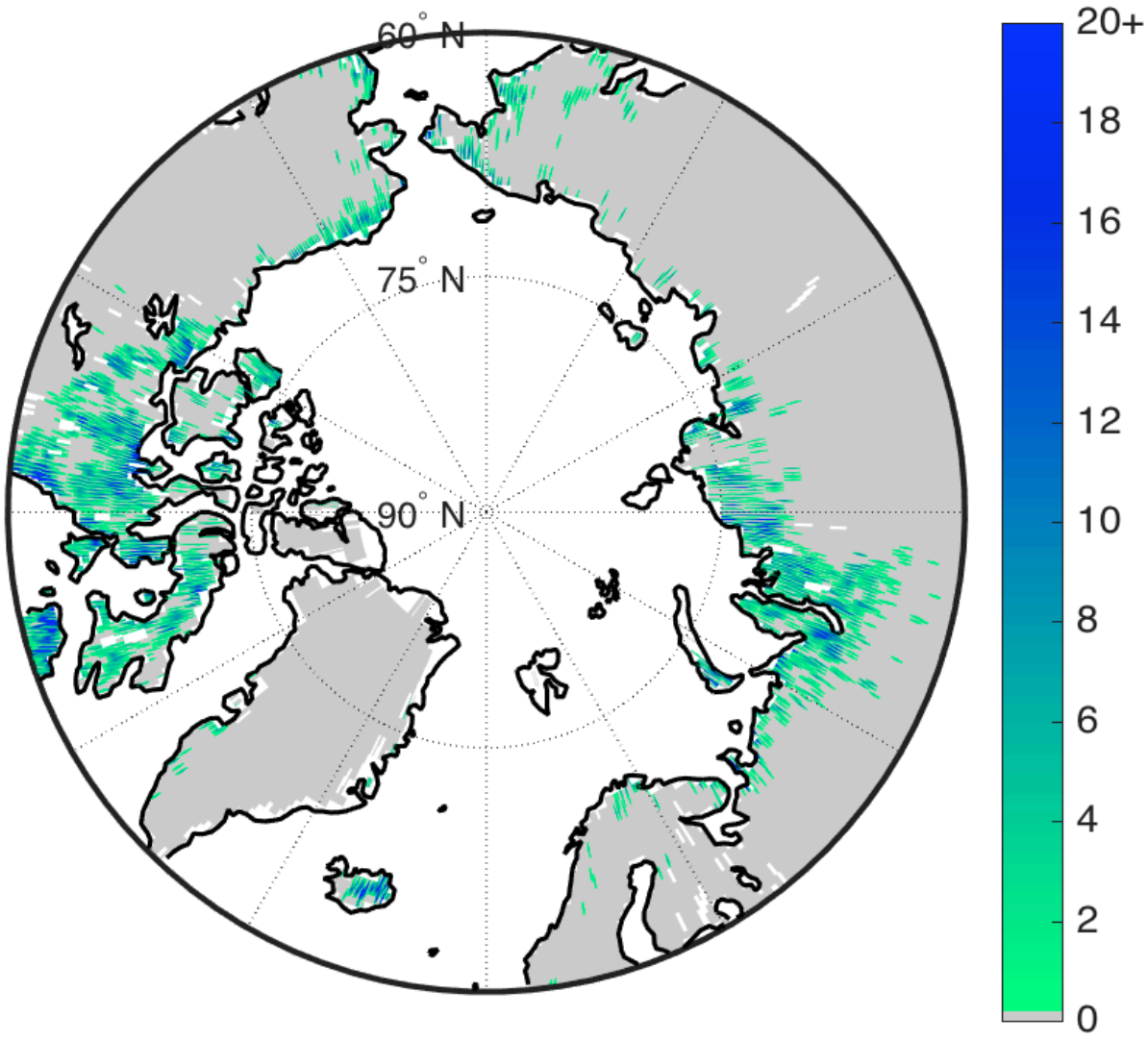

Figure 3.1. Regional distribution of all ROS events detected in Method over the nine-year period. The color bar indicates the frequency of events within a particular 25 km x 25 km grid cell.

Based on the observed Method 1 output, a trend in the frequency of detected ROS events over the nine-year period was not evident, which is a conclusion not supported by current literature. Although it is important to note that two winter seasons were missing, and a substantial amount of area was not covered, therefore the determination that Method 1 ROS events have no clear trend does not have strong standing. Figure 3.11 plots the cumulative number of grid cells with ROS events for each day of the winter season over the nine-year study

period. Figure 3.11 shows a peak in ROS events in the middle of the winter season during the month of February, reaching a peak of 400 detected grid cells. One could hypothesize more ROS events at the beginning and/or the end of the winter season when air temperature fluctuations near the freezing point are more likely to occur. However, most snow-cover occurs in the middle of the winter season, which may be the reason for the increase.

The average CATCHMENT estimated snow depth for all Method 1 ROS events was about 0.47 m. The atmospheric reanalysis (MERRA-2) that provided the boundary conditions to CATCHMENT estimated an average air temperature of approximately 265 K and 1.6 mm of precipitation for all the ROS events detected. Three histograms in Figure 3.3 show the frequency of MERRA-2 daily-averaged near-surface air temperature and precipitation in addition to the CATCHMENT estimated daily-averaged snow depth for all Method 1 detected ROS events. A majority of the detected grid cells (98%) fall below the freezing point, according to MERRA-2 near-surface air temperatures. MERRA-2 daily-averaged precipitation values were quite low with about 51% of all detected grid cells in a range between 0 and 0.08 mm. With almost all of the MERRA-2 air temperatures estimated below freezing, one can foresee issues when comparing Method 1 output to Method 2 detected ROS events. CATCHMENT estimated daily-averaged snow depth on the day of the detected ROS event had a fairly large range from slightly above 0.0193 m to 2.2 m. Figure 3.3 is instrumental in showing the large differences between output using satellite observations and model estimates. Overall, CATCHMENT estimates do not agree with Method 1 detected ROS events because low daily-averaged precipitation amounts, and daily-averaged near-surface air temperatures were estimated on the day of detected ROS events.

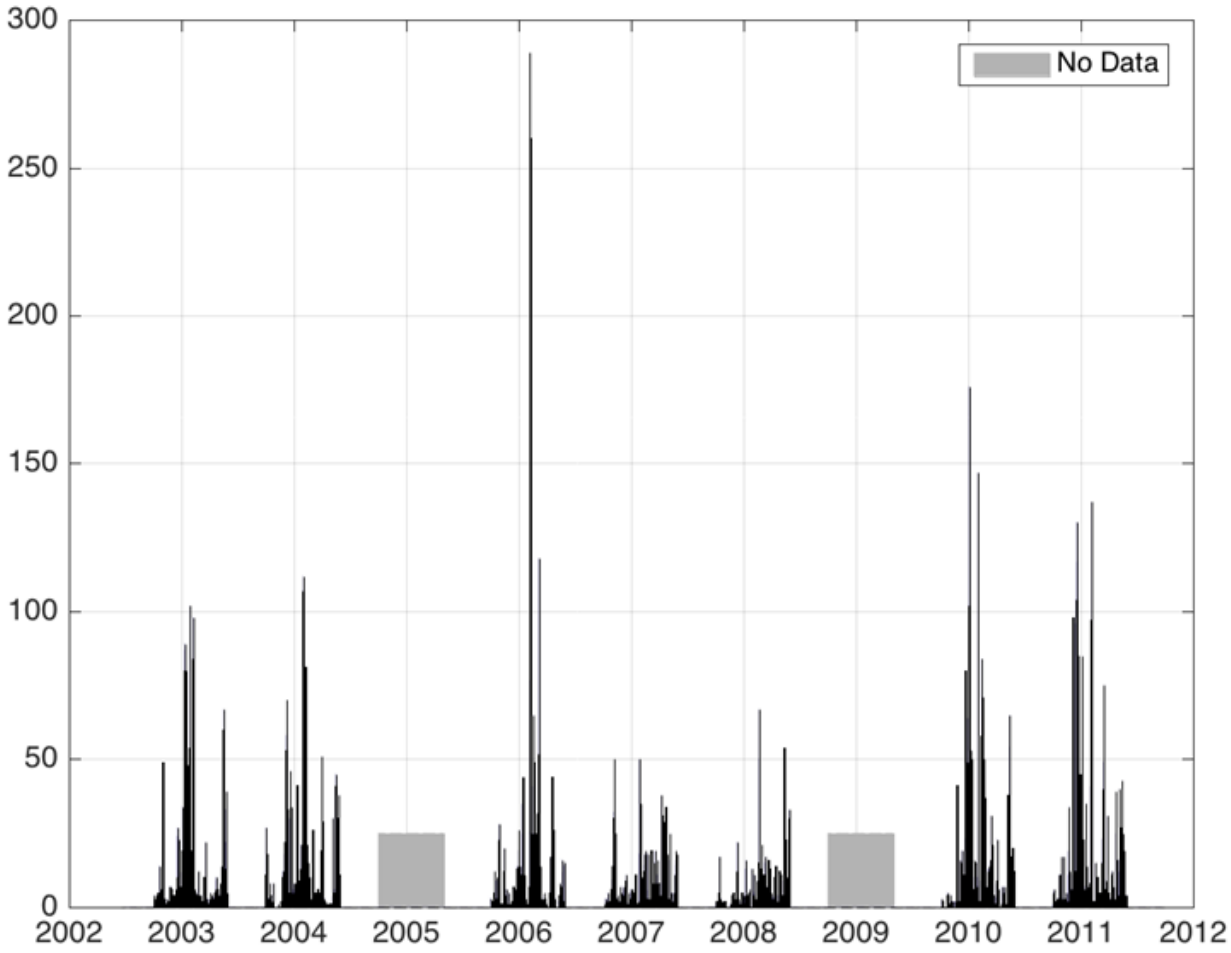

Figure 3.2. The total number grid cells with a Method 1 ROS detection calculated for each day over the nine-year study period. The gray bars indicate two winter seasons where there was no algorithm output. The months of May through September are excluded from the analysis.

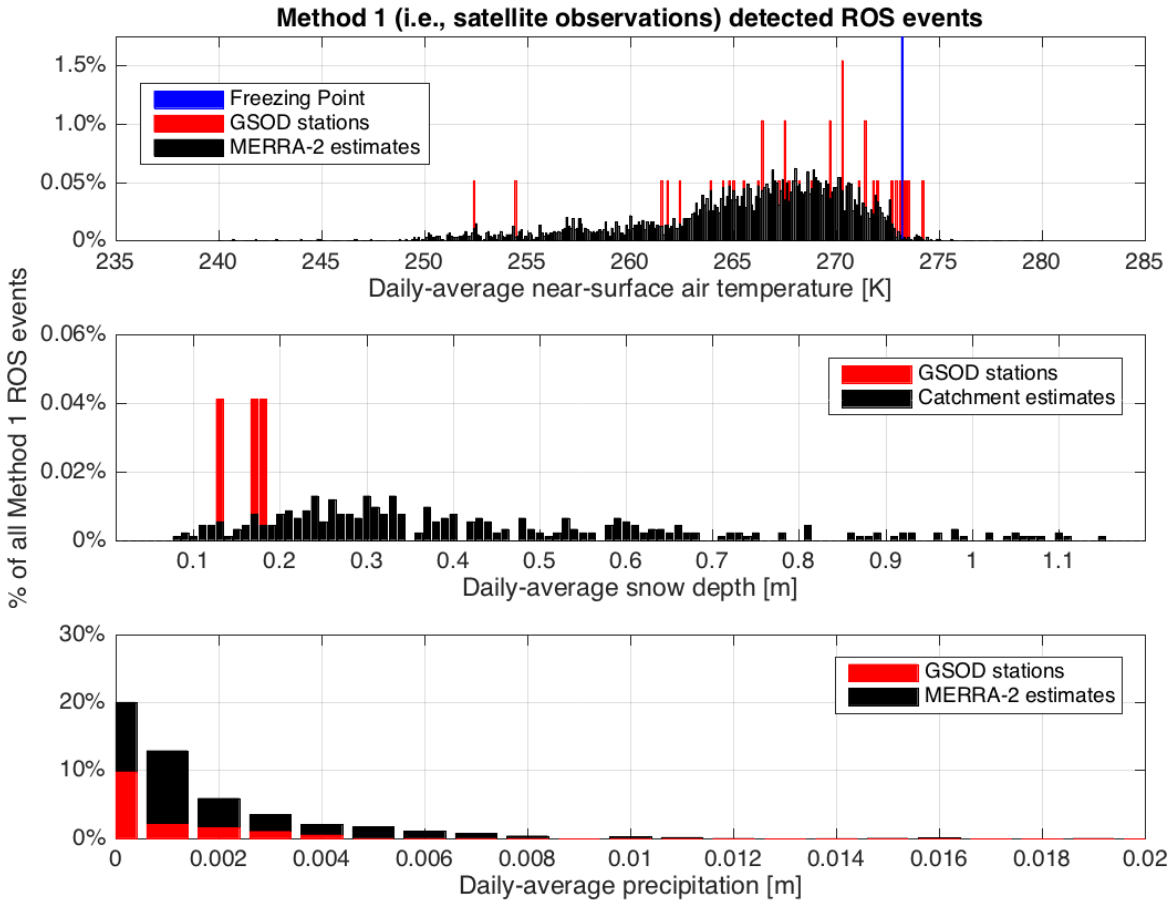

Figure 3.3. Three histograms presenting the frequency of Method 1 ROS detected grid cells for MERRA-2 daily-averaged air temperature and precipitation, CATCHMENT daily-averaged estimated snow depth, in addition to the NOAA GSOD ground station daily-averaged near-surface air temperature, daily-averaged precipitation and daily-averaged snow depth measurements.

Using the National Oceanic and Atmospheric Association (NOAA) Global Summary of the Day (GSOD) database, the average snow depth of all Method 1 detected grid cells that contained a station with available data was approximately 0.266 m. The average daily near-surface air temperature was approximately 268 K with a daily average precipitation of about 0.6 mm. Similar to the observations seen in Figure 3.3, the GSOD network also suggests low daily-averaged surface air temperatures and little daily-averaged precipitation for the detected events in Method 1. Such findings also foreshadow disagreement between Method 1 and Method 3

where daily-averaged near-surface air temperatures were well below freezing with little or no recorded daily-averaged precipitation.

3.3 Method 2: ROS Detection using Model Estimates

Method 2 ROS detection used the estimates of an atmospheric re-analysis tool (MERRA-2) in addition to estimates from a land surface model (CATCHMENT). The method was composed of four conditional statements;

(1) Previous day CATCHMENT daily-averaged estimated snow depth ≥ predefined threshold value.

(2) Current day CATCHMENT daily-averaged estimated snow depth ≥ predefined threshold value.

(3) MERRA-2 daily-averaged near-surface air temperature ≥ predefined threshold value.

(4) MERRA-2 daily-averaged precipitation ≥ predefined threshold value.

Two different versions of Method 2 (i.e., Method 2a and Method 2b) were generated. Each version used a different threshold for the conditional statements, which are summarized in Table 3.1. The values used in Method 2b were determined from recorded snow depths and air temperatures of the three known ROS events.

Table 3.1. Description of Thresholds used for Method 2 (i.e., model estimate-based) ROS Detection

Version	Previous and Current Day Snow Depth [m]	Current Day Total Precipitation [m]	Current Day Air Temperature [K]
2a	> 0	> 0	≥ 273.15
2b	≥ 0.0127	≥ 0.1524	≥ 273.15

Method 2a detected the tail end of the Banks Island ROS event. However, neither version (2a or 2b) detected the southern Yamal Peninsula or Daring Lake ROS events. Further investigation revealed that although sufficient snow depth and precipitation was detected, air temperature estimates were too far below freezing to warrant an ROS detection based on the established thresholds.

Method 2a detected approximately 76.7% of all ice-free, land-classified grid cells possible for ROS detection. Alternatively, Method 2b detected approximately 13.1% of all grid cells that could potentially detect ROS events, which is illustrated in Figure 3.4. Method 2a spans over almost all of the entire region of interest (excluding parts of eastern Russia) and has nearly six times the number of detected grid cells as compared to Method 2b. Method 2b contains higher thresholds for snow depth and precipitation estimates, and subsequently has a limited distribution that is concentrated mainly in Iceland, Norway, western Russia, Alaska, and Yukon Territory. It is important to note that Figure 3.4 does not show where the highest concentrations of ROS detection occurred. Appendix A provides figures displaying the regional distribution of all ROS events detected using Method 2a and 2b in Figure A.1 and Figure A.2, respectively. Method 2a possessed the highest concentrations of ROS events in the Alaska and Yukon Territories, as well as in Scandinavia. Method 2b ROS detections are more prevalent along the coast of Norway, the southern tip of Greenland, and the southeastern edge of Alaska.

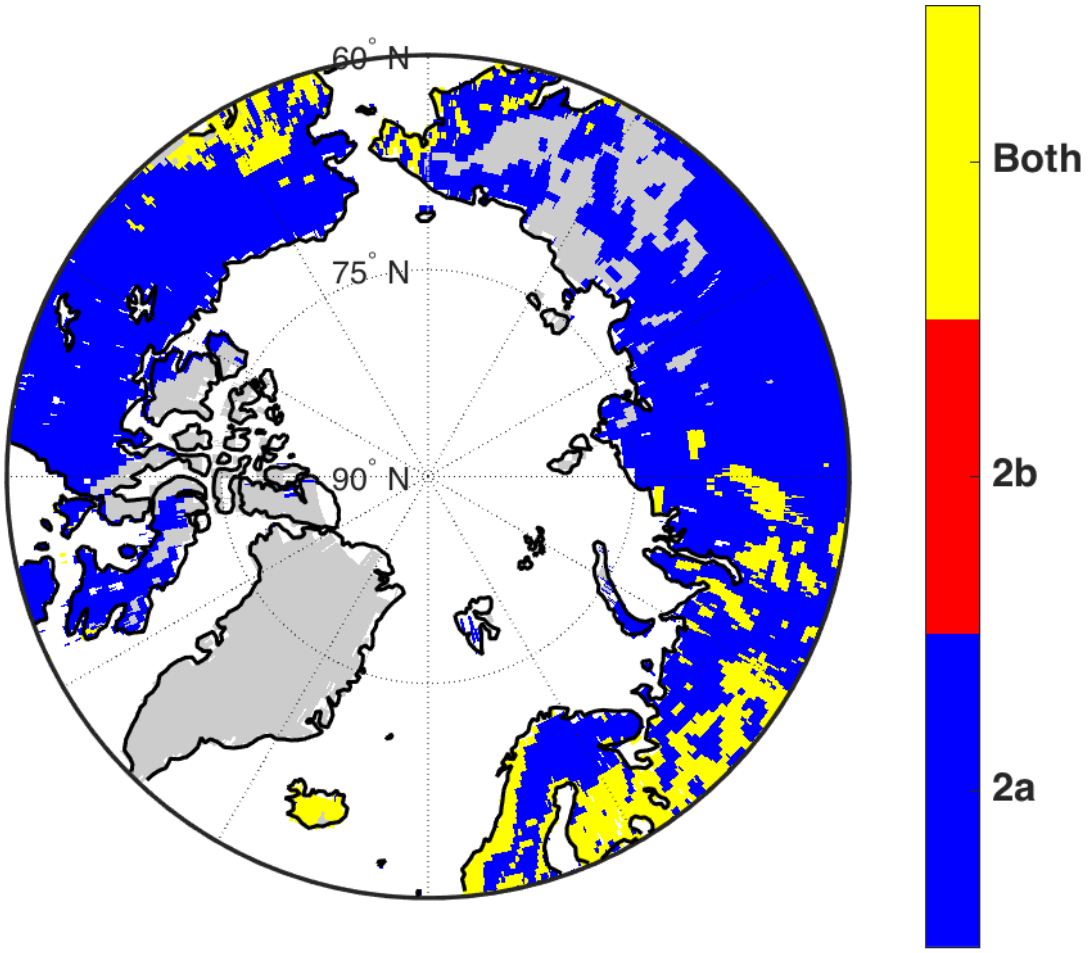

Figure 3.4. Regional distribution of all Method 2 ROS detected grid cells. Map illustrates the vast areas covered by each version (2a and 2b) and the regions in which they overlap. Note that color does not indicate frequency of ROS events, only distribution.

As anticipated the method containing more relaxed bounds, Method 2a, yielded considerably larger numbers of ROS detected grid cells than Method 2b as indicated in Figure 3.5. Comparable to the findings in Method 1, both versions of Method 2 do not reveal any apparent trend in ROS events over the nine-year period. However, a distinct difference between the versions in Method 2 is the distribution of ROS detected grid cells over a given winter. Method 2a detects the largest number of ROS events occurring at the beginning and end of the winter season. Method 2b displays the opposite, peaking in the middle of the winter season when snow cover is at a seasonal maximum, which is a pattern consistent with Method 1 results.

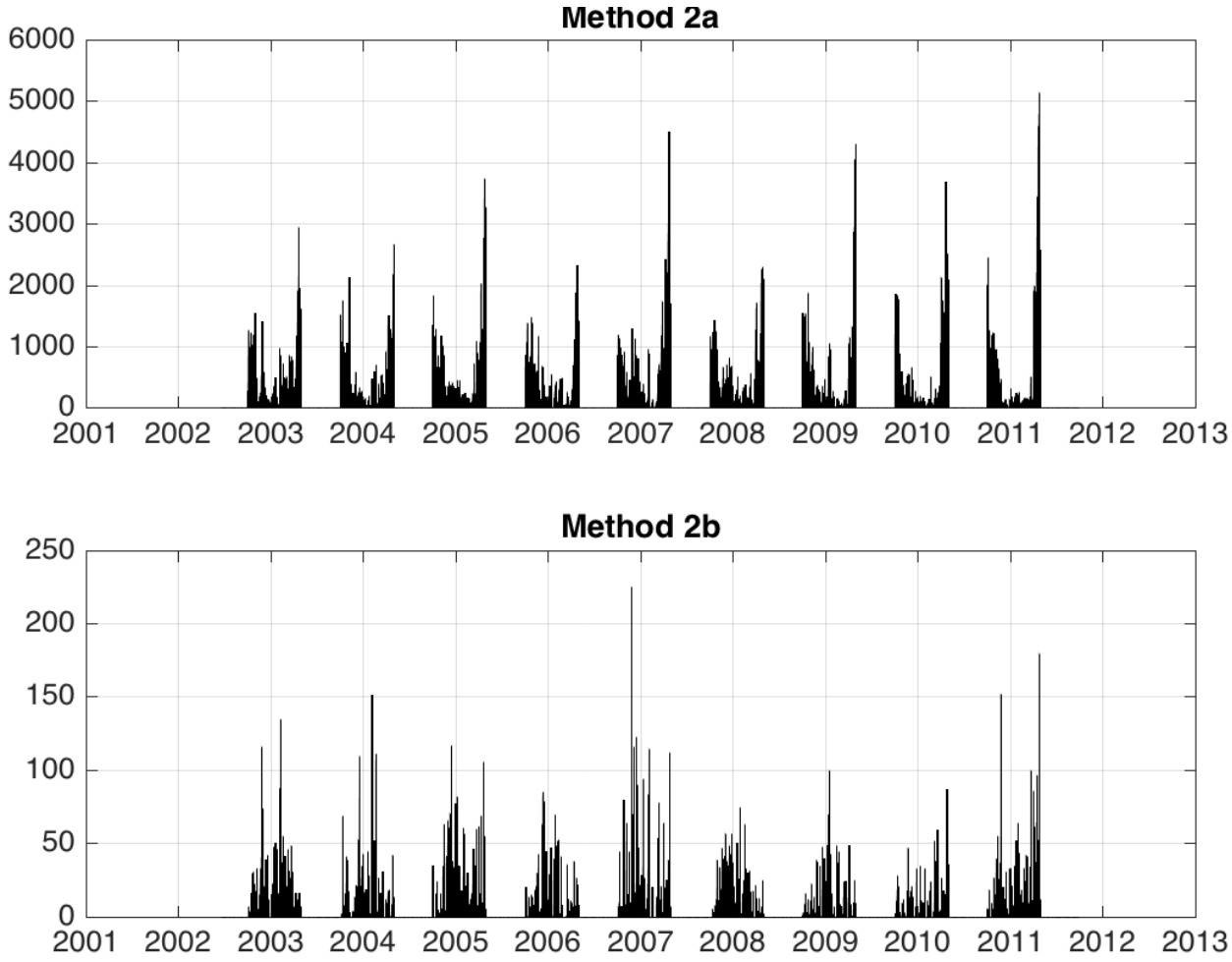

Figure 3.5. The total number grid cells with a Method 2a or 2b ROS detection calculated for each day over the nine-year study period. The months of May through September are excluded from the analysis.

Method 2 ROS detection is beneficial because values can be estimated as often as needed and at better spatial resolutions than satellite observations. Conversely, it is important to note the CATCHMENT model output is largely dictated by the boundary conditions applied to the model. High latitude MERRA-2 air temperatures and precipitation values may be unreliable, which can cause the CATCHMENT to inaccurately estimate state variables and consequently Method 2 to miss an ROS event or detect a false positive ROS event.

3.4 Method 3: ROS Detection using In-situ Measurements

Method 3 only used measurements obtained from the National Oceanic and Atmospheric Administration (NOAA) Global Summary of the Day (GSOD) network, a system of stations that is sparse and unevenly distributed above the 60th parallel. Thresholds for conditional statements varied depending on the two different versions (i.e., Method 3a and Method 3b) the details of which are listed in Table 3.2. Similar to Method 2, the conditional statements use recorded measurements of;

(1) Previous and current day daily-averaged snow depth.

(2) Current day daily-averaged precipitation.

(3) Current day surface air temperature.

Two different surface air temperatures were used (depending on the version): mean daily surface air temperature or maximum daily surface air temperature. The thresholds used in Method 3b for precipitation and snow depth were determined from records of the three known ROS events and are the same as the values used in Method 2b.

Table 3.2. Description of Thresholds used for Method 3 (i.e., in-situ measurements-based) ROS Detection

Version	Previous and Current Day Snow Depth [m]	Current Day Total Precipitation [m]	Current Day Air Temperature [K]
3a	> 0	> 0	Mean Air Temperature ≥ 270.15
3b	≥ 0.0127	≥ 0.1524	Maximum Air Temperature ≥ 273.15K

Neither version in Method 3 detected any of the three known ROS events. The Daring Lake ROS event was not detected in Method 3 because the mean air temperature was in the 258-262 K range, which reflects temperatures that are too low to meet established thresholds. Precipitation and snow depth were both recorded as non-zero. GSOD ground stations in the area

did not record any precipitation for the southern Yamal Peninsula and Banks Island events thereby preventing detection.

Figure 3.6 displays the clustered distribution of all Method 3 ROS detected grid cells. Detected regions were concentrated mainly in Norway, Sweden and Finland. Some were widely dispersed throughout Russia and others clustered together in Alaska. Approximately 282 grid cells were detected to have an ROS event in Method 3a and 130 grid cells in Method 3b. The reduction in ROS detected events from Method 3a to Method 3b is a direct result of the increase in threshold values for both the snow depth and air temperatures in Method 3b. The most overlap between the different versions occurred in Alaska and Norway. Maps illustrating the distribution of ROS event frequency for all Method 3 ROS detected grid cells over the nine-year study period is shown in Appendix A as Figure A. and Figure A.. Both figures show the highest number ROS events occurring in Norway where many ground stations appear to be located. These maps and Figure 3.8 highlight just how sparse the network of ground stations is, in high latitude polar regions, which severely limits the applicability of Method 3 for ROS detection.

Figure 3.7 plots the total number of Method 3 ROS detected grid cells for the entire nine-year period. One can see that Method 3a detects more than ten times the number of ROS events detected in Method 3b, associated with the relaxed thresholds used in Method 3a. Like the two previously described methods, there was no apparent trend in the number of detected ROS events over the nine-year study period. A typical winter time series differs between versions (same as for Method 2), but not to such a large extent. Method 3a tends to peak in detected ROS events at the beginning and end of the season whereas Method 3b peaks in the middle of the snow season in a similar manner as witnessed in Method 1.

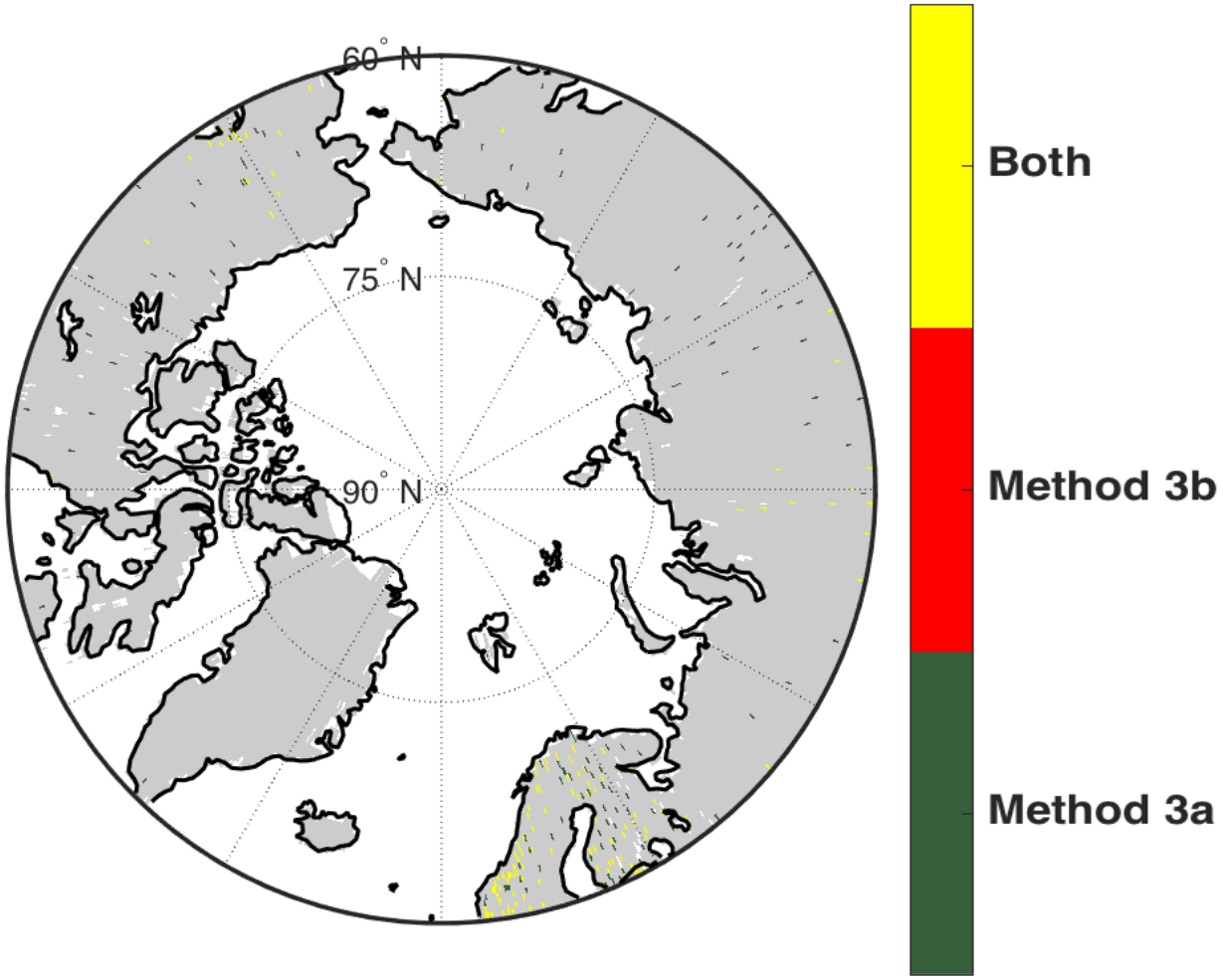

Figure 3.6. Regional distribution of all Method 3 ROS detected grid cells. Map illustrates the concentrated areas covered by each version (Method 3a and Method 3b) and the regions in which they overlap. Note the uneven distribution of the GSOD network in these high latitude regions is reflected in the ROS detection where regions with detection are only in areas where GSOD contain available data. Other areas without stations could have ROS events, but Method 3 would not detect them.

A typical winter time series differs between versions (same as for Method 2), but not to such a large extent. Method 3a tends to peak in detected ROS events at the beginning and end of the season whereas Method 3b peaks in the middle of the snow season in a similar manner as witnessed in Method 1. It appears that the versions detecting sizeable numbers of ROS events tend to have a consistent pattern of peaking in the middle of the winter season when snow cover is at a seasonal maximum.

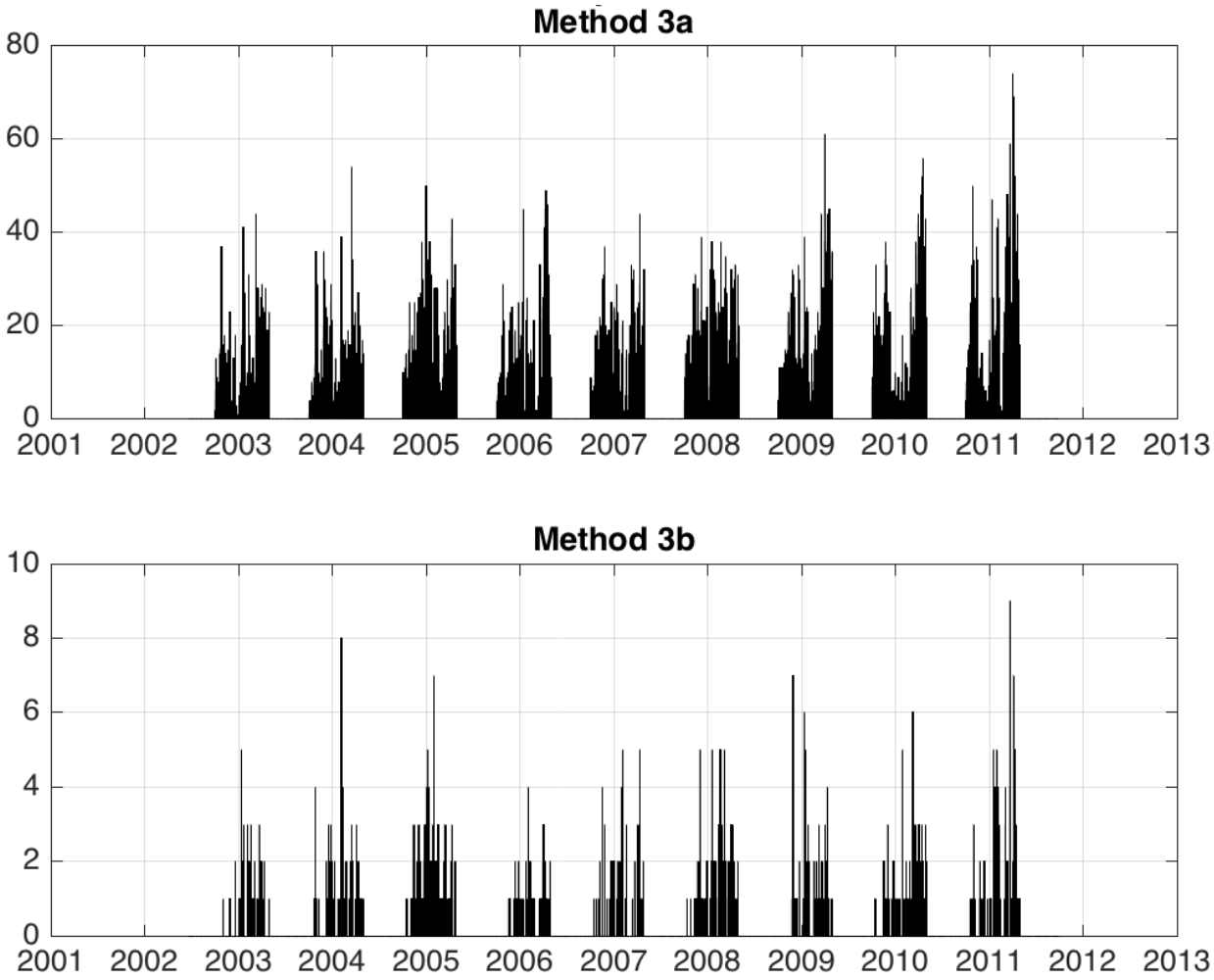

Figure 3.7. The total number grid cells with a Method 3a or 3b ROS detection calculated for each day over the nine-year study period. Notice the different y-axis limits in each of the different subplots. The months of May through September are excluded from the analysis.

The clustering of detected ROS events shown in Figure 3.6 foreshadows the difficulty with merging the output of Method 3 with others as it is highly constricted to grid cells that have stations with available data. The findings from Method 3 detection stress the importance of establishing a more robust ground-based network in polar regions to help better validate model estimates and satellite-based retrievals.

3.5 Method 4: ROS Detection using Multiple Data Types

Method 4 involved comparing the output of Methods 1-3 in order to find any ROS events that were detected in more than one method (i.e., dataset type). Method 4 incorporates one or more dataset types to detect an ROS event, which is advantageous in mitigating the shortcomings of each previously listed method and helps narrow the total number of ROS events detected down to those that most likely occurred, since they were detected using more than one method.

After generating numerous combinations (i.e., versions) of the first three ROS detection methods, there was no agreement among all three methods over the nine-year study period in regions north of the 60th parallel. Bounds of the conditional statements in Methods 2 and 3 were expanded to the greatest extent to find any agreement that still made theoretical sense. Method 1 output remained untouched as only one version was generated. Snow depth and precipitation thresholds were set at any values greater than zero, and air temperatures greater than freezing. Thresholds for air temperature were lowered even further for Method 3 to slightly below freezing. The justification of lowering of air temperatures to slightly below freezing was based on our understanding that rainfall can still occur in sub-freezing temperatures. The estimated or recorded near-surface air temperature may not be representative of the air temperature in the atmosphere above. Air temperatures could be warmer in the atmosphere when precipitation occurs, more conducive to rain, even though the near-surface air temperature is at a sub-freezing range. The lack of agreement between methods is most likely a result of the restrictions with using Method 3 where ROS detection could only occur in grid cells for which there is a ground-based GSOD station with available data (see Figure 3.8). Of the 16,204 stations used in NOAA's GSOD database, only 2.49% had any data available to use for detection in regions north of the 60th parallel. Once gridded onto the EASE-Grid 2.0 grid, only about 1.68% of the grid cells had

the potential for an ROS event to be detected using Method 3. Not only were there few grid cells containing data, but often that data was not available on a consistent daily basis. As a result, Method 3 is believed to be the "weakest link" in the Method 4 theory. When mapped on the same grid as Method 1 and Method 3, only 1.3% of all the total grid cells were eligible to have agreement from both methods, which likely contributed to the general lack of agreement. A further limitation in the agreement between Method 1 and Method 2 or Method 3 was the lack of ROS detection for two winter seasons in Method 1 (2004-2005 and 2008-2009) as a result of missing data.

After concluding that there were no versions of Method 4 that could be produced where Methods 1, 2 and 3 detected an ROS event, the study then considered versions comparing output between just two methods. Table 3.3 contains a summary of the different combinations (i.e., versions) explored.

Table 3.3. Description of each version used in Method 4 ROS Detection

Version	Method 1 version	Method 2 version	Method 3 version	Number of ROS Events
4a	1a	-	3a	1
4b	1a	2a	-	22
4c	-	2b	3b	94

Method 4a compared Method 1 detection (i.e. satellite observations-based) output with Method 3 (i.e. in-situ measurements-based) detection output. Only one ROS event covering one grid cell was found in agreement between the two different methods as shown in Figure 3.10. The ROS event was located in Nunavut Territory, Canada, on 19 December 2010 next to Baker Lake and home to eleven native Inuit groups. On the day of the ROS event, the CATCHMENT estimated approximately 0.33 mm of precipitation and an air temperature of approximately 269 K. The Nunavut Territory appears to have a high number ROS events detected using Method 1,

as shown in Figure 3.1. For Method 4a, the threshold for near-surface daily-averaged air temperature in Method 3 was lowered to 270 K. Method 3a needed to have a low threshold for any agreement with Method 1 to occur. Since the near-surface air temperature was a daily-average, theoretically the temperatures could have spiked higher than 270 K during the precipitation event.

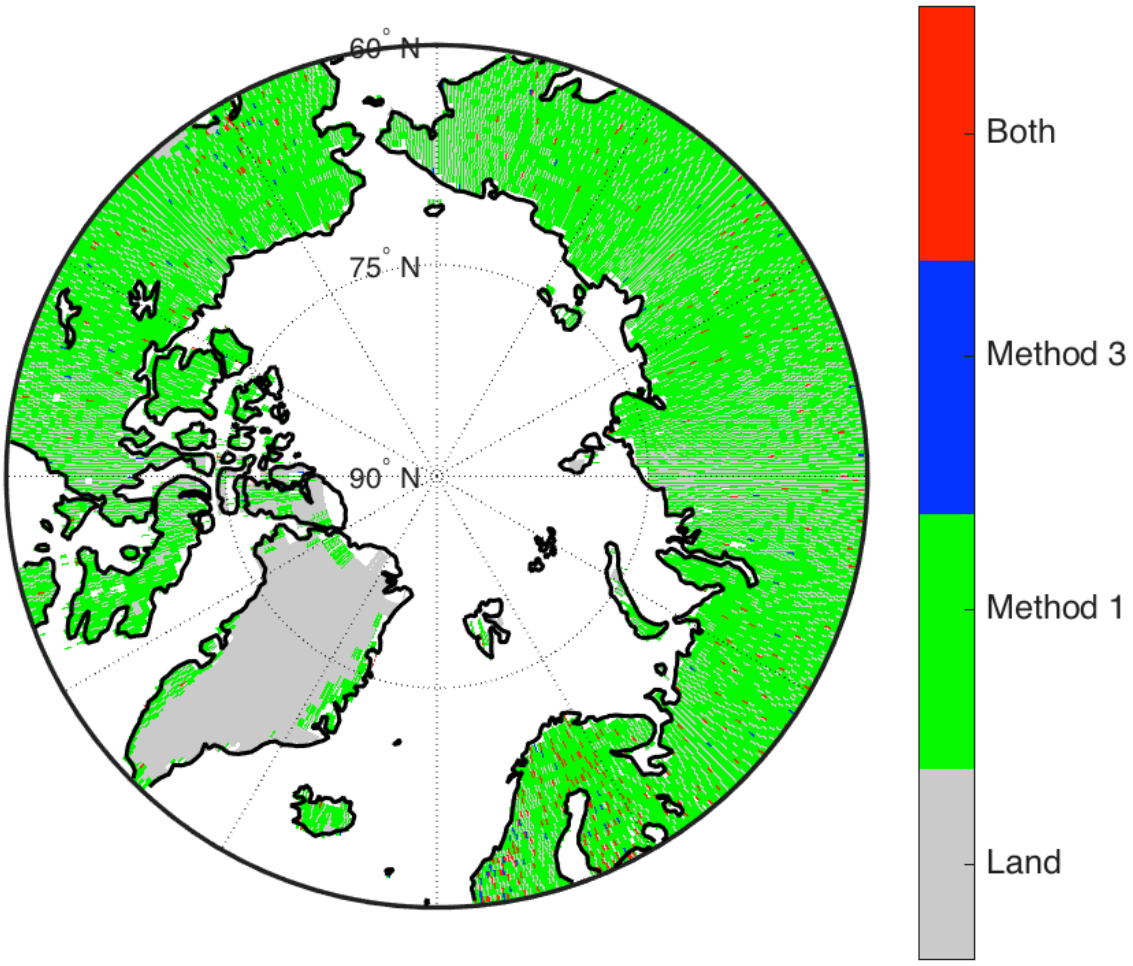

Figure 3.8. Regional distribution of all grid cells that could possibly be detected in Method 1, Method 3 or both. Map illustrates the relatively high concentration of grid cells containing GSOD stations in Northwestern Europe and Yukon Territories. Approximately 1.3% of all grid cells contained GSOD ground stations where both detection could occur (in red) leading to limited agreement between Method 1 and 3.

A second version of Method 4 (Method 4b) was created to investigate the ROS events detected using Methods 1 and 2. Using the most relaxed bounds from Method 2a, only 25 grid

cells over the entire study period were marked or flagged for possible ROS events. These 25 events occurred where the precipitation amount was greater than zero and the daily-averaged air temperature was above freezing, Figure 3.10 shows the regional distribution. The limited agreement between these methods is likely due to the fact that only 0.6% of all the ROS events detected in Method 1 had estimated MERRA-2 air temperatures above freezing, and only about 17.6% were above 270.13 K. A majority of the time, the MERRA-2 forcings used in Method 2 would estimate precipitation, but at air temperatures well below freezing. Perhaps using a model with forcings more conducive to high latitude regions would produce additional overlap between methods. Liquid precipitation can occur in subfreezing temperatures given the right conditions, but such occurrence is relatively rare. Nonetheless, as a result, MERRA-2 precipitation forcings and consequently the CATCHMENT (i.e., Method 2) ROS detection could be incorrect. Figure 3.9 would suggest a decreasing trend in ROS detections over the nine-year study period. However, such a conclusion is not statistically significant due to such a small sample size of 25 events.

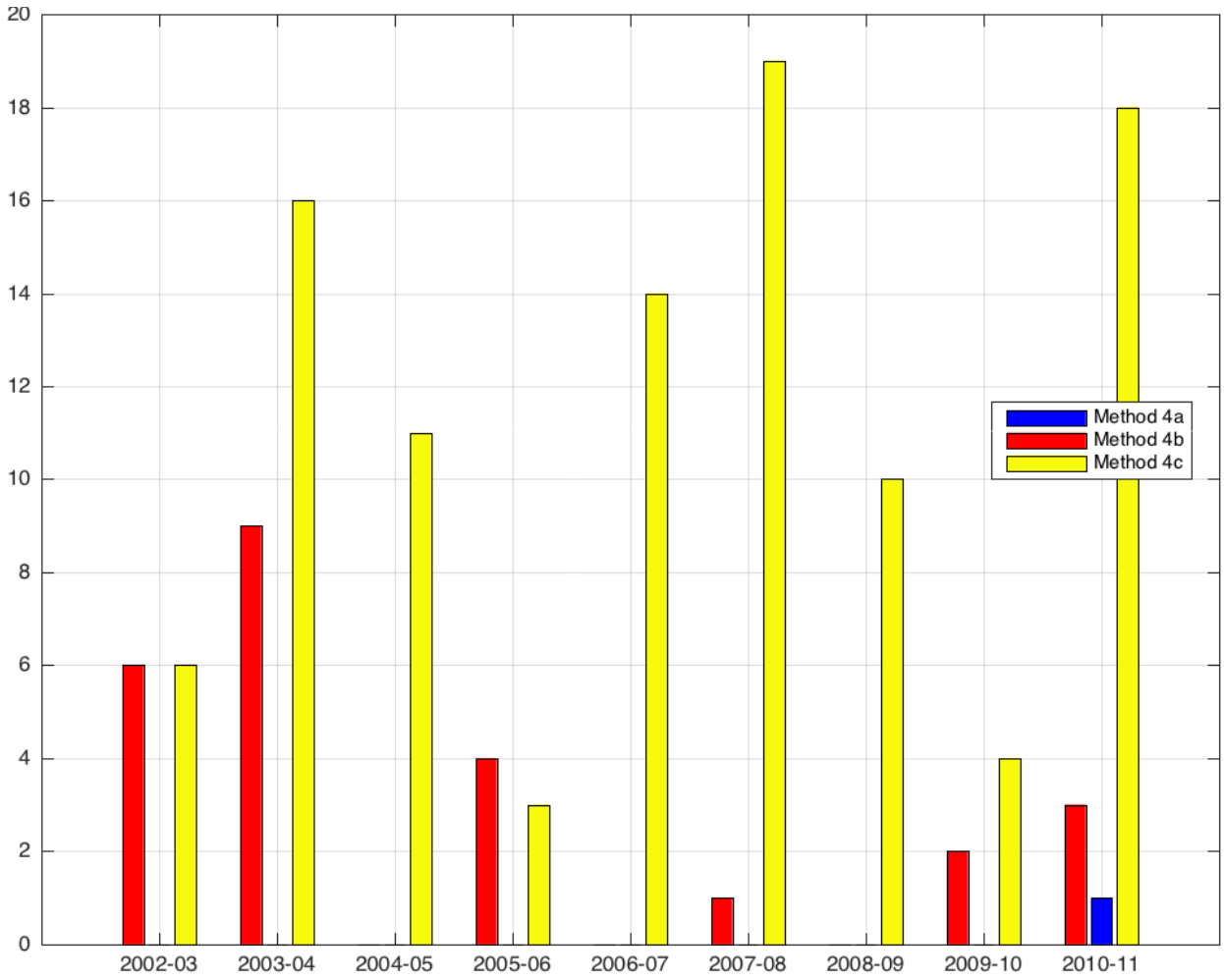

Figure 3.9. Total number of ROS detected grid cells over a winter season (i.e., October-April) for Methods 4a-4c within the nine-year study period.

Finally, a third version (Method 4c) was created to look at ROS events detected using versions from Methods 2 and 3. Method 4c detected 101 grid cells with ROS events (see Figure 3.10). Address the total number of ROS events detected over the nine years and distribution. Figure 3.9 does not show any trend on frequency of ROS events over the nine-year period, similar to the conclusions made in Methods 1-3.

Figure 3.10 shows the global distribution of all ROS events detected over the nine-year time period for the versions used in Method 4. Note how different versions of Method 4 (Method 4a - Method 4c) detect ROS events in different regions of the northern hemisphere. Method 4a is

heavily isolated from any other detected events in Method 4. Method 4b detects ROS events mainly in Greenland, Russia and Northern Alaska. Method 4c is more concentrated in Norway and southeastern Alaska.

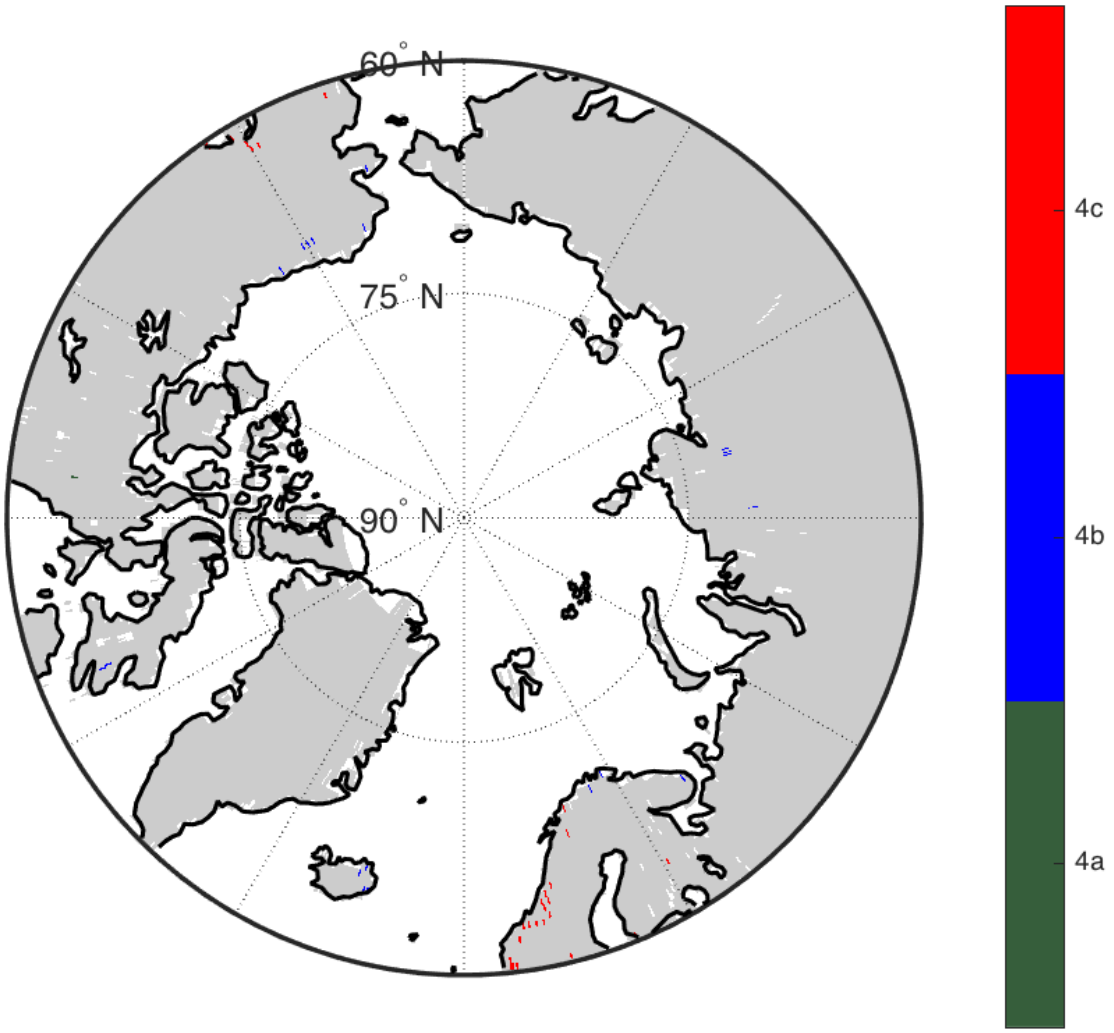

Figure 3.10. Regional Distribution of all grid cells detected over the nine-year study period for Methods 4a-4c.

The final analysis conducted in Objective A was to look at the average number of ROS events detected over a winter season as illustrated in Figure 3.11. Method 4b and 4c show similar patterns to Methods 2 and 3 where the version with the larger number of detected events

has the highest frequency at the beginning and end of the winter seasons. Method 4c peaks in February, similar to Method 1.

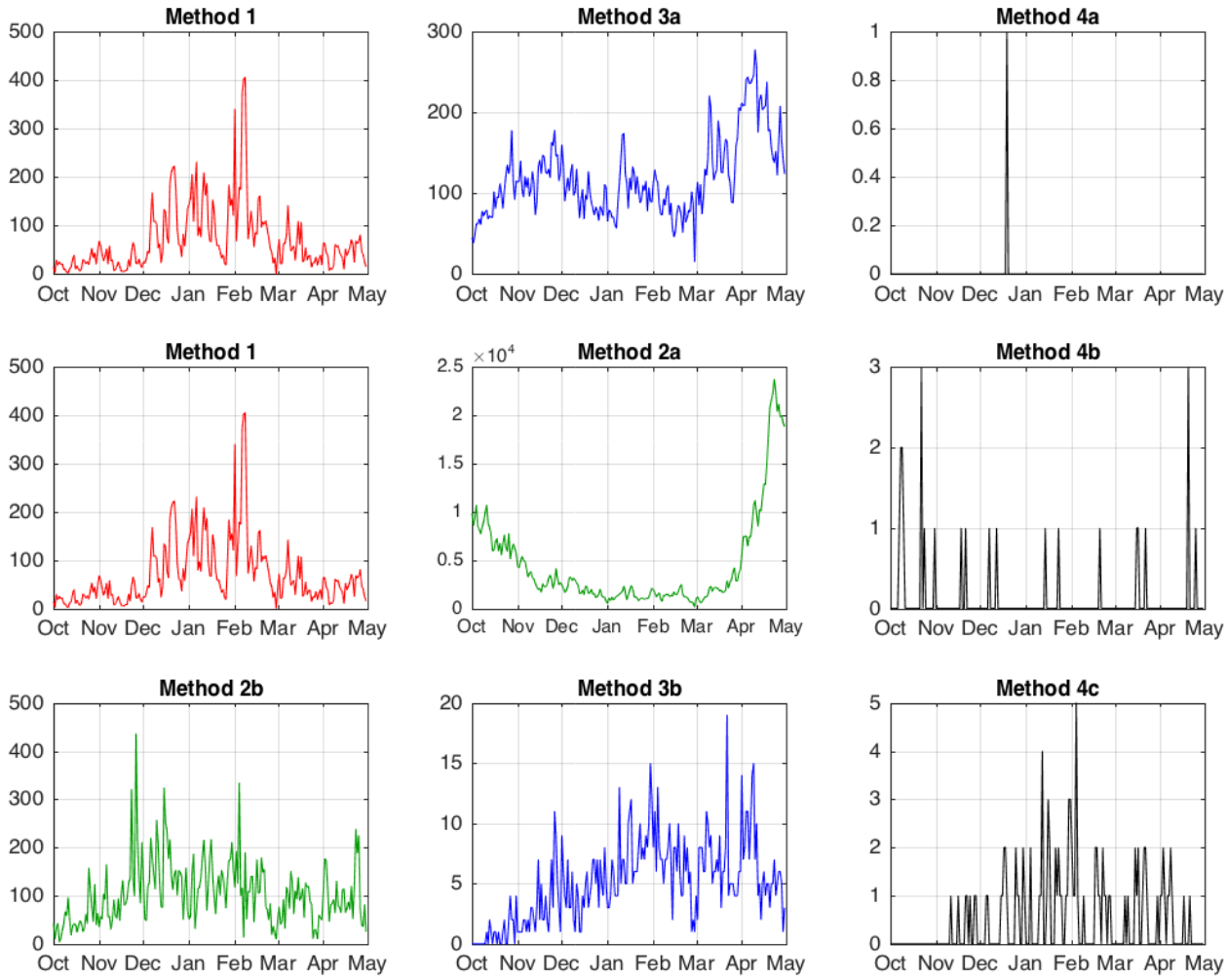

Figure 3.11. Total number of ROS detected grid cells over a winter season (i.e., October-April) over the nine-year time period. Method 1: ROS detection using satellite observations only. Method 2a-2b: ROS detection using CATCHMENT estimates only. Method 3a-3b: ROS detection using only ground-based station networks. Method 4a-4c: ROS detection by finding agreement among three previous methods. The months of May through September are excluded from the analysis.

3.6 Discussion of ROS Detection Results

The theory behind combining different data types to detect ROS events was based on the hypothesis that combining data types could help mitigate the limitation of each type, and in turn, better detect the ROS events.

3.6.1 Method 1: ROS Detection using Satellite Observations

Method 1 (i.e., ROS detection using satellite observations only) provides good spatial and temporal resolution, however lacks sub-pixel variability since a small-scale ROS event could go undetected within a single 625 km^2 grid cell. Conversely, an ROS event may be detected for an entire grid cell when in reality the event may have occurred on a smaller scale. An ROS event could have also occurred in an area covered by multiple grid cells, resulting in all the grid cells to detect an ROS event, when in reality it was just in a portion of each. Analogously, events that happened over a short time span (e.g., hours) or over a certain time of day may go undetected, or even detected the day after they actually occurred, given that the AMSR-E sensor may only pass over a particular location once a day. Method 1 used an algorithm to detect ROS events based on changes in Tb to indicate a liquid layer or ice crust within the snowpack. A detected liquid layer or ice crust could be a result of a different phenomenon (e.g., snow melt without rain) and hence not reflective of an ROS event. Further, natural features impacting satellite observations (i.e., overlying vegetation, complex terrain, open water bodies, coastal regions, wet snow and ice crusts) pose issues with accuracy of satellite observations; the latter two essentially describe an ROS event.

Regridding the output of Method 1 resulted in the loss of approximately 22.7% of the original area used for detection, as a result of regridding from a polar grid to a global grid. Removal of approximately 22.7% of the area creates some sparsity in the distribution of ROS events, as any ROS events that did occur in those 22.7% of grid cells is not represented. Method 1 produced the most regional distribution of ROS events, concentrating in in Iceland, Quebec, Newfoundland and Labrador regions, as well as the northwestern coast of Russia. There was no trend in the frequency of ROS events detected during the nine-year study period, although two

winter seasons (2004-05, 2008-09) were not reviewed because a number of data sets were not available during these particular winter seasons. Over a typical winter season, the frequency of ROS events appeared to peak in February. Method 1 detected all three of the known ROS events. Review of the CATCHMENT estimates and ground station data available for all ROS detected grid cells revealed near-surface daily averaged air temperatures well below freezing and relatively small precipitation totals. These findings were used to determine the thresholds for conditional statements in Method 2 and Method 3 in order to better optimize agreement using Method 4.

3.6.2 Method 2: ROS Detection using Model Estimates

Method 2 (i.e., ROS detection using CATCHMENT estimates only) provided an improved temporal and spatial resolution over both Method 1 and Method 3. However, there are larger uncertainties in the estimated state variables, relative to the observed or recorded data. CATCHMENT forcings via MERRA-2 are crucial to the accuracy of snow depth estimates. Likewise, MERRA-2 surface daily-averaged air temperature and daily-averaged precipitation are constrained by the accuracy of its forcings. The application of MERRA-2 precipitation to polar regions may also bring added error due to a limited number of ground-based stations for use in conditioning the MERRA-2 reanalysis product. All CATCHMENT forcings and variables used in the conditional statements for Method 2 (i.e., precipitation, surface air temperature and snow depth) were an average of the entire day, from 00:00 to 23:59. Consequently, many ROS events likely went undetected if they occurred over a short time period during the day or spanned over multiple days. The CATCHMENT estimates were initially generated on a 9 km x 9 km grid and then aggregated up to a 25 km x 25 km grid by computing the arithmetic average. Consequently, precipitation values within the grid cell are spread out among the entire grid cell, so localized

ROS events may go undetected or an entire grid cell could be marked with an ROS event when in reality only a small portion of the grid cell was affected.

Two versions of Method 2 were created, one with the most relaxed bounds possible and the other slightly more constrained. Thresholds were based on the observations and records of the three known ROS events. Method 2 detected only the last day of the Banks Island ROS event and none of the other known events. Average daily air temperature appeared to be the biggest constraint as an ample amount of snow depth and precipitation were estimated throughout the winter seasons. ROS events detected using Method 2a (with the most relaxed bounds) spans over almost the entire region of interest (excluding eastern Russia) and has nearly six times the number of detected grid cells compared to Method 2b. Method 2b contains higher thresholds for snow depth and precipitation estimates, and subsequently has a limited distribution concentrated mainly in Iceland, Norway, western Russia, Alaska, and the Yukon Territory. Similar to Method 1, there was no trend in frequency of ROS events over the nine-year study period for Method 2. Method 2a detected the most ROS events at the beginning and end of the winter season, whereas Method 2b (with more constrained bounds) detected the highest frequency of ROS events in the middle of the winter season.

3.6.3 Method 3: ROS Detection using In-situ Measurements

Method 3 (i.e., ROS detection using ground station measurements only) had a much better chance of catching more localized ROS events. However, similar to Method 2, hourly records were averaged up to a daily value, which could potentially mask events occurring over a period of a few hours or less. Stations with available are not evenly dispersed, which led to studying ROS events detected only at stations with available measurements. Unfortunately, ground stations can break down often (e.g., spent batteries, fully data loggers) for long periods of

time leading to large data gaps. Stations were also limited by the technology used and may be unable to determine the state of precipitation (e.g. liquid versus solid), which is valuable information for ROS detection. Only one station is needed to detect an ROS event for an entire 25 km x 25 km grid cell. Such an assumption brings uncertainty to the ROS events detected.

Two versions of Method 3 were created (i.e., Method 3a and Method 3b), one with relatively relaxed bounds and the other slightly more constrained, respectively. Neither version detected the three known ROS events. Detected regions were concentrated mainly in Norway, Sweden, and Finland. Some were widely dispersed throughout Russia and others clustered together in Alaska. The most overlap of detected events between versions is in the Alaska and Norway regions. The highest number of ROS events was detected in Norway where many ground stations are located. The frequency of ROS events for both version showed no trend over the nine-year study period. Similar to Method 2, Method 3a (more relaxed bounds) detected more ROS events at the beginning and end of the ROS event, whereas Method 3b (more constrained) showed a peak in ROS events in the middle of the winter in a similar manner as Method 1. Only approximately 1.7% of the region of interest had the potential for an ROS event to be detected using Method 3. The lack of working high latitude ground stations was a severe crutch for Method 3 ROS detection and subsequently for Method 4, too.

3.6.4 Method 4: ROS Detection using Multiple Data Types

Combining all three data types could strengthen the accuracy of ROS detection but unfortunately, the particular datasets used were not conducive to a combination approach because finding agreement between all three methods did not occur. Regridding Method 1 caused the loss of approximately 22.7% of the study area associated with the conversion of a polar grid to global grid. In addition, there were two winter seasons (2004-2005 and 2008-2009)

with missing output. Although ample amounts of precipitation and snow depth were estimated, the CATCHMENT estimated air temperatures well below freezing making it difficult to securely detect an ROS event. Lastly, and likely the biggest reason why there was no agreement between all three methods; only approximately 1.7% of the region studied had the potential for an ROS event to be detected using Method 3 due to the sparsity of ground-based observation stations north of the 60th parallel.

As a result, three different combinations or versions of Methods 1-3 were used to make up Method 4. All three versions (Methods 4a-4c) detected ROS events in different regions;

Method 4a

- Combination of Method 1 and Method 3a
- One ROS event estimated in the Nunavut Territory, Canada

Method 4b

- Combination of Method 1 and Method 2a
- 22 ROS events concentrated in the Northern Alaska and Russia

Method 4c

- Combination of Method 2b and Method 3b
- 94 ROS Events concentrated in Norway and Southeastern Alaska

All three versions showed no trend in the frequency of ROS events over the nine-year study period. Method 4b had a peak in ROS events at the beginning and end of the winter season whereas Method 4c had a peak in ROS event frequency the middle of the season.

These results are limited in terms of applicability as Method 3 only has ROS detection in areas with ground stations. ROS events of all intensities are compared, hence, an ROS event with

very small amount of precipitation has equal weight to an ROS event that yields large amounts of rainfall. Analogously, one with a relatively small snow depth is equal in weight to one with deep snowpack. The ROS events in Method 4b have smaller snowpack depths and precipitation values relative to those in Method 4c. None of the versions in Method 4 (i.e., Method 4a-4c) detected the three known ROS events further questioning the validity of the ROS detection method used.

The goal of detecting ROS events using multiple data sources was not just to find more historical ROS events, but also to find historical ROS that likely occurred and could have potentially impact $SWE_{AMSR\text{-}E}$. The results demonstrate just how difficult such a task is. Exploring models with forcings better suited for polar regions and using more robust ground-based networks can improve ROS detection that uses multiple data types.

Chapter 4: Analysis of the Impact ROS Events on SWE_{AMSR-E}

4.1 Introduction

Chapter 4 addresses Objective B, which is the investigation of if/how ROS events impact local AMSR-E based SWE retrievals (i.e. SWE_{AMSR-E}). Objective B, was first explored by analyzing the three known ROS events followed by analyzing those detected in Objective A, using Method 4. Chapter 4 first summarizes all the current knowledge on the three known ROS events and based on that knowledge, estimates a 'true' SWE time series. Each ROS event would theoretically have its own unique time series depending on the snowpack characteristics before the event, and the intensity and duration of the event. The 'true' SWE time series was than compared to the SWE_{AMSR-E} for each event.

The following section explores the SWE_{AMSR-E} for all the detected events in Method 4a – Method 4c. Lastly, a preliminary and brief analysis of the effect of particular characteristics of an ROS event (i.e., duration, frequency, initial snow depth, timing or location) on SWE_{AMSR-E}. Chapter 4 ends with a general discussion on the findings to address Objective B.

4.2 Analysis of SWE_{AMSR-E} for Documented ROS Events

Section 4.2 provides a general summary of all local observations (anecdotal evidence), CATCHMENT estimates, and GSOD records for each of the three documented ROS events was examined and compared to formulate a 'true' SWE time series for the event, which would then validate or invalidate the SWE_{AMSR-E} estimates for that ROS event.

4.2.1 Banks Island, Canada ROS Event (09/27-10/03/2003) Description

The Banks Island ROS event is likely the most infamous of all known ROS events and is believed to have caused the largest known 'die off 'of ungulates, with a death toll of over 20,000 musk oxen (Grenfell, et al., 2008). Hunters had observed starved musk oxen searching for food on pack ice that drifted out to sea (Grenfell, et al., 2008). Local inhabitants reported several days of 'drizzly' freezing rain on a snowpack that was approximately 15 cm thick, proceeding with a quick decrease to subfreezing temperatures. The ice layer was estimated to be several inches thick and exist at the base of the snowpack (Soil thermal and ecological impacts of rain-on-snow events in the circumpolar arctic, 2008). Unfortunately, meteorological data does not exist for the ROS event, since very few ground stations are located on the island. In fact, ground stations do not exist in the affected area, which was on the northern half of the island. The closest station was about 30-45 km from the affected area and only a trace of rain was recorded (Grenfell, et al., 2008). The Sachs Harbour Station of the Atmospheric Environment Service of Canada logged air temperatures just before the event increasing from approximately 265.15 K to 273.15 K, and then reaching a high of about 276 K during the event. The same station also recorded a low-pressure system moving through, as air pressure dropped significantly, and the cloud cover showed a near-maximum value (Grenfell, et al., 2008). Approximately four days after the event, recorded air temperatures returned to below freezing and maintained a normal decrease to the seasonal minimum at the end of February (Grenfell, et al., 2008).

Of all the GSOD stations on the island, only three of the eight stations recorded data during the period of the ROS event. Two of the three stations were actually on the northern part of the island where the event occurred. According to the data available, precipitation did not occur, mean air temperatures hovered around 270 K during the event and dropped quickly after

to approximately 265 K. During the last four days of the event, the maximum air temperature was recorded at slightly above freezing. The snow depth increased from approximately 8 cm to 18-20 cm and remained at that depth for at least five days following the event.

CATCHMENT estimates show a steady increase in daily mean snow depth throughout the ROS event. Estimates begin at 10 cm before the event and steadily increase to 18 cm over the course of the storm and remain steady at 18 cm following the event. Estimated mean air temperatures hovered around 270 K during the event with a steep decrease to subfreezing temperatures approximately two days after the event ended. Approximately 0.09 cm of precipitation was estimated on the last day of the ROS event, otherwise no other precipitation was estimated. Interestingly, the largest precipitation estimates occurred within 3 to 5 days after the ROS event ended. However, this could have been another snowstorm, since measured temperatures were well below freezing during the precipitation event.

Based on the observations of local inhabitants, GSOD records, and CATCHMENT estimates, a SWE time series over for the Banks Island ROS event would likely appear to initially decrease during at the start of the event because of warm temperatures and the introduction of liquid water into the system that likely caused further melting. Precipitation likely percolated through the snowpack, which caused some melting or wet snow metamorphism to occur. However, a decrease in SWE was probably small because the temperatures were only a few degrees below freezing and relatively little rainfall was observed, estimated, and recorded. Therefore, it is possible that not much water left the system. In the middle of the event, SWE estimates may have then started to steadily increase. Both the estimated and recorded snow depth increased throughout the event and then remained constant following the event which suggests that large amounts of water were not leaving the system and perhaps were trapped within the

system. Therefore, the SWE would increase as well. After the event, the observations, estimates, and records agree that air temperatures dropped drastically. Such a quick drop would likely cause any liquid water to freeze into an ice crust; local inhabitants observed ice crusts. One would expect SWE to level, as further water was not being added to the system. Such a conclusion could be supported because of the leveling off seen in both the estimated and recorded snow depth following the event. Some increase in SWE could occur after the ROS event since MERRA-2 did estimate precipitation occurring following the ROS event and temperatures were well below freezing, which could result in the accumulation of more snow.

In summary, based on the available data, a 'true' SWE time series would have a small initial drop in SWE at the start of the event, followed by a sharp increase in the middle to end of the event, and then a slow, gradual increase after the ROS event when precipitation continued as snow rather than as rain.

4.2.2 Southern Yamal Peninsula, Russia ROS Event (11/05-11/07/2006) Description

The ROS event that occurred on the southern Yamal Peninsula impacted a fairly large region relative to the other two known ROS events. Over approximately 48 hours, two periods of rainfall occurred separated by heavy snowfall, which caused two distinct ice crusts to form within the snowpack (see Figure 1.1). The Southern Yamal Peninsula ROS event is considered to have caused the loss of about 25% of reindeer herds in the region because it critically impacted migration routes and casued wide spread starvation (Detection of snow surface thawing and refreezing in the eurasian arctic with quikscat: implications for reindeer herding, 2010). The region then experienced another ROS event a few months later in January 2007 (Passive-Microwave-Based Detection of Rain-on-Snow Events over sub-Arctic Regions, 2014).

Of the 45 GSOD stations in the area, eight stations had available data during the time of the ROS event, while only one station was actually located at the center of the region impacted by the ROS event. GSOD stations recorded 0.03 cm of precipitation the day before the event, but no precipitaion during or following the known time period of the ROS event. Recorded air temperatures remained well below freezing (around 260 K) for entire time period of interest. However, on the last day of the event, a maximum air temperature of 271 K was measured. Snow depth measurements were missing on the last day of the event, but at the start of the ROS event it was around 0.35 m and then dropped to 0.20 m during the event and then subsequently increaed to 0.45 m the day after the event ended.

MERRA-2 estimates revealed similar near-surface air temperatures to GSOD station measurements remained around 260 K for the entire event. The snow depth was estimated at approximaetly 60 cm before the event and steadily increased to about 70 cm where it then leveled off. MERRA-2 estiamted precipitation remained at a steady rate of about 8 mm for each of the three days (before, day of, and day following the ROS event).

Based on the observations, records, and esimations, a 'true' SWE time sereies for the soutehrn Yamal Penninsula ROS event might start as an initial slow decrease, based on the decreased snow depth recored by GSOD stations and the introduction of rainfall observed by local inhabitants. During the ROS event, a large steady increase in SWE between the two rainfall events (based on increases to CATCHMENT-derived snow depths, GSOD station meausrements, and local hunter observvations). Following the last rainfall event and the conlcusion of the ROS event, a continued increase of SWE as further snow accumulates on the snowpack. Estimated cold air temperatures coupled with observed snowfall, suggests that minimal water left the system and, hence, a steady increase in SWE after the first initial rainfall.

4.2.3 Daring Lake, Canada ROS Event (04/08/2007) Description

The Daring Lake ROS event was small when compared to the two previously described known events. The event only lasted a day with light rainfall recorded in the afternoon. There were no apparent ecological impacts as a result of the Daring Lake ROS event either. The ice crust developed on the surface of the snowpack and was approximately 3 mm thick. Temperatures were recorded as only slightly above freezing for approximately 3 hours. The Daring Lake ROS event was also thoroughly studied by a field campaign using ground-based radiometers (Observed and modelled effects of ice lens formation on passive microwave brightness temperatures over snow covered tundra, 2010)

Of the GSOD five stations located in the area, two had available data. A daily-average of roughly 2 cm of precipitation was recorded on the day of the event, with a slight dip in snow depth measurements from approximately 0.75 m to 0.65 m. However, the snow depth returned to about 0.75 m the day after the event ended. Steady increases in mean air temperatures were recorded at least five days leading up to the ROS event, with a peak at about 267 K on the day of the event and for a few days after.

CATCHMENT estimated a consistent increase in air temperature preceding the ROS event, (similar to GSOD station measurements) and hovered just below freezing (about 270 K) on the day of the ROS event and for about a week following the event. Precipitation was estimated at 0.02 cm on the day of the event, which is analogous to the GSOD records. Estimated snow depths start at approximately 40 cm before the event and slowly decline following the event, likely due to approaching spring season.

The observations, station measurements, and CATCHMENT estimates for the Daring Lake ROS event suggested a slight decrease in SWE on the day of the event since snow depth

was recorded and shown to decrease on the day of the ROS event, followed by a slight increase the day after the event since an ice crust was observed and the recorded snow depth increased. If the ice crust formed on the top of the snowpack and a small amount of precipitation was both recorded and estimated, then one could theorize that water did not drain from the snowpack, thereby suggesting a slight increase in SWE immediately following the ROS event. However, a steeper decline in SWE likely occurred during the week following the ROS event as air temperatures lingered near the freezing point and the snow depth continued to decrease. Since additional precipitation did not occur after the event and temperatures remained high, the snowpack was likely melting (or sublimating), which resulted in a decrease in SWE as the spring season approached.

4.2.4 SWE_{AMSR-E} of the Three Known ROS Events

A 31-day time series (10 days before the last day of the ROS event and 20 days after the ROS event ended) for each of the three known ROS events is shown in Figure 4.1. All three events vary in duration making them difficult to compare to one another using a time series. Therefore, the last day of each ROS event (dark vertical line) was indicated to compare the SWE_{AMSR-E} on the final day and those following the event. Due to the duration and intensity of the Banks Island and southern Yamal Peninsula ROS events, the SWE_{AMSR-E} for those storms yielded considerably larger changes relative to the Daring Lake event. An apparent pattern in the Banks Island and southern Yamal Peninsula ROS events of an initial decline in SWE_{AMSR-E} followed by a steep increase is evident. Such a pattern was expected for both of these events based on the anecdotal evidence, ground station measurements, and model estimates. The Daring Lake event matches its anticipated SWE time series for the days preceding and following the

ROS event. Interestingly, there appears to be an increase a week or so afterwards, which could possibly be explained by the further metamorphism of the ice crust.

It is difficult to discern whether or not changes in SWE_{AMSR-E} are accurate because either an increase or a decrease can be justified theoretically, depending on the characteristics of the ROS event. For example, a decrease in SWE (i.e., water leaving the system) during the ROS event could be due to the melting of the snowpack because of warm air temperatures or liquid water percolating though the snowpack, further accelerating snowpack melt. An increase in SWE (i.e., water accumulating in the system) during the ROS event could be a result of liquid precipitation that freezes and is retained within the snowpack. An increase in SWE preceding or following the event could be due to a separate snow event completely independent of the ROS event. However, if air temperatures remain high, a decline in SWE following an ROS event could also be justified since further melt might occur. As a result, the variability in a SWE time series for an ROS event should be noted and considered when trying to determine the accuracy of SWE_{AMSR-E} estimates.

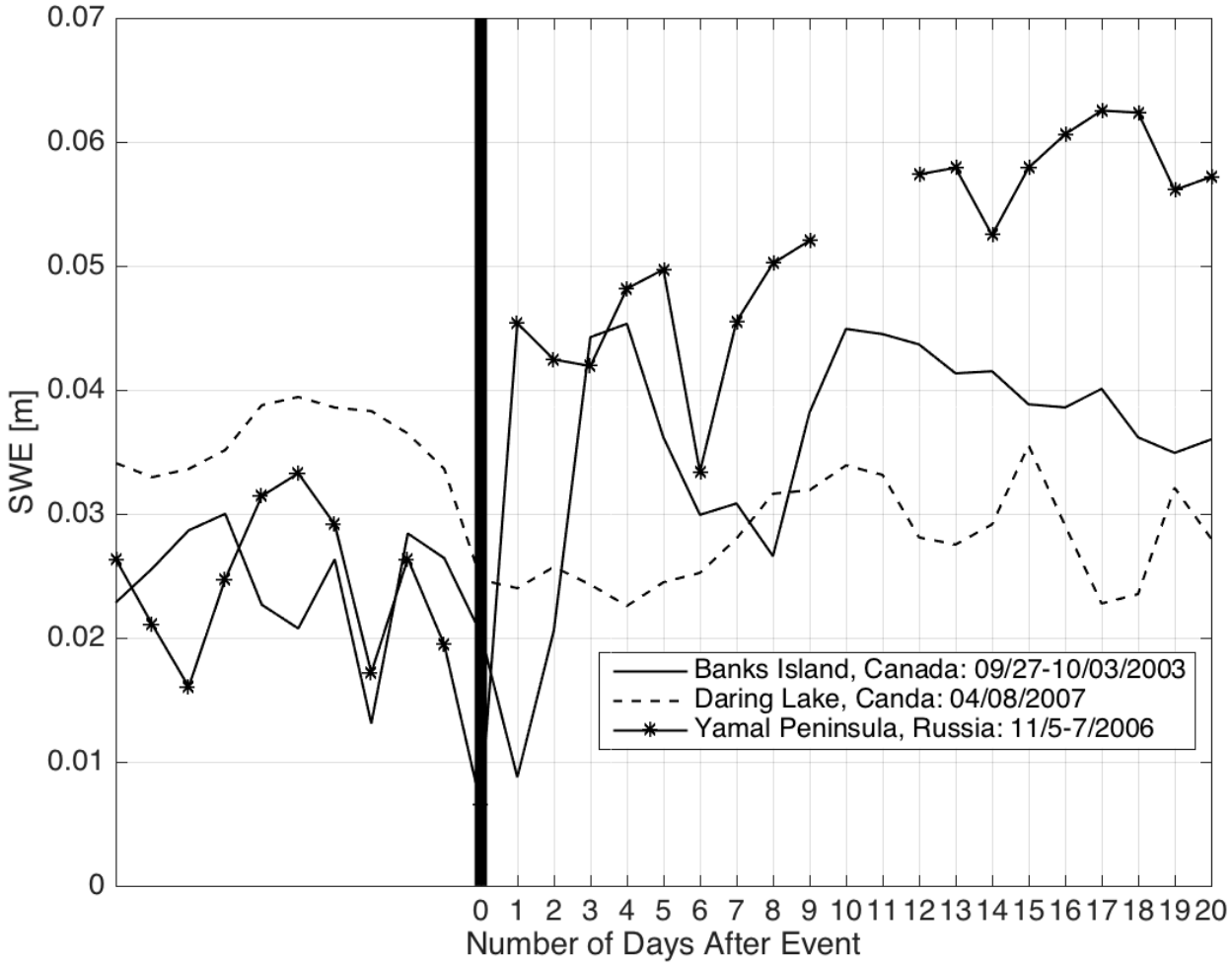

Figure 4.1. Time series of domain-averaged SWE_{AMSR-E} estimates for each of the three known ROS events. Solid black line represents the last day of the ROS event. Ten days before the last day of the ROS event and twenty days after the ROS event ended.

Figure 4.2 shows the daily change in SWE_{AMSR-E} for each of the three known ROS events. Figure 4.2 is beneficial in the visualization and comparison of trends concerning the changes of SWE_{AMSR-E} over an ROS event. The steady decline and then an abrupt, steep increase is evident in SWE_{AMSR-E} following the southern Yamal Peninsula ROS event.

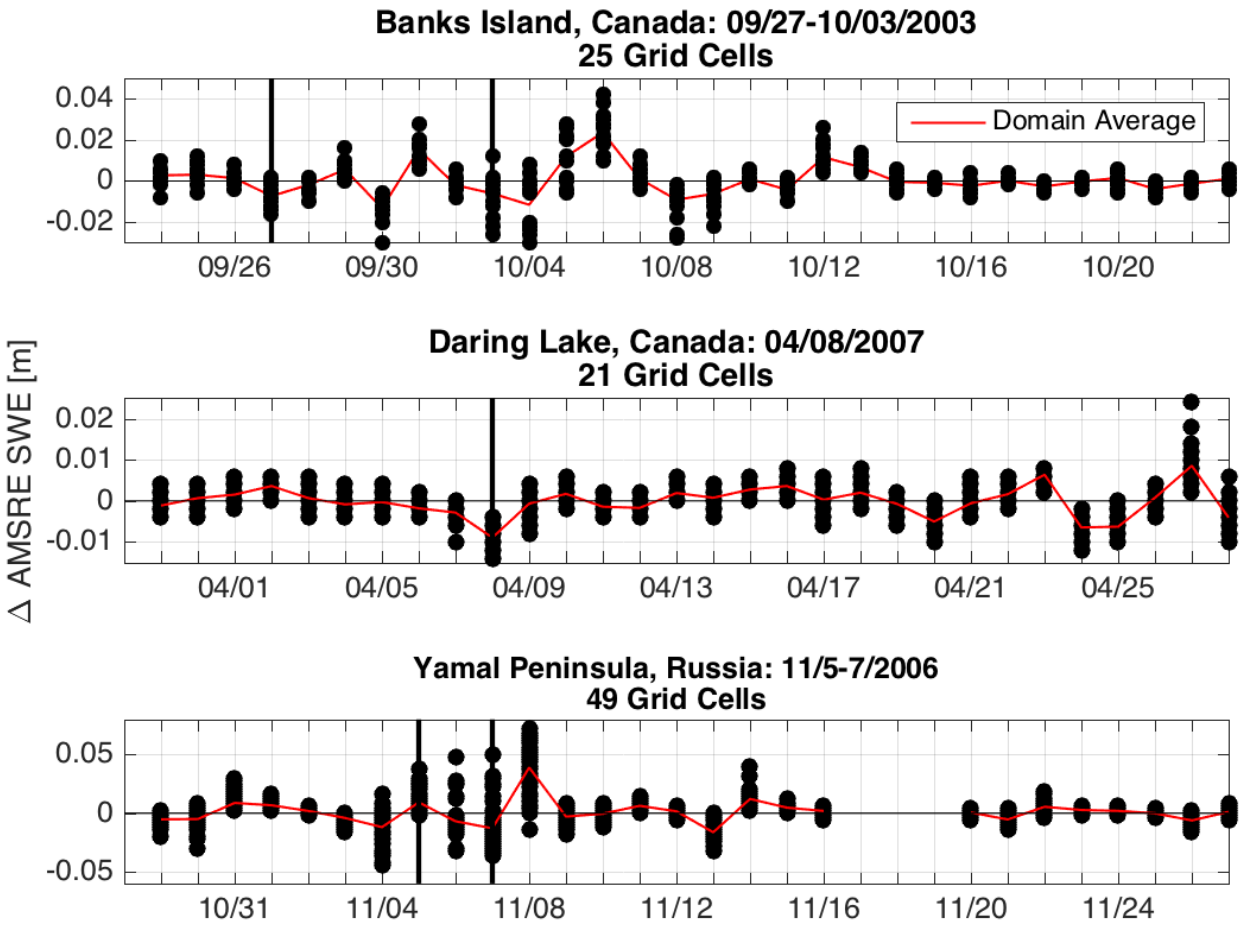

Figure 4.2.Domain-averaged daily change in SWE_{AMSR-E} for each of the three known events. Bolded black lines represent the start and end of the ROS event, and for the case of the Daring Lake ROS event, which only occurred over one day, a single black line.

Additionally, for all three ROS events, a decline in estimates is evident either on the day of or throughout the time span of the ROS event, followed by a subsequent increase after the ROS event. A general pattern is evident by the red line in Figure 4.2 even though small fluctuations in SWE_{AMSR-E} occur on a daily basis. It is important to determine if the fluctuations during an ROS event are statistically significant and whether or not that suggests inaccuracy in the SWE_{AMSR-E} or if it is a true reflection of the system response.

The variation in each SWE_{AMSR-E} time series for ROS events shows that an ROS event can alter a snowpack SWE_{AMSR-E}, depending on the characteristics of the ROS event. Due to the

lack of in-situ SWE measurements taken for known high latitude ROS events, it is difficult to determine if the SWE_{AMSR-E} estimates are accurate or if it should be flagged (i.e. may require additional modification). By utilizing local ground-based observations, model estimates and ground station measurements one can hypothesize a true SWE profile to determine if these ROS events are adversely impacting satellite observations in such a manner for which the retrieval algorithms do not account. Locating additional ROS events (i.e., detected ROS events) to study could help address such a concern.

4.3 Analysis of SWE_{AMSR-E} for Detected ROS Events

ROS events were detected using Method 1- Method 4, described in Chapter 2 and Chapter 3. Method 4 involved comparing the output generated in Methods 1- Method 3. Three different versions of Method 4 (Method 4a, Method 4b, and Method 4c) were created in order to highlight suspected ROS events that are detected by at least two of the three different methods. The detected ROS events from these three versions were used in the following analyses.

For all analyses conducted, an ROS event has been classified as one 25 km x 25 km grid cell detecting an event. In some cases, several adjacent grid cells detected an ROS event on a given day. Such events were then grouped as described in the section of Chapter 2. Grouped ROS events were then labeled as "regional ROS events", and then a domain-average was calculated for each event's daily SWE_{AMSR-E}. Table 4.3 displays the number of regional ROS events for each version of Method 4. Calculating the domain-average of adjacent ROS detected grid cells eliminated having multiple grid cells representing the same ROS event, which may become an issue when every ROS event SWE_{AMSR-E} time series is plotted and then averaged.

Additionally, any grid cell that detected an ROS event for two or more consecutive days was removed to try to remove potential snowpacks that could have odd SWE_{AMSR-E} time series

due to long lasting ROS events and thus difficult to compare with other ROS events. As shown in Table 5, these decisions narrowed the number of ROS events analyzed to 1 event in Method 4a, 16 events in Method 4b and 64 events in Method 4c. Collectively, a total of 81 detected regional ROS events have been estimated.

Table 4.1. Summary of the grouping or elimination of some Method 4 detected ROS events based on location and duration.

Method	Total number of grid cells with ROS detection	Total number of Regional ROS events	Total number of Regional ROS events occurring over one day
4a	1	1	1
4b	25	22	16
4c	101	94	64
			Total: 81

The daily change in SWE_{AMSR-E} estimates for the detected regional ROS events in Method 4 is shown in Figure 4.3. Different behaviors are evident in each version. An increase in SWE_{AMSR-E} on the day of the event followed by further increases once the ROS event has ended is evident for Methods 4a and 4b. A relatively clear pattern of decrease in SWE_{AMSR-E} on the day before and of the regional ROS event followed by subsequent increases in SWE_{AMSR-E} is evident for Method 4c.

An investigation of the detected regional ROS events CATCHMENT and MERRA-2 estimates was done to further analyze the SWE_{AMSR-E} shown in Figure 4.3. On the day of the ROS event, the average snow depth was approximately 0.35 m and 0.44 m, in Method 4a and Method4b, respectively. These values are less than half of the average snow depth estimated in Method 4c, which was approximately 0.83 m. Method 4a and Method 4b also had significantly

smaller precipitation amounts of roughly 0.33 mm and 2.4 mm, respectively. Method 4c had an average precipitation amount of about 21 mm, which is approximately nine times greater than the other two versions of Method 4. Such low precipitation over shallow snowpacks would theoretically produce small changes in SWE values, which can be seen by the range in $SWE_{AMSR\text{-}E}$ of the first two plots in Figure 4.3. An average MERRA-2 near-surface air temperature of approximately 274.23 K was estimated on the day of all detected regional ROS events.

An increase in $SWE_{AMSR\text{-}E}$ after the suspected regional ROS events for all three versions of Method 4 is evident, which could be explained theoretically by additional precipitation (snow) continuing after the regional ROS event when temperatures decreased to below freezing. However, the average MERRA-2 air temperatures for all Method 4 regional ROS events remained around freezing for multiple days following the event, which would theoretically decrease SWE estimates. Such findings may point to the necessity to flag ROS event $SWE_{AMSR\text{-}E}$.

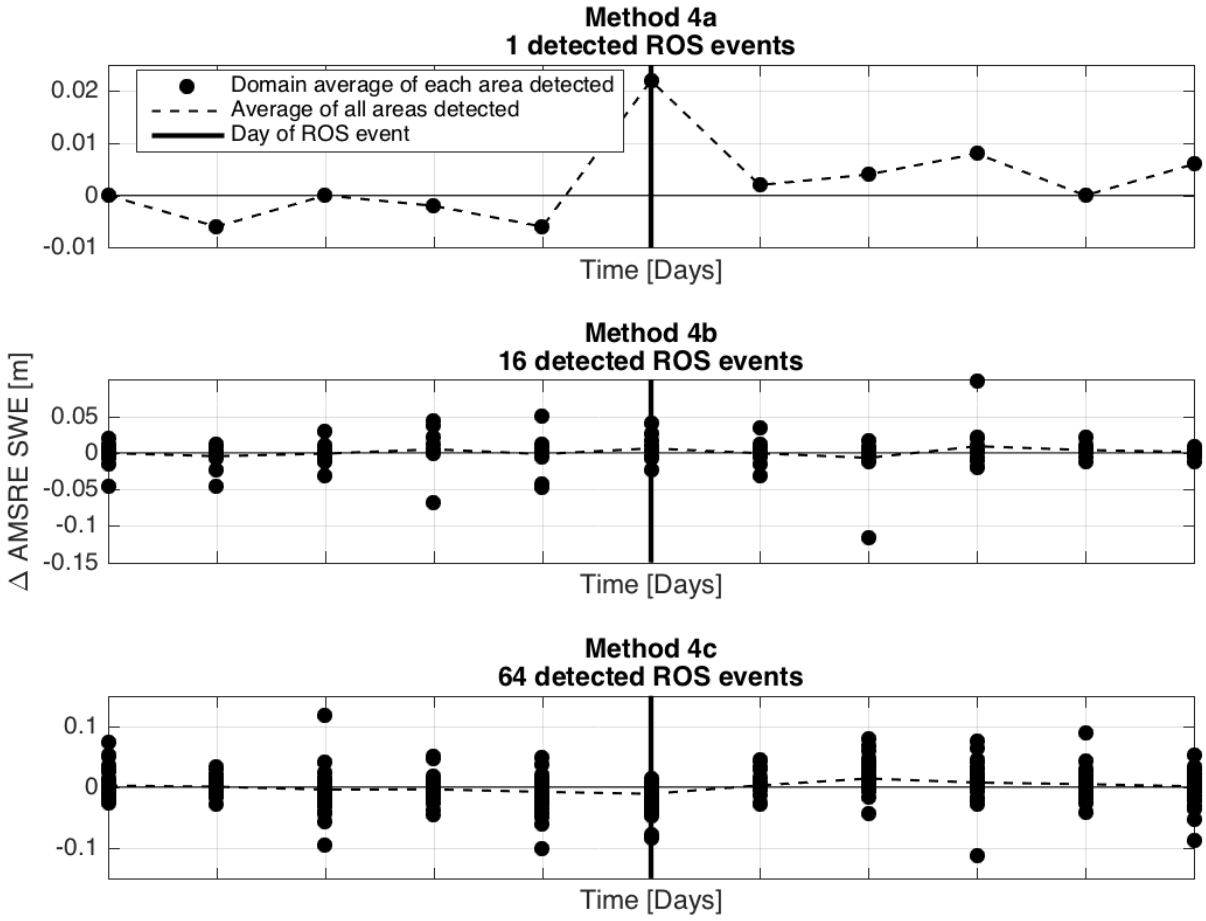

Figure 4.3. Time series of daily change in domain-averaged SWE_{AMSR-E} for all 81 ROS events detected in Method 4 versions (4a-4c). Black line indicates day of ROS event.

Table 4.2 lists the percentages of regional ROS events with a positive, negative or zero change in SWE_{AMSR-E} for the day before, of, and up to three days following an ROS event. Table 4.2 also includes SWE_{AMSR-E} from the three known ROS events. Shaded sections show that a majority of ROS events have a decrease in SWE_{AMSR-E} on the day before and on the day of the ROS event. Even though Method 4a and Method 4b show an increase in SWE_{AMSR-E} on the day of the regional ROS event, the majority of the detected regional events are in Method 4c (i.e., 64 of the 81 events) which have a decrease in retrieval on the day of the ROS event. Since a

decrease in SWE_{AMSR-E} for all three known ROS events was also observed, a negative trend was concluded for the day of the ROS event.

Table 4.2 concludes an overall positive increase in SWE_{AMSR-E} in the days following an ROS event; however there appears to be large number fluctuations in SWE_{AMSR-E} in the days following the event. Regardless if there is a positive or negative trend over the span of the ROS event, it is important to determine if those changes are significant or just random fluctuations. Statistically significant changes in SWE_{AMSR-E} could raise concern about the accuracy of the product. However, a justification can be made that significant changes are in fact occurring in the natural system. Analysis was conducted as a preliminary look to see what kind of SWE_{AMSR-E} fluctuations occur with ROS events.

Table 4.2. Summary of the percentage of cells with a positive, negative or no change in domain- averaged SWE_{AMSR-E} for detected ROS events in Method 4 and the three known events. Grey blocks denote which sign dominated the majority of change on a given day.

	Δ	4a	4b	4c	Known			Total
					Banks Island	Daring Lake	Yamal Peninsula	
Total # of ROS Events		1	16	64	1	1	1	84
Day Before ROS Event	+	0%	62%	22%	17%	0%	12%	18%
	-	100%	31%	59%	79%	86%	88%	72%
	0	0%	8%	19%	4%	14%	0%	10%
ROS Day	+	100%	69%	16%	17%	0%	16%	19%
	-	0%	31%	50%	67%	100%	84%	66%
	0	0%	0%	34%	17%	0%	0%	15%
1 Day After ROS Event	+	100%	36%	33%	17%	38%	96%	50%
	-	0%	43%	23%	75%	43%	2%	28%
	0	0%	21%	44%	8%	19%	2%	22%
2 Days After ROS Event	+	100%	50%	73%	67%	67%	18%	54%
	-	0%	50%	13%	21%	5%	67%	31%
	0	0%	0%	14%	13%	29%	14%	15%
3 Days After Event	+	100%	62%	62%	100%	5%	35%	53%
	-	0%	31%	27%	0%	52%	37%	29%
	0	0%	8%	11%	0%	43%	29%	18%

4.3.1 Factor Analysis: Impact of ROS Event characteristics on SWE_{AMSR-E}

A factor analysis was conducted to determine if regional ROS events detected (1) over multiple days, (2) with varied snowpack particular depths, (3) on certain times in the winter season, or (4) in specific regions heavily influenced the time series of daily changes in SWE_{AMSR-E} (i.e., ΔSWE_{AMSR-E}). An analysis was conducted to explore various characteristics of ROS events and to investigate if certain regional ROS events were more impactful on the SWE_{AMSR-E} than others.

4.3.1.1 SWE_{AMSR-E} for Multi-day ROS Events versus Single Day ROS Events

Detected ROS events occurring over multiple days in Method 4 were removed from the analyses so that only ROS events of similar characteristics were compared since daily changes in SWE_{AMSR-E} was the main strategy to observe the impact ROS events had on SWE_{AMSR-E} estimates. Therefore, any events that have the potential to yield anomalous SWE_{AMSR-E} estimates due to long durations were removed. Results showed that SWE_{AMSR-E} analyses for the removed 46 multi-day ROS events were found to differ minimally from those that occurred over a single day.

4.3.1.2 SWE_{AMSR-E} for ROS Events with Various Snowpack Depths

All domain-averaged CATCHMENT-derived snow depths for each regional ROS event on the day before the event occurred were calculated and placed into four groups based on the magnitude of snow depth. Daily-averaged snowpack depth on the day before the regional event was chosen to pair suspected regional ROS events with similar snowpack sizes. Snowpack depths on the day of the regional ROS event are likely impacted by the event, hence, grouping them by the day before provides a better way of comparing events. Once groups were established, daily ΔSWE_{AMSR-E} for each individual regional ROS event was plotted in Figure 4.4.

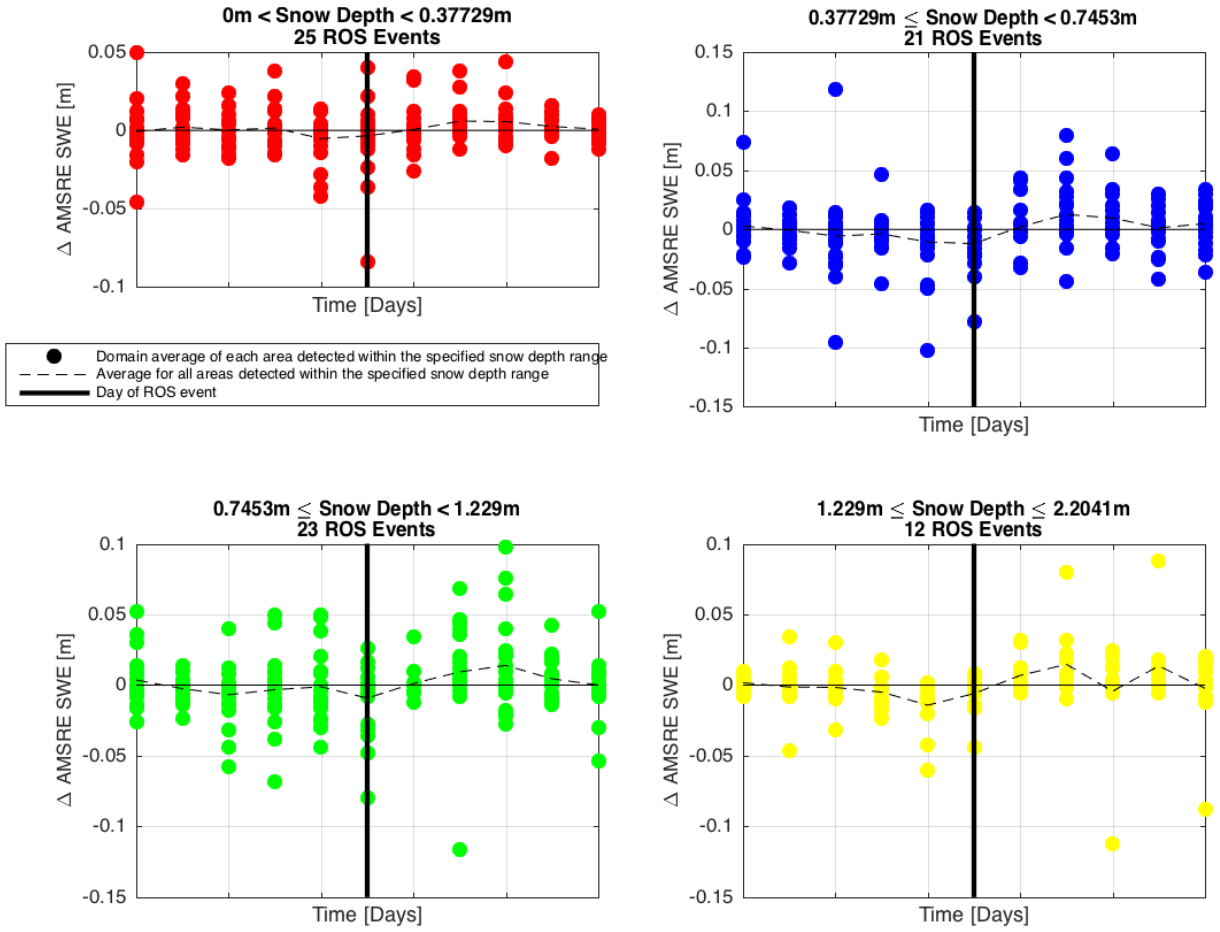

Figure 4.4. Daily changes in SWE_{AMSR-E} for all Method 4 detected ROS events separated by the domain-averaged CATCHMENT snow depth estimated the day before the event. Solid vertical line represents the day of the suspected ROS event.

Figure 4.4 indicates that shallow snowpacks, in general, yield changes in ΔSWE_{AMSR-E} similar in scale to the deeper snowpacks. Table 4.3 summarizes the number of regional ROS events in each snow depth category and how many of those come from each version of Method 4. The highest number of regional ROS events was in the shallow snowpack group (0 m - 0.38 m) and comprise a majority of the detected events in Method 4b, which have very small snowpack depths. All four groups show the same trend with slight decreases in SWE_{AMSR-E} preceding and on the day of the regional ROS event and followed by a few days of increase in SWE_{AMSR-E}.

Table 4.3. Summary of the total number of regional ROS events in each snow depth grouping

	Total number of ROS events	Total number of Method 4a ROS events	Total number of Method 4b ROS events	Total number of Method 4c ROS events
Snow depth < 0.38 m	25	1	11	13
0.38 m $\leq$ Snow depth < 0.75 m	21	0	1	20
0.75 m $\leq$ Snow depth < 1.2 m	23	0	3	20
1.2 m $\leq$ Snow depth	12	0	1	11
Total	81	0	16	64

The results suggest that snow depth has minimal impact on the variation in SWE_{AMSR-E} among detected regional ROS events. However, it is important to note that the regional ROS events in Method 4a and 4b are masked by those in Method 4c since about 79% of all the ROS events reviewed were detected in Method 4c.

4.3.1.3 SWE_{AMSR-E} for ROS Events at Various Times in the Winter Season

Seasonal timing was determined by grouping all detected ROS events into three different time periods: Early-Winter (October-November), Mid-Winter (December-February) and Late-Winter (March-April). Figure 4.5, Figure 4.6 and Figure 4.7 plot the SWE_{AMSR-E} for each respective group. The detected ROS events that fall within each group are then further divided by which version (Method 4a- Method 4c) they were detected in. Such an analysis was done to reduce the number of ROS events detected in Method 4c, which detects about 79% of all the ROS events studied and to look at the variability of ROS events within each group.

Regardless of the version in Method 4 (i.e., Method 4a – Method 4c), it appears that the time series of daily ΔSWE_{AMSR-E} remains consistent, except for Method 4b during Late-winter. In the Early and Mid-winter times of year, Method 4b displays a pattern of positive ΔSWE_{AMSR-E} before, during and after the regional ROS event. A slightly larger increase (+0.005 m and 0.03

m, respectively) on ROS day, but that does not appear to be significant, since similar magnitudes can be seen a few days before and after the event. Late-winter Method 4b regional ROS events show the exact opposite with a consistent negative $\Delta SWE_{AMSR\text{-}E}$, which may be associated with the encroaching spring season. Another reason could be due to the highly evolved snowpack at the end of the season that ultimately produced a wide range of results.

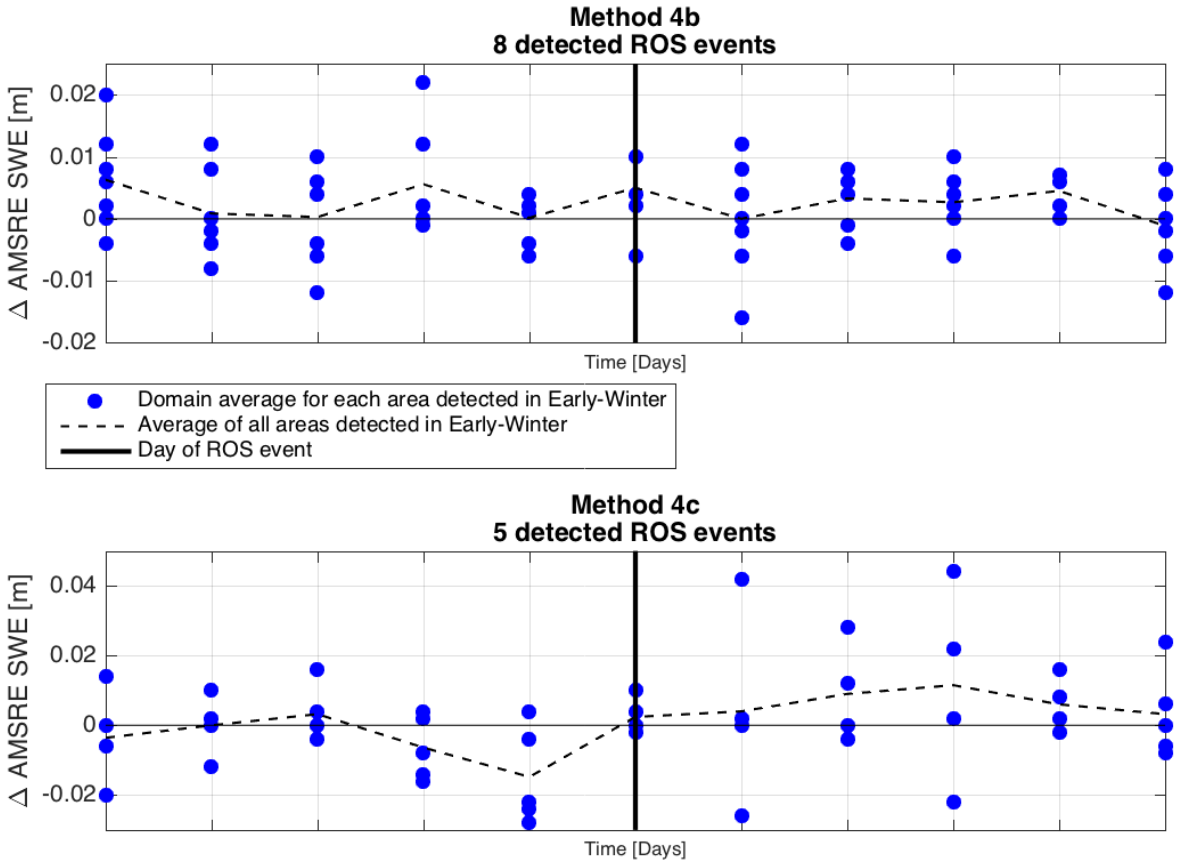

Figure 4.5.Daily change in domain-averaged $SWE_{AMSR\text{-}E}$ for all regional ROS events detected in Method 4 during Early-winter (i.e., October-November).

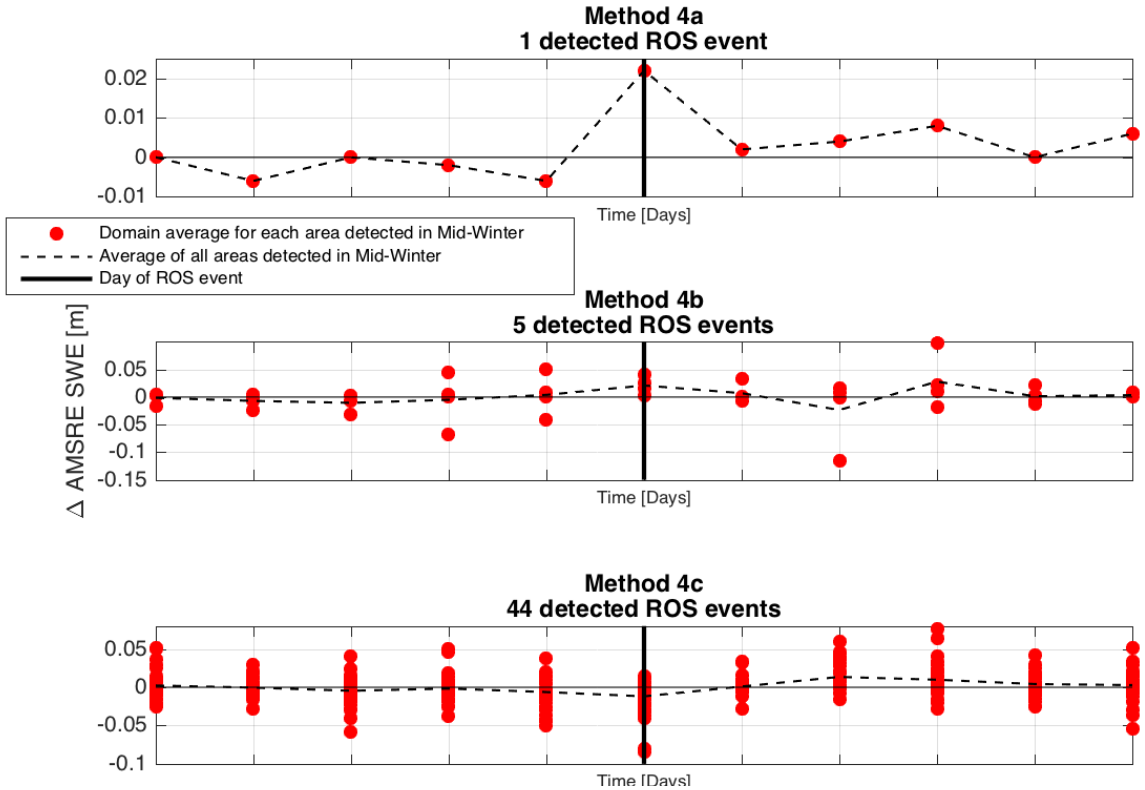

Figure 4.6. Daily change in domain-averaged $SWE_{AMSR\text{-}E}$ for all regional ROS events detected in Method 4 during Mid-winter (i.e., December-February).

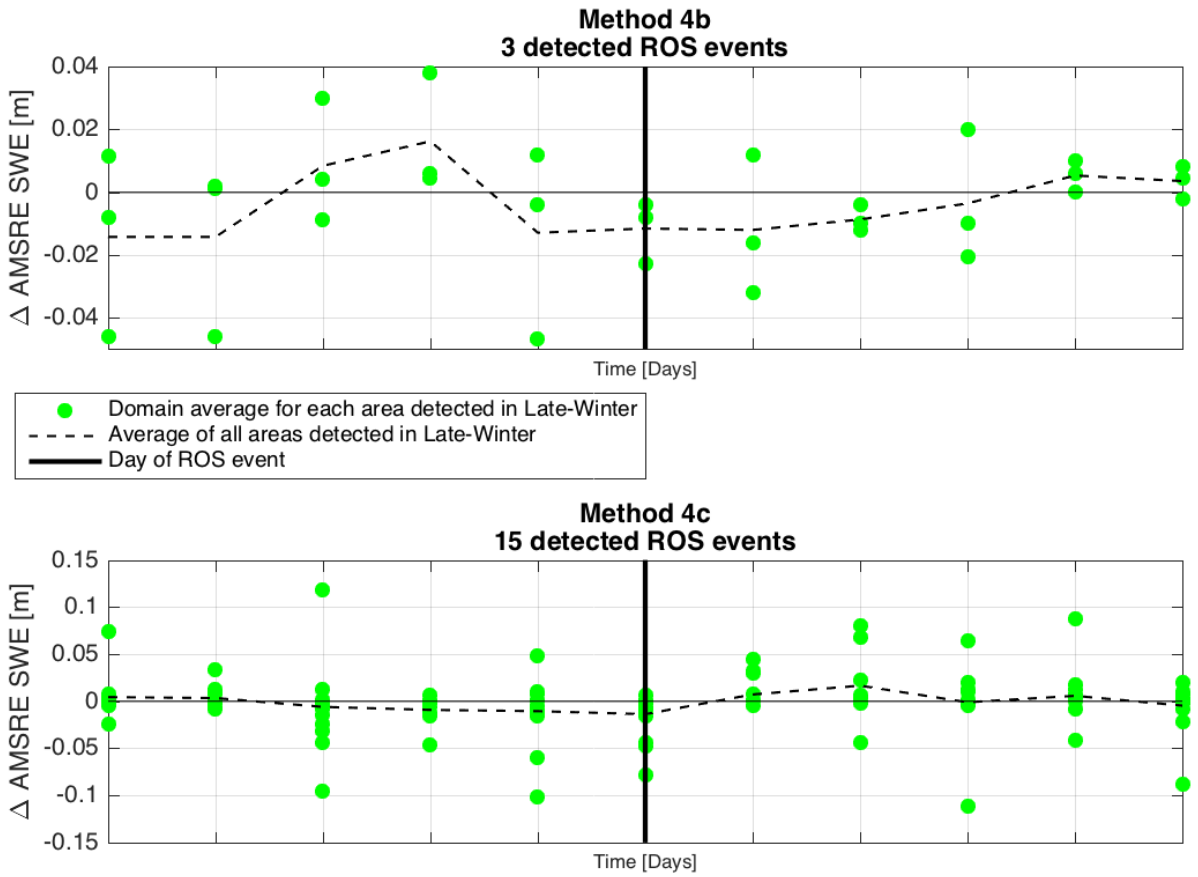

Figure 4.7. Daily change in $SWE_{AMSR\text{-}E}$ for all regional ROS events detected in Method 4 during Late-winter (i.e., March-April).

81% of all Method 4b ROS events fall within the first two groups (i.e., Early and Mid-winter), so it is difficult to place a lot of confidence on the results seen in Late-winter since only three regional ROS are detected. Method 4c has a slightly different pattern in Early-winter than Mid and Late-winter, with a negative $\Delta SWE_{AMSR\text{-}E}$ on the day of the regional ROS events. Method 4a has only one regional event, occurring in Mid-Winter and has a similar time series to Method 2b.

One would expect seasonality results to be similar to the snow depth analysis findings, because various times series as the winter season progresses, so does the depth of the snowpack. Unlike the snow depth analysis, when comparing ROS events strictly within the same version,

ΔSWE seems to fluctuate differently depending on the timing in the winter season. Ranges in daily $\Delta SWE_{AMSR\text{-}E}$ are larger towards the end of the winter season than in the beginning.

4.3.1.4 $SWE_{AMSR\text{-}E}$ for ROS Events Occurring in Various Regions

Lastly, a regional analysis was conducted where all the regional ROS events detected in Method 4 were mapped and placed into six groups according to where they occurred (see Figure 4.8). Each version in Method 4 detected regional ROS events in the same general areas that almost never interlap with other versions (see Figure 3.10). Therefore, the regional analysis was not anticipated to bring any new findings to the study as the $\Delta SWE_{AMSR\text{-}E}$ time series for each version have already been plotted in Figure 4.3. However, for Methods 4b and Method 4c there are at least two different areas where regional ROS events were clustered together and the regional analysis could help determine if there was a difference in $SWE_{AMSR\text{-}E}$ estimates among versions or between regions. The regional analysis was also not anticipated to reveal any new findings since the entire region of interest is located above the 60th parallel and has the same tundra biome; however, precipitation may be more frequent in areas due to weather patterns and thus have the potential to show varied $SWE_{AMSR\text{-}E}$ time series.

Method 4c only detected regional ROS events in Region 1 and 3 (see Figure 3.10**)** because Method 4c required agreement with ground stations, which are predominantly found in Regions 1 and 3 (see Figure 3.8). Approximately 73% of all the regional ROS events in Method 4b were detected in Region 1. Method 4a only detected one ROS event, which was located far way from all other detected regional ROS events. Method 4b had the most widespread distribution that included detections in Region 1, 2, 3, 5, and 6.

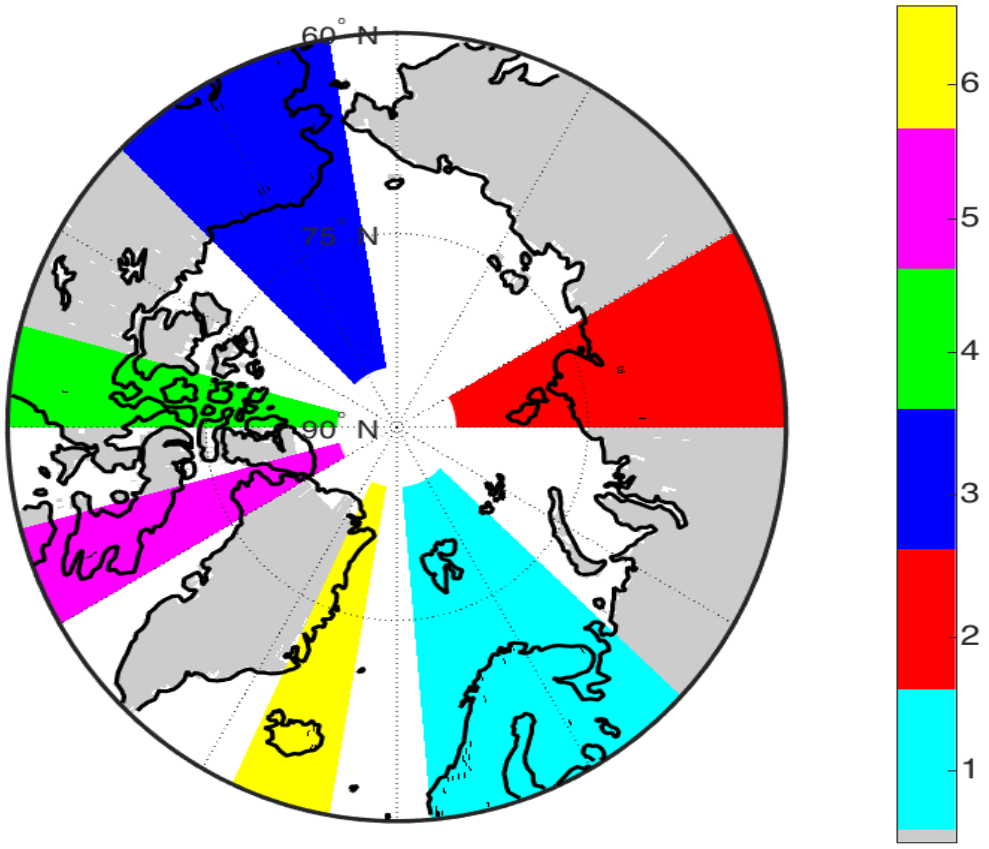

Figure 4.8. Delineation of regions Method 4 ROS events were divided into. The grid cells with an ROS detection are darkened.

The daily change in SWE_{AMSR-E} time series for Method 4c events in Region 1 and 3, showed the same SWE_{AMSR-E} patterns. Namely, a negative ΔSWE_{AMSR-E} was witnessed on the day before and of the regional ROS event and then a positive ΔSWE_{AMSR-E} the day after. Method 4b showed a positive ΔSWE_{AMSR-E} on the day of the regional ROS event for Region 1 and 3, which was contrary to Method 4c but had the same positive ΔSWE_{AMSR-E} following the regional ROS event. Method 2c showed similar patterns of change at similar magnitudes among the two regions it detected regional ROS events. Method 4b showed a variety of behaviors, depending on the regions of detection. The only regions that showed similar behavior were Regions 1 and 6. Such variability may suggest these profiles look different according to where they are located.

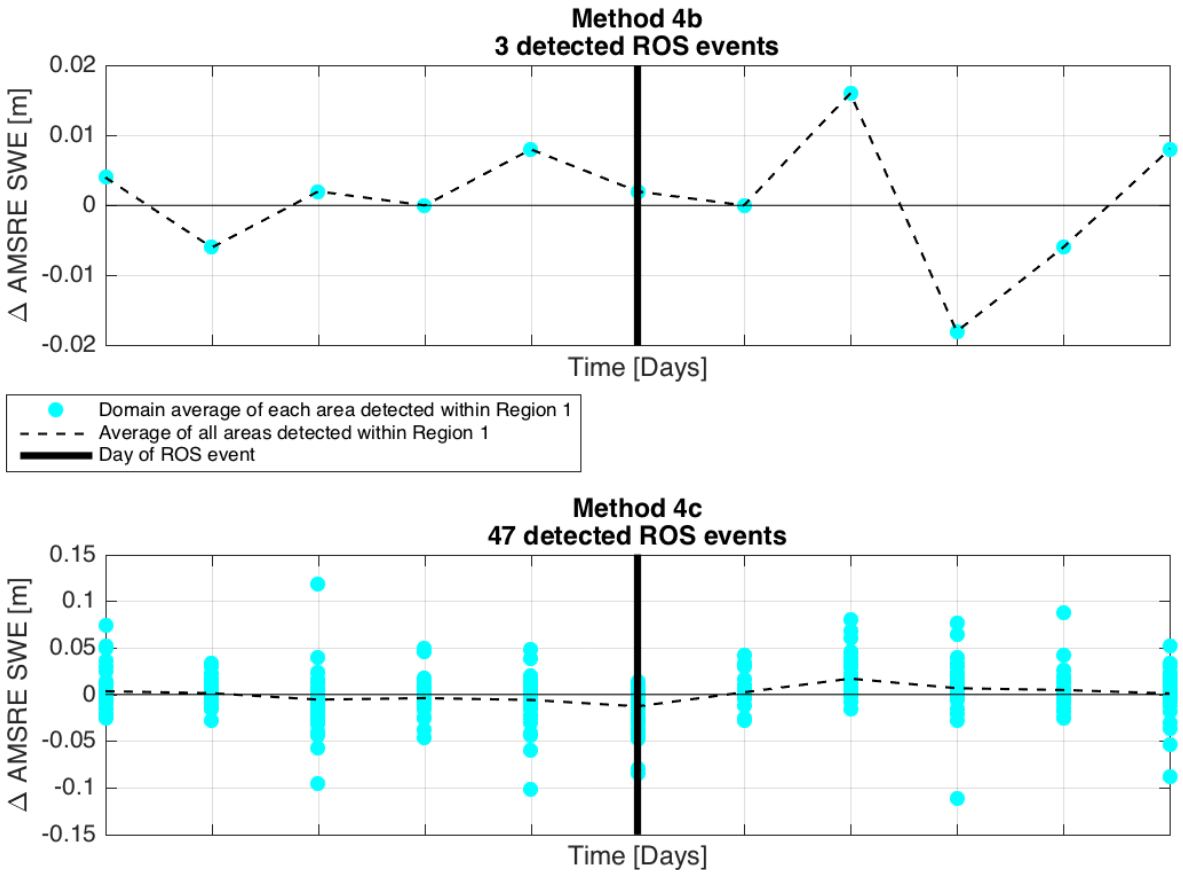

Figure 4.9. Daily changes in domain-averaged $SWE_{AMSR\text{-}E}$ for all ROS events detected in Method 4 that fall within Region 1 (50 grid cells total), as shown in Figure 4.8.

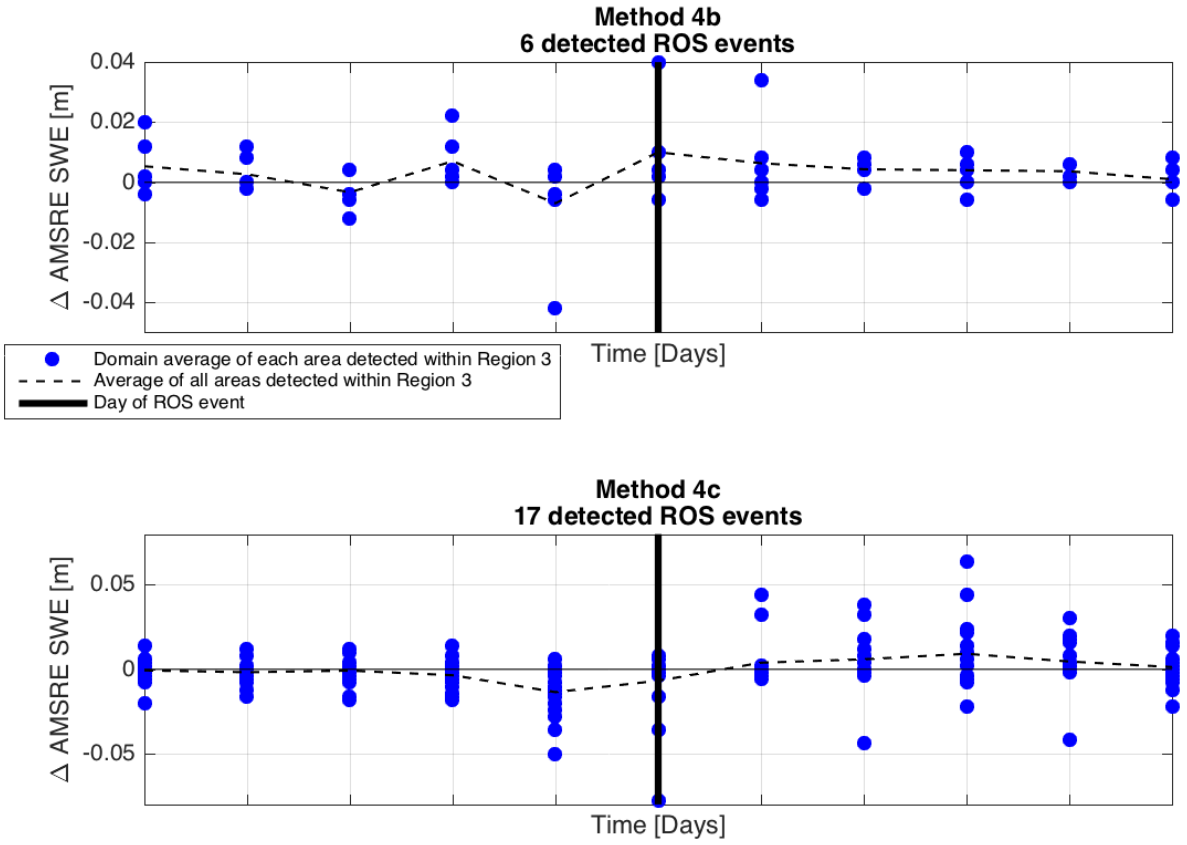

Figure 4.10. Daily change in domain-averaged $SWE_{AMSR\text{-}E}$ for all ROS events detected in Method 4 that fall within Region 3 (23 grid cells total), as shown in Figure 4.8.

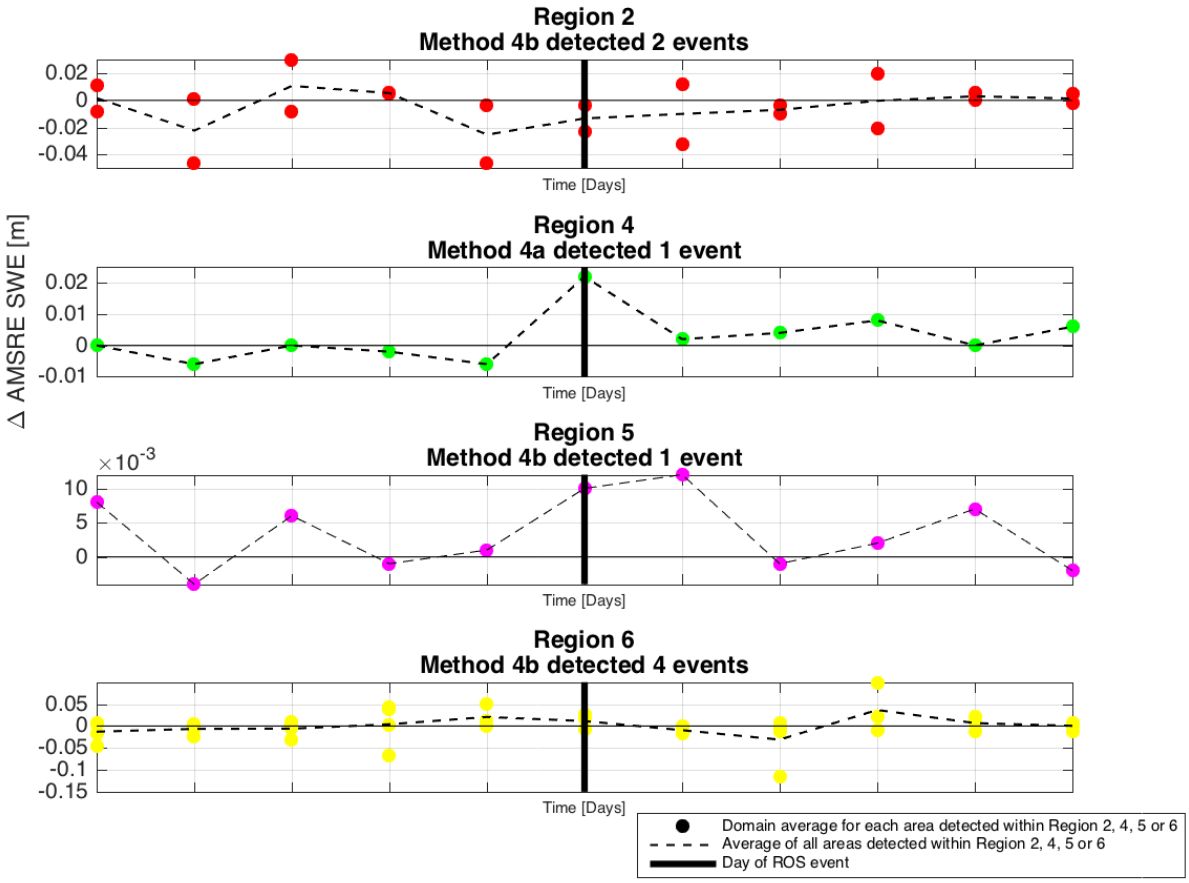

Figure 4.11. Daily change in domain-averaged $SWE_{AMSR\text{-}E}$ for all ROS events detected in Method 4 that fall within Region 2, 4, 5 or 6, as shown in Figure 4.8.

However, the number of regional ROS events actually reviewed per region is small for Method 4b, ranging from one to six. Such a small sample size makes it difficult to say that the variation among one another is significant. Method 4a ΔSWE time series are most like Method 4b in Region 3; however, only one regional ROS event is used in comparison of which statistical significance cannot be based on.

4.4 Discussion of ROS Impact on SWE_{AMSR-E}

Although it is unclear whether or not the SWE_{AMSR-E} is correctly estimating these changes, all events (both known and suspected) show a change in SWE_{AMSR-E} resulting around the ROS event, which suggests that ROS events are likely influencing SWE_{AMSR-E}.

4.4.1 SWE_{AMSR-E} of Documented ROS Events

Two of the three known ROS events (i.e., Banks Island, Canada and southern Yamal Peninsula, Russia) were so large that they caused massive die offs of ungulates in the region. The southern Yamal Peninsula event resulted in the generation of two ice crusts within the snowpack. The Daring Lake ROS event was relatively light and only resulted in a thin ice crust on the surface of the snowpack. Based on local observations, CATCHMENT estimates and station records the SWE_{AMSR-E} appears to reflect what occurred. In general, the SWE_{AMSR-E} decreased right before (and during) the ROS event and was then followed by a sharp increase and subsequently leveling off. The Daring Lake ROS event does not reflect such a pattern, however, that may be due to the relatively low intensity ROS event and the fact that it occurred at the end of the winter season. It is difficult to discern if the SWE_{AMSR-E} was accurate based on the information available because positive or negative changes could be justified at any part of the ROS event. It appeared that each individual ROS events' time series varied depending on the individual characteristics of that event. Depending on how the air temperatures fluctuated during the ROS event, it is possible that one could witness an increase or decrease in SWE_{AMSR-E}. In addition, the fact that SWE_{AMSR-E} is an daily-averaged value based on when the sensor passed over the region led to more variability with the timing in the ROS event for which AMSR-E observed the snowpack. Uncertainty could be removed by observing the SWE_{AMSR-E} of the

detected events, but it is abundantly clear that there is direct method for determining if the SWE_{AMSR-E} was accurate without comparing the retrieval to in-situ SWE measurements.

4.4.2 SWE_{AMSR-E} of Detected ROS Events

Any ROS detected grid cells in Method 4 that were detected over consecutive days were removed from the SWE_{AMSR-E} analysis in order to compare ROS events that only occurred on a single day. Additionally, adjacent grid cells that detected an ROS event were grouped together and their SWE_{AMSR-E} value was domain-averaged. Therefore, reducing the ROS events studied to the following; 1 ROS event in Method 4a, 16 ROS events in Method 4b, and 64 ROS events in Method 4c. The first two versions (Method 4a and Method 4b) show an increase in SWE_{AMSR-E} on the day of the event followed by further increases once the ROS event ends. Method 4c shows a relatively clear pattern of decrease in SWE_{AMSR-E} on the day before and of the ROS event, followed by steady increases in SWE_{AMSR-E}. Method 4a and Method 4b also had ROS events with significantly smaller precipitation amounts and snowpack depths, relative to Method 4c, and may be why Method 4a and 4b have relatively small changes in SWE_{AMSR-E} values. An increase in SWE_{AMSR-E} following the ROS events for all three versions can be seen, which can be explained by rationalizing that an ice crust or further precipitation continued after the ROS event as temperatures were dropping back down below freezing. However, daily-averaged MERRA-2 air temperatures for all Method 4 regional ROS events hover around freezing for multiple days following the event, which would theoretically decrease SWE_{AMSR-E} estimates. Such findings may point to the necessity of SWE_{AMSR-E} to be flagged.

Table 4.2 lists the percentages of ROS events with a positive, negative, or no change in SWE_{AMSR-E} for the day before, of, and up to three days following an ROS event. Even though Method 4a and Method 4b show an increase in SWE_{AMSR-E} on the day of the ROS event, a

majority of regional ROS events detected are in Method 4c which have a decrease in SWE_{AMSR-E} on the day of the event. Additionally, the three known events show a decrease in SWE_{AMSR-E} during the event, thus a general conclusion of a decrease in SWE_{AMSR-E} on the day of the ROS event was made.

Table 4.2 concludes an overall positive increase in SWE_{AMSR-E} for the days following an ROS event. However, a relatively weak trend as there is considerable fluctuation in SWE_{AMSR-E} in the days following the event. Significant changes in SWE_{AMSR-E} could raise concern about the accuracy of the product, however a justification can also be made that significant changes should in fact occur in the natural system.

A factor analysis was conducted to see if ROS events detected 1) over multiple days, 2) with varied snowpack particular depths, 3) on certain times in the winter season, or 4) in specific regions, heavily impacted the daily changes in SWE_{AMSR-E}. Analysis was conducted to explore various characteristics of ROS events to investigate if one was more impactful on SWE_{AMSR-E}. Results showed almost no impact in patterns of daily SWE_{AMSR-E} for regional ROS events occurring over multiple days versus just over one day. When ROS events were divided by their snowpack depth, results suggested that snow depth has little to no impact on the variation in daily ΔSWE_{AMSR-E} among the detected ROS events. However, it is important to note that the number of ROS events detected in Method 4a and Method 4b are relatively small compared to those in Method 4c. Seasonal timing was determined by grouping all detected ROS events into three different time periods: Early- winter (October-November), Mid-winter (December-February) and Late-winter (March-April). Approximately 81% of all Method 4b ROS events fall within the first two groups (i.e., Early and Mid-winter), so it is difficult to put a lot of weight on the results seen in Late-winter because only 3 detected regional ROS events are in that group.

One would expect seasonality results to be similar to the snow depth analysis because as the winter season progresses, in general so does the depth of the snowpack. Nonetheless, unlike the snow depth analysis, when comparing ROS events strictly within the same version of Method 4, $\Delta SWE_{AMSR\text{-}E}$ seems to fluctuate differently depending on the timing in the winter season. Ranges in daily $\Delta SWE_{AMSR\text{-}E}$ are larger towards the end of the winter season than in the beginning, perhaps because the snowpack is deeper later in the snow season. Lastly, a regional analysis was conducted where all the ROS events detected in Method 4 were mapped and placed into six groups according to where they occurred. Method 4a only occurred in one region and was not close to any other detected ROS events thereby making it difficult to compare to other. There is variability in the pattern of daily $\Delta SWE_{AMSR\text{-}E}$ for ROS events detected in Method 4c, depending on the region they occurred, insinuating there may be some correlation between region and $SWE_{AMSR\text{-}E}$ fluctuations.

The $SWE_{AMSR\text{-}E}$ contains numerous errors; hence, there are inconsistencies in $SWE_{AMSR\text{-}E}$ when comparing the time series of daily change for ROS events in different versions. The ROS detection methods used to investigate $SWE_{AMSR\text{-}E}$ were not able to agree with one another for any given ROS event. Also, there was not adequate regional distribution of the detected ROS events due to the preference of grid cells to certain ROS detection methods. ROS events are highly variable in duration, intensity and frequency, which impact the SWE of the snowpack. The $SWE_{AMSR\text{-}E}$ of ROS events of all intensities are compared such that an ROS event with a small amount of precipitation has equal weight to an ROS event that yields large amount of rainfall. Therefore, comparing the $SWE_{AMSR\text{-}E}$ of a bunch of different ROS events may not be the best strategy. A majority of the ROS events detected using ground-based stations were concentrated mainly in Norway and Alaska, adding partiality to any $SWE_{AMSR\text{-}E}$ findings to those

regions. Frequent ROS events could create a snowpack with a very unique SWE_{AMSR-E} time series due to wet snow and ice crust metamorphism within the snowpack. Coastal regions or nearby lakes, especially in northern Canada include additional error in the SWE_{AMSR-E} (and suspected ROS events) associated with sub-grid variability from surface water bodies. ROS events appear to impact horizontally-polarized measurements more so than vertically-polarized measurements. However, AMSR-E retrieval algorithms mainly depend on the vertically-polarized channels. The assumptions made for the AMSR-E based SWE retrieval or SWE_{AMSR-E} (homogenous and dry snowpack) are violated in the presence of a ROS event of which is comprised of (ice crusts and wet snow). The SWE retrieval analysis conducted highlights the importance of using of ROS event in-situ SWE measurements in well-characterized snowpacks in order to further validate (or invalidate) the findings to better determine whether or now SWE_{AMSR-E} should be flagged during ROS events.

Chapter 5: Conclusions, Future Directions, and Closing Remarks

5.1 Introduction

Findings of the study are just a preliminary investigation of the limited information regarding when and where ROS events occur and their subsequent impact on observation-based snowpack characterization.

5.1.1 ROS Detection

While there are many different ways to detect historical ROS events, each approach comes with its own limitations and benefits. The theory behind combining different data types to detect ROS events was based on the rationale that combining multiple data types could help mitigate the limitations inherent to each data type (i.e., method) to improve the accuracy of detecting ROS events.

Method 1 (i.e., ROS detection using satellite observations only) provides good spatial and temporal resolution, however lacks sub-pixel variability because a small-scale ROS event could go undetected within a single 625 km^2 grid cell. Conversely, an ROS event may be detected for an entire grid cell when in reality the event could have occurred on a smaller scale. ROS events occurring in multiple adjacent grid cells may also be misrepresented where the entire grid cell may be flagged (i.e. may require additional modification) or perhaps not flagged as a result of only a portion of the grid cell being affected by the ROS event. Analogously, events that happened over a short time span (e.g., hours) or over a certain time of day may go undetected or perhaps detected the following day, given that the AMSR-E sensor may only overpass a particular location once a day. Method 1 used an algorithm to detect ROS events based on changes in Tb to indicate a liquid layer or ice crust within the snowpack. A detected liquid layer

or ice crust could be a result of a different phenomenon (e.g., a melt or thaw event) and not reflective of an ROS event. Also, natural features impacting satellite observations (i.e., vegetation, complex terrain, open water bodies, coastal regions, wet snow, and ice crusts) pose issues with accuracy of said observations. Two of those natural features listed, wet snow and ice crusts, are the main components of an ROS event. The regridding of Method 1 output resulted in only approximately 77.3% of the original area available for detection, a result of the conversion of a polar grid to a global EASE-Grid 2.0 grid. Removal of 22.7% of the total area creates some effect in the distribution of ROS events, as that 22.7% will not be represented.

Method 1 produced the most regional distribution of ROS events that were primarily concentrated in Iceland, Quebec, Newfoundland, and Labrador, as well as the northwestern coast of Russia. A trend was not uncovered when reviewing the frequency of ROS events over the nine-year study period; however, two winter seasons (2004-2005 and 2008-2009) were not reviewed because of a lack of available data. Over a typical winter season, the frequency of ROS events appeared to peak around February. Unlike Method 2 and 3, Method 1 detected all three of the known historical events. Review of the CATCHMENT forcing and estimates and available ground station data for all grid cells detected with an ROS event suggested that the ROS events detected in Method 1 were well below the freezing point and with a relatively small amount of average-daily precipitation taking place. Findings were used to help determine the thresholds for conditional statements used in Method 2 and Method 3, and to optimize agreement using Method 4.

Method 2 (i.e., ROS detection using only CATCHMENT forcing and estimates) provided improved temporal and spatial resolution over both Method 1 and 3. However there are larger uncertainties (i.e., decreased accuracy) in estimated state variables relative to any observed or

recorded data. CATCHMENT forcings from MERRA-2 are crucial to the accuracy of snow depth estimates, and likewise, MERRA-2 air temperature and precipitation are only as accurate as the forcings in that re-analysis. The application of MERRA-2 precipitation to polar regions may also introduce added error due to data sparsity in these regions, which impacts the conditioning process used to generate MERRA-2. All variables used in the conditional statements for Method 2 (i.e., precipitation, air temperature and snow depth) and Method 3 (i.e., measured precipitation, air temperature and snow depth) were an average of the entire day, computed from 00:00 to 23:59. Averaging in both space and time smooths out extremes, therefore many ROS events likely went undetected as short periods of warm events or precipitation may be masked when using a daily average. For example, a grid cell's near-surface

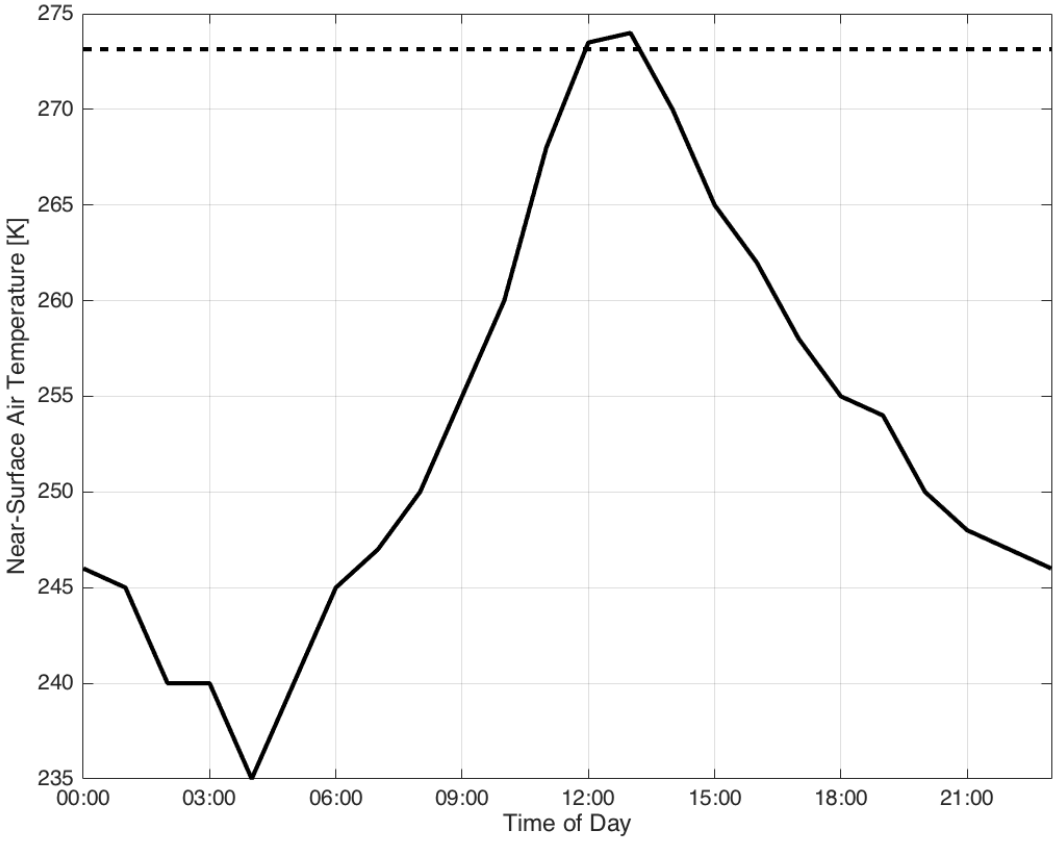

Figure 5.1. Daily change in domain-averaged $SWE_{AMSR\text{-}E}$ for all ROS events detected in Method 4 that fall within Region 2, 4, 5 or 6, as shown in Figure 4.8.

air temperature hourly profile could look like that in Figure 5.1. The daily average was 253.06K, but one can clearly observe that for a couple hours of the day the air temperature was above freezing. If precipitation coincided with the peak in air temperature, an ROS event could have occurred and would have been missed using Method 2, 3 or 4. The CATCHMENT forcings and estimates were generated on a 9 km x 9 km grid and then aggregated up to a 25 km x 25 km grid by computing the arithmetic average. Values within the grid cell can be spread out among the entire grid cell, so an ROS event may not be detected due to too little precipitation spread over the entire grid cell when it actually occurred in a concentrated part of the grid cell. Method 2 allowed for the most flexibility in thresholds because of such increased temporal and spatial resolution. Two versions were generated, one with the most relaxed bounds possible and the other slightly more constrained. Thresholds were based on the observations and records of the three known ROS events. Method 2 detected only the last day of the Banks Island ROS event, and none of the other known events. Average daily air temperature appeared to be the biggest constraint as ample amount of snow depth and precipitation were estimated throughout the winter seasons. ROS events detected using Method 2a (with the most relaxed bounds) spans over almost the entire region of interest (excluding eastern Russia) and has nearly six times the number of detected grid cells compared to Method 2b. Method 2b contains higher thresholds for snow depth and precipitation estimates, and subsequently has a limited distribution: concentrated mainly in Iceland, Norway, western Russia, Alaska and Yukon Territory. Like Method 1, there was no trend in frequency of ROS events over the nine-year study period. The Method 2a detected the most ROS events at the beginning and end of the winter season and the Method 2b (with more constrained bounds) detected the highest frequency of ROS events in the middle of the winter season.

Method 3 (i.e., ROS detection using only ground station measurements) had a higher chance of detecting smaller more localized ROS events. However, similar to Method 2, hourly records were daily averaged, which likely masks some events that occurred over a period of a few hours. Stations with available data are not evenly dispersed, which can introduce a partiality in ROS events detected to only those locations with working stations. Working stations also could break down for long periods of time leading to large data gaps. Stations were also limited by the technology used and may be unable to determine the state of precipitation (i.e., liquid versus solid), which is invaluable information for ROS detection. Only one station is needed for the entire grid cell to be flagged with an ROS event. Such an assumption brings uncertainty to the ROS events detected. The ground station could be malfunctioning and record false values causing a false positive ROS event. The ROS event could be localized to the area just around the ground station and since Method 3 marks the entire grid cell, there an overestimation of the area impacted. Lastly, if an ROS event span over multiple grid cells, some of which do not have ground stations, the ROS event may also be misrepresented. Two versions of Method 3 were created, one with very relaxed bounds (Method 3a) and the other slightly more constrained (Method 3b). Method 3 ROS detection was concentrated mainly in Norway, Sweden, and Finland. Additionally, some were widely dispersed throughout Russia and others clustered together in Alaska. The highest number of ROS events was detected in Norway, where many ground stations are located. Similar to Method 2, the version with more relaxed bounds (Method 3a) detected more ROS events at the beginning and end of the ROS event. Whereas the version with more constrained bounds (Method 3b) showed a peak in ROS events in the middle of the winter like Method 1 and Method 2b. Only about 1.68% of the region of interest contained working ground-based stations, hence, had the potential for an ROS event to be detected using

Method 3. The lack of working high latitude ground stations was a severe limitation for Method 3 ROS detection, and by construct, Method 4.

Combining all three data types could strengthen the accuracy of ROS detection but unfortunately the particular datasets used were not conducive to the combination approach because finding agreement between all three methods did not occur. Regridding Method 1 from a polar grid to a global grid caused the loss 22.7% of the study area. Further, there were two winter seasons (2004-2005 and 2008-2009) with missing output. Although ample amounts of precipitation and snow depth were estimated, MERRA-2 estimated very low air temperatures making it difficult to accurately detect an ROS event. Lastly, and likely the biggest reason why there was no agreement between all three methods, only 1.68% of the region studied had the potential for an ROS event to be detected using Method 3 due to the sparse distribution of ground-based measurements. As a result, three different combinations or versions of Methods 1-3 were used to make up Method 4. All three versions (i.e., Methods 4a - Method4c) detected ROS events in different regions and had no trend in the frequency of ROS events over the nine-year study period. Method 4b had a peak in ROS events at the beginning and end of the winter season whereas Method 4c had a peak in ROS event frequency the middle of the season. ROS events of all intensities are compared, so an ROS event with very small amount of precipitation has equal weight to an ROS event that yields large amounts of rainfall. Analogously, one with a relatively small snow depth is equal in weight to one with deep snowpack. The ROS events in Method 4b have smaller snowpack depths and precipitation values, relative to those in Method 4c. None of the versions in Method 4 (i.e., Method 4a - Method 4c) detected the three known events, further questioning the validity of the ROS detection method used.

5.1.2 Impact of ROS Events on SWE_{AMSR-E}

After the analysis of three documented and 81 detected regional ROS events, results were not able to suggest whether ROS events negatively impact local SWE_{AMSR-E} estimates. ROS events vary greatly in duration, intensity, and frequency making it difficult to make generalized observations about these events difficult. The lack of in-situ SWE measurements of ROS impacted regions also limits the capability of the study to address the impact ROS events have on the accuracy of satellite-based snowpack characterization. Results suggest that SWE_{AMSR-E} estimates minimally fluctuate during and after an ROS event. However, the question remains if these changes are accurate according to what actually is occurring within the snowpack, as a variety of responses observed could be explained theoretically. For example, during an ROS event:

(a) A decrease in SWE could be due to the melting of the snowpack as a result of warm air temperatures or wet snow metamorphism (i.e., liquid water percolating though the snowpack melting the snowpack).

(b) An increase in SWE could be to the addition of water accumulating on the surface or percolating into the snowpack, but not leaving the system.

Further, following an ROS event:

(a) An increase in SWE could be due to the addition of an ice crust into the snowpack or further accumulation of solid precipitation (snow) as air temperatures drop and the precipitation event transitions from liquid to solid phase.

(b) A decline in SWE could also be justified because further melt could occur once the event ended if air temperatures remained above freezing.

An apparent pattern was noticed for two of the three known events with a decrease in SWE_{AMSR-E} leading up to or during the event. Once the ROS event ended, an increase in SWE_{AMSR-E} was seen within the next 3 days preceding the event. The Daring Lake event was small in duration and area of extent, relative to the other two events, and does not show as definitive of a pattern or change.

The goal of the study was not to detect all of the historical ROS events, but instead the ones that most likely happened and perhaps the events that had the greatest impact on the SWE_{AMSR-E}. Issues with determining a reliable detection method led to issues with SWE_{AMSR-E} retrieval analysis. Daily change in SWE_{AMSR-E} over a detected ROS event differed depending on the version (Method 4a – Method4c) of the ROS detection used.

Atmospheric simulations show wintertime warming increasing and becoming more frequent in sub-Arctic regions which may mean that ROS events will become less frequent as the amount of time in the winter season with snow cover shortens. Nonetheless, both ROS detection and the impact of ROS events on SWE_{AMSR-E} need further exploration to validate the conclusions made.

5.2 Future Directions

5.2.1 ROS Detection

Future directions could include continued exploration into methods of ROS detection by the use of each data type (i.e., satellite observations, model estimates, and ground station measurements). Variables such as snow density, snow liquid water content (SLC) and air pressure can be indicative of a recent storm, which could also be utilized in ROS detections. Moving to an hourly detection instead of a daily detection could also pick up the shorter ROS

events. Analogously, using data at finer spatial resolutions to detect those ROS events that are more localized. Analysis could be done with the use of more evenly dispersed polar region ground station networks or perhaps models run at smaller resolutions using finer resolution boundary conditions. ROS detection using polarization ratios has shown promising results and should continue to be investigated (Development of a rain-on-snow detection algorithm using passive microwave radiometry) (Langlois, et al., 2017). A thorough literature review and research campaign to find historical ROS events can help validate these methods.

5.2.2 Exploration of the Impact of ROS Events on SWE_{AMSR-E}

Gathering in-situ SWE measurements of snowpacks known to have been impacted by ROS events to compare to Tb-based SWE estimates would be instrumental in answering the question explored (i.e., if the SWE_{AMSR-E} should be marked as" user beware" or flagged). Observing the AMSR-E SWE retrieval of the grid cells surrounding the detected cells can give some insight into: (1) if the detection method is capturing all of the ROS event, and 2) the changes in the retrieval of snowpacks that are theoretically unaffected by the detected ROS event. Although adding another layer of complexity, observing SWE_{AMSR-E} in regions below the north 60^{th} parallel would also contribute to the further investigation of the ways that SWE_{AMSR-E} estimates are impacted. The methods used are not necessarily applicable to those regions as there was no vegetation, complex terrain, or urban environments to introduce more electromagnetic interference between the snowpack and the sensor. Comparisons of other SWE estimates to the SWE_{AMSR-E} estimates during an ROS event could also help address the accuracy of the retrieval. The daily change in SWE_{AMSR-E} was explored but computing multi-day changes to SWE_{AMSR-E} over an ROS event could also help further answer the question posed. Since AMSR-E calculated snow depth is a significant component of the SWE_{AMSR-E} estimate, further investigation into the

ways that Tb-based snow depth (rather than SWE_{AMSR-E}) is impacted by an ROS event would also be of value. Determining a way to differentiate ROS events from melting episodes, and then comparing the SWE_{AMSR-E} of each type can identify the relevant issues with the estimation. Comparisons of SWE retrieval in snowpacks with known ice crusts or wet snow could also provide information on the accuracy of SWE_{AMSR-E} for ROS events.

5.3 Closing Remarks

The analysis conducted was only a preliminary investigation into both ROS detection and the impact of ROS events on Tb-based snowpack characterization. The findings here emphasize the necessity for further exploration of both objectives. The assumptions made for the AMSR-E based SWE retrieval (i.e., homogenous and dry snowpack) directly contradict the composition of an ROS event (i.e., ice crusts and wet snow). Throughout the time period in which the study was conducted, it has become increasingly clear within the remote sensing community of the limitations of AMSR-E SWE retrieval, and the findings here further support that such a concern is justified as the question of whether or not SWE_{AMSR-E} should be flagged was not clearly answered.

Appendix A: Regional ROS Event Distribution for Methods 2 and 3

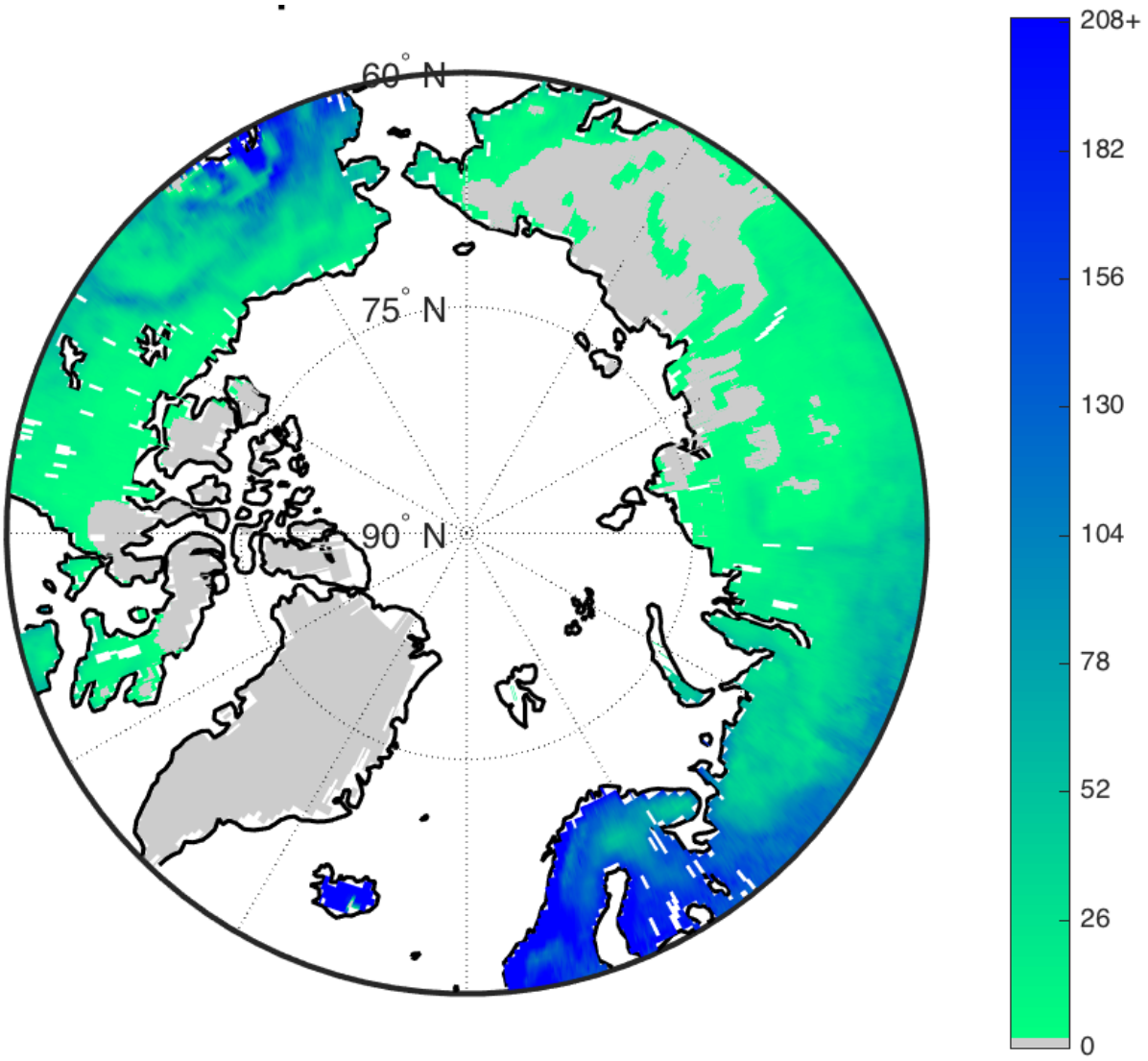

Figure A.1. Regional distribution of all Method 2a ROS detected grid cells over the nine-year period where the color bar indicates the frequency of events for a particular 25 km x 25 km grid cell.

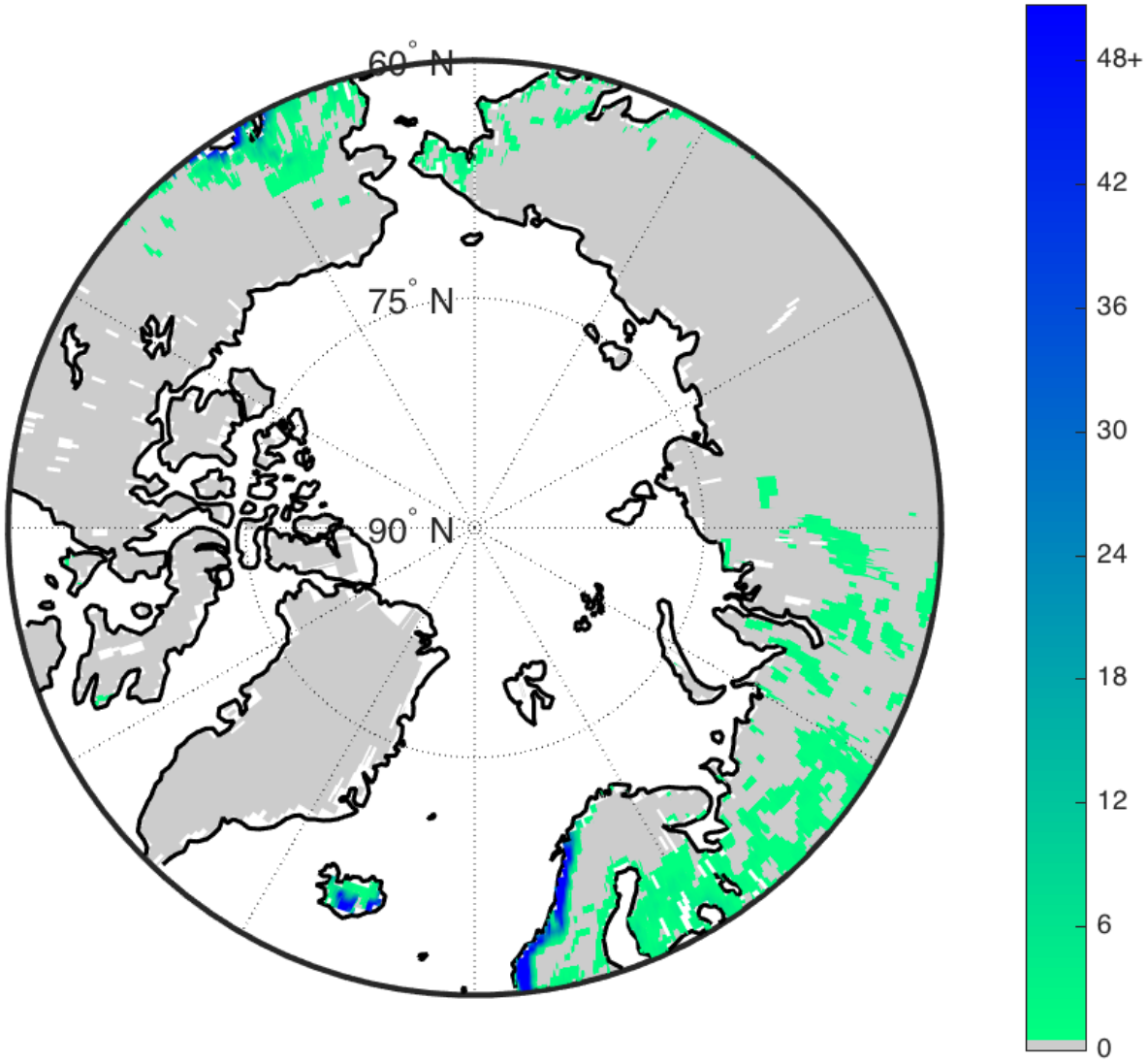

Figure A.2. Regional distribution of all Method 2b ROS detected grid cells over the nine-year period where the color bar indicates the frequency of events for a particular 25 km x 25 km grid cell.

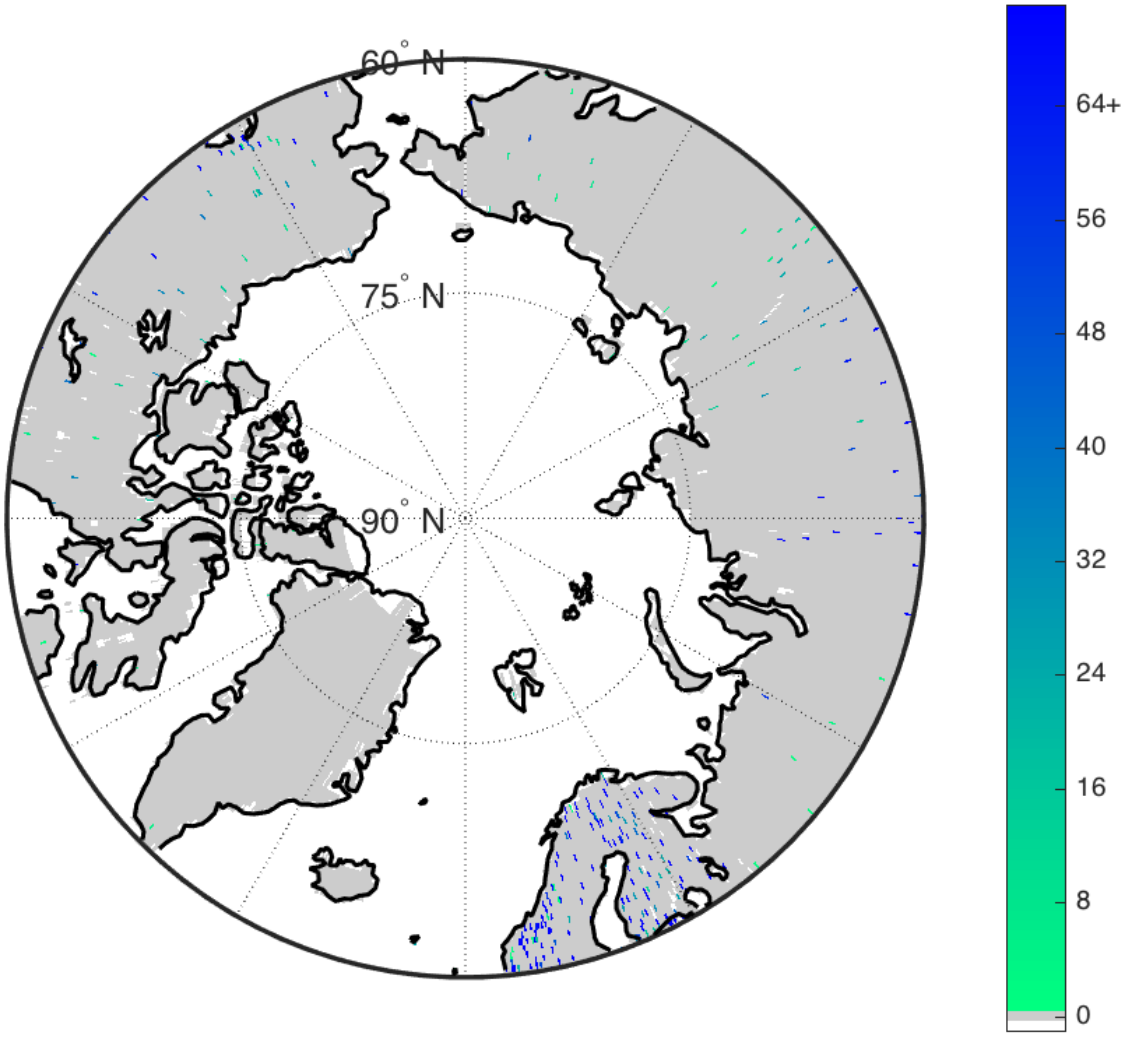

Figure A.3. Regional distribution of all Method 3a ROS detected grid cells over the nine-year period where the color bar indicates the frequency of events for a particular 25 km x 25 km grid cell.

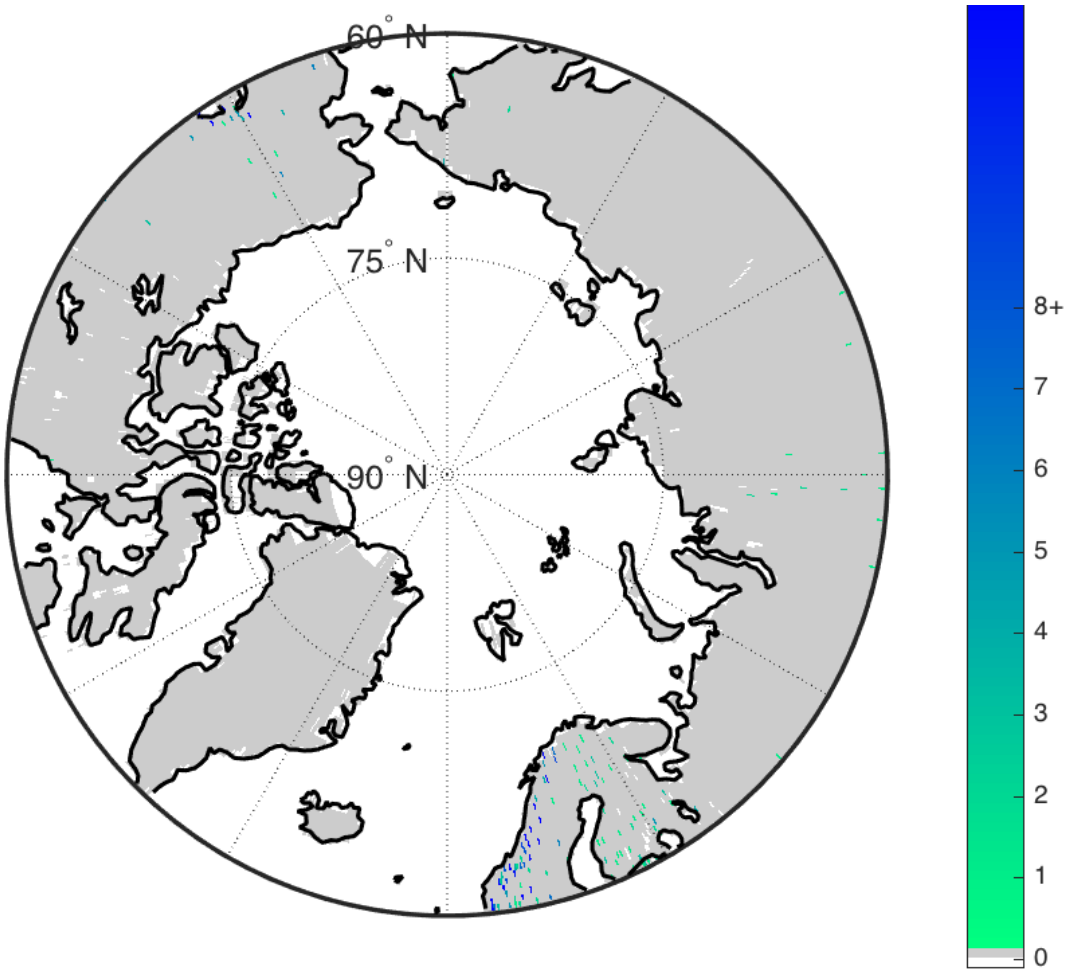

Figure A.4. Regional distribution of all Method 3b ROS detected grid cells over the nine-year period where the color bar indicates the frequency of events for a particular 25 km x 25 km grid cell.

References

A catchment-based approach to modeling land surface processes in a general circulation model 1. Model Structure. **Koster, Randal D., et al. 2000.** D20, 2000, Journal of Geophysical Research, Vol. 105, pp. 24,809-24,822.

A Comparison of AMSR-E/Aqua Snow Products with in situ Observations and MODIS Snow Cover Products in the Mackenzie River Basin, Canada. **Tong, Jinjun and Velicogna, Isabella. 2010.** 2010, Remote Sensing, pp. 2313-2322.

A Prototype AMSR-E Global Snow Area and Snow Depth Algorithm. **Kelly, Richard E. and Chang, Alfred T. 2003.** 2, 2003, IEEE Transactions on Geoscience and Remote Sensing, Vol. 41, pp. 230-242.

A Seasonal Snow Cover Classification System for Local to Global Applications. **Sturm, Matthew, Holmgren, Jon and Liston, Glen E. 1995.** 1995, American Meteorological Society, pp. 1261-1283.

A Simple Algorithm for Identifying Periods of Snow Accumulation on a Radiometer. **Lapo, Karl E., et al. 2015.** 2015, Water Resources Research, pp. 7820-7828.

Armstrong, R. L., et al. 1993. Snow depths and grain-size relationships with relevance for passive microwave studies. *Annals of Glaciology.* 1993, Vol. 17, pp. 171-176.

Ashcroft, Peter and Wentz, Frank J. 2000. *Algorithm Theoretical Basis Document AMSR Level 2A Algorithm.* Santa Rosa, CA : Remote Sensing Systems, 2000. Technical Report.

Assessment and Enhancement of MERRA Land Surface Hydrology Estimates. **Reichle, Rolf H., et al. 2011.** 2011, Journal of Climate, pp. 6322-6388.

Bjerke, J.W., et al. 2011. Contrasting sensitivity to extreme winter warming events of dominant sub-arctic heathland bryophyte and lichen species. *J. of Ecology.* 2011, Vol. 99, 6, pp. 1481-1488.

Brodzik, M.J. and Knowles, K. 2011. *EASE-Grid 2.0 Land-Ocean-Coastline-Ice Masks Derived from Boston University MODIS/Terra Land Cover Data, Version 1.* [prod.] NASA National Snow and Ice Data Center Distributed Active Archive Center. Boulder, CO, USA : s.n., 2011. doi: http://dx.doi.org/10.5067/VY2JQZL9J8AQ.

Brodzik, M.J., et al. 2014. Correction: Brodzik, M. J. et al. EASE-Grid 2.0: Incremental but Significant Improvements for Earth-Gridded Data Sets. ISPRS International Journal of Geo-Information 2012, 1, 32-45. *ISPRS International Journal of Geo-Information.* 2014, Vol. 3, 3, pp. 1154-1156.

Brodzik, M.J., et al. 2012. EASE-Grid 2.0: Incremental but Significant Improvements for Earth-Gridded Data Sets. *ISPRS International Journal of Geo-Information.* 2012, Vol. 1, 1, pp. 32-45.

Callaghan, T.V., et al. 2010. A new climate era in the sub-Arctic: Accelerating climate changes and multiple impacts. *Geophys. Res. Lett.* 2010, Vol. 37, 14705.

Cavalieri, D.J., Markus, T. and Comiso, J.C. 2014. AMSR-E/Aqua Daily L3 12.5 km Brightness Temperature, Sea Ice Concentration, & Snow Depth Polar Grids Version 3. *Boulder, Colorado USA. NASA National Snow and Ice Data Center Distributed Active Archive Center.* [Online] 2014. http://dx.doi.org/10.5067/AMSR-E/AE_SI12.003.

Colbeck, S.C. 1982. An Overview of Seasonal Snow Metamorphism . *Rev. Geophys.* . 1982, Vol. 20, pp. 45-61.

Detection of rain-on-snow (ROS) events and ice layer formation using passive microwave radiometry: A context for Peary caribou habitat in the Canadian Arctic. **A. Langlois, A., et al. 2017.** 2017, Remote Sensing of Environment, Vol. 189, pp. 84-95.

Detection of snow surface thawing and refreezing in the eurasian arctic with quikscat: implications for reindeer herding. **Bartsch, A., et al. 2010.** 2010, Ecological Applications, Vol. 20, pp. 2346-2358.

Development of a rain-on-snow detection algorithm using passive microwave radiometry. **Dolant, C., et al.** Hydrological Processes.

Development of the GEOS-5 atmospheric general circulation model: evolution from MERRA to MERRA2. **Molod, A., et al. 2015.** 5, 2015, Geosci. Model Dev., Vol. 8, pp. 1339-1356.

Ecological Implications of Changes in the Arctic Cryosphere. **Vincent, Warwick F., et al. 2011.** s.l. : Springer, 2011, AMBIO, Vol. 40, pp. 87-99.

Estimating the Spatial Distribution of Snow Water Equivalence in a Montane Watershed. **Elder, Kelly, Rosenthal, Walter and Davis, Robert E. 1998.** 1998, Hydrological Processes, pp. 1793-1808.

Forbes, Bruce C., et al. 2016. Sea ice, rain-on-snow and tundra reindeer nomadism in Arctic Russia. *Biology Letters.* 2016, Vol. 12, p. 20160466.

Forman, Barton A. and Reichle, Rolf H. 2015. Using a Support Vector Machine and a Land Surface Model to Estimate Large-Scale Passive Microwave Brightness Temperatures Over Snow-Covered Land in North America. *IEEE Journal of Selected Topics in Applied Earth Observations and Remote Sensing* . Sept. 2015, Vol. 8, 9, pp. 4431-4441.

Galloway, Kevin, et al. 2014. Winter 2013-2014: A Memorable Weather Season in Alaska. *Alaska Climate Dispatch A State-wide Seasonal Summary and Outlook.* March 2014, pp. 1-12.

Gelaro, R., et al. 2017. The Modern-Era Retrospective Analysis for Research and Applications, Version 2 (MERRA-2). *J. Climate.* 2017, Vol. 30, pp. 5419-5454.

Global Estimates of Snow Water Equivalent from Passive Microwave Instruments: History, Challenges and Future Developments. **Clifford, Debbie. 2010.** 14, 2010, International Journal of Remote Sensing, Vol. 31, pp. 3707-3726.

Grenfell, T.C. and Putkonen, J. 2008. A method for the detection of the severe rain-on-snow event on Banks Island, October 2003, using passive microwave remote sensing. *Water Resources Research.* s.l. : American Geophysical Union, March 25, 2008.

Guarino, Ben. 2016. Starvation killed 80,000 reindeer after unusual Arctic rains cut off the animals' food suppy. *The Washington Post.* November 16, 2016.

Hansen, Brage B, et al. 2014. Warmer and wetter winters: characteristics and implications of an extreme weather event in the High Arctic. *Environ. Res. Lett.* 2014, Vol. 9, 114021, pp. 1-10.

Hydrometeorological Characteristics of Rain-on-Snow Events Associated with Atmospheric Rivers. **Guan, Bin, et al. 2016.** 2016, Geophysical Research Letters, pp. 2964-2973.

Jentsch, A., Kreyling, J. and Beierkuhnlein, C. 2007. A new generation of climate-change experiments: events, not trends. *Frontiers in Ecology and the Environment* . 2007, Vol. 5, 7, pp. 365-374.

Kelly, R. 2009. The AMSR-E snow depth algorithm: Description and initial results. *Journal of the Remote Sensing Society of Japan.* 2009, Vol. 29.

Koike, Tosio and Suhama, Tomoyuki. 1993. Passive-microwave remote sensing of snow. *Annals of Glaciology.* 1993, Vol. 18, pp. 305-308.

Kumar, D. Nagesh and Reshmidevi, T.V. . 2013. Remote Sensing Applications in Water Resources. *Journal of the Indian Institute of Science.* Apr.-Jun. 2013, Vol. 93, 2, pp. 163-187.

Land Surface Precipitation in MERRA-2. **Reichle, Rolf H., et al. 2016.** 2016, Journal of Climate (MERRA-2 Special Collection).

Langlois, A., et al. 2017. Detection of rain-on-snow (ROS) events and ice layer formation using passive microwave radiometry: A context for Peary caribou habitat in the Canadian Arctic. *Remote Sensing of Environment.* 2017, Vol. 189, pp. 84-95.

Liston, G.E. and Hiemstra, C.A. 2011. The changing cryosphere: Pan-Arctic snow trends (1979-2009). *J. Climate.* 2011, Vol. 24, 11.

Mankin, Justin S, et al. 2015. The potential for snow to supply human water demand in the present and future. *Environ. Res. Lett.* 2015, Vol. 10, 114016.

MERRA: NASA's Modern-Era Retrospective Analysis for Research and Applications. **Rienecker, Michele M, et al. 2011.** 2011, Journal of Climate, Vol. 24, pp. 3624-3648.

Observational evidence of recent change in the northern high-latitude environment. **Serreze, M.C., et al. 2000.** 2000, Climate Change, Vol. 46, pp. 159-207.

Observed and modelled effects of ice lens formation on passive microwave brightness temperatures over snow covered tundra. **Rees, A., et al. 2010.** 1, 2010, Remote Sensing of the Environment , Vol. 114, pp. 116-126.

Oskal, A. 2008. Old livelihoods in new weather: Arctic indigenous reindeer herders face the challenges of climate change. *Development Outreach, World Bank Institute Special Paper.* 2008, pp. 22-25.

Passive-Microwave-Based Detection of Rain-on-Snow Events over sub-Arctic Regions. **Brucker, Ludovic, Ivanoff, Alvaro and Maynard, Nancy G. 2014.** 2014, Personal Communication .

Putkonen, J. and Roe, G. 2003. Rain-on-snow events impact soil temperatures and affect ungulate survival. *Geophys. Res. Lett.* 2003, Vol. 30, 4.

Radar hydrology: rainfall estimation. **Krajewski, W.F. and Smith, J.A. 2002.** s.l. : Elsevier, May 12, 2002, Advances in Water Resources, pp. 1387-1394.

Reichle, R.H., et al. 2017. Land Surface Precipitation in MERRA-2. *Journal of Climate* . 2017, Vol. 30, 5, pp. 1643-1664.

Remote Sensing Applications in Water Resources. **Reshmidevi, T.V. and Kumar, D. Nagesh. 2013.** 2, 2013, Journal of the Indian Institute of Science, Vol. 93.

Rosen, Yereth. 2014. Forget snowfall -- winter rain becoming new normal in Alaska and Arctic. *Alaska Dispatch News.* January 28, 2014.

—. 2014. Rain on snow takes a toll on wildlife and the natural environment in the far north. *Alaska Dispatch News.* February 1, 2014.

Salick, Jan and Byg, Anja. 2007. *Indigenous Peoples and Climate Change.* Oxford : Tyndall Centre for Climate Change Research, 2007. Report of Symposium.

Satellite Rainfall Climatology: A Review. **Kidd, C. 2001.** 2001, International Journal of Climatology, pp. 1041-1066.

Soil thermal and ecological impacts of rain-on-snow events in the circumpolar arctic. **Rennert, K. J., et al. 2008.** 2008, Journal of Climate.

Stemp-Morlock, Graeme. 2008. Mysterious "Rain on Snow" Events Tracked in Arctic. *National Geographic.* March 04, 2008.

Synergistic Use of Remote Sensing for Snow Cover and Snow Water Equivalent Estimation. **Muñoz, Jonathan, et al. 2013.** 2013, British Journal of Environment and Climate Change, pp. 612-627.

Tedesco, M. 2012. *Algorithm Theoretical Basis Document NASA AMSR-E Product.* s.l. : NASA, 2012. Internal Document.

Tedesco, M., et al. 2004. *AMSR-E/Aqua Daily L3 Global Snow Water Equivalent EASE-Grids. Version 2.* Boulder, Colorado : USA: NASA National Snow and Ice Data Center Distributed Archive Center, 2004. Digital Media. doi: 10.5067/AMSR-E/AE_DYSNO_002.

Trends and Variability in Rain-on-Snow Events. **Cohen, Judah, Ye, Hengchun and Jones, Justin. 2015.** 2015, Geophysical Research Letters, pp. 7115-7122.

White water: Fifty years of snow research in WRR and the outlook for the future. **Sturm, M. 2015.** 2015, Water Resources Research, Vol. 51, pp. 1-18. . doi:10.1002/2015WR017242..

Winter Rain on Snow and its Association with Air Temperature in Norther Eurasia. **Ye, Hengchun, Yang, Daqing and Robinson, David. 2008.** 2008, Hydrological Processes, pp. 2728-2736.

World Meteorological Organization (WMO). *Review of Remote Sensing of the Snow Cover and on Methods of Mapping Snow.* s.l. : World Meteorological Organization.